UNIVERSITÄTSKLINIKUM HAMBURG-EPPENDORF

Institute of Medical Microbiology, Virology and Hygiene

Prof. Dr. med. Martin Aepfelbacher

Characterization of *Mycobacterium abscessus* EsxU/EsxT complex

Dissertation

to obtain the doctoral degree PhD
at the Medical Faculty of the University of Hamburg

presented by:

Flor del Milagro Vásquez Sotomayor
Lima-Peru

Hamburg 2021

UNIVERSITÄTSKLINIKUM HAMBURG-EPPENDORF

Characterization of *Mycobacterium abscessus* EsxU/EsxT complex

Accepted by the Faculty of Medicine on **16.02.2022**
Published with the permission of the Medical Faculty of the University of Hamburg.

Examination Board:
Chairperson: Prof. Dr. Florian Maurer
2nd reviewer: Prof. Dr. Matthias Wilmanns

DEDICATORIA

Dedico este trabajo y todo mi esfuerzo a mis padres, quienes siempre me han dado amor y me han apoyado a lo largo de este camino. Gracias por enseñarme que las cosas, con esfuerzo, se consiguen, y por ser parte de mis alegrías. Agradezco a Dios por mi familia entera y mis amigos, por habernos protegido durante la pandemia y por permitirme realizar mis sueños. Pido por la eterna paz de aquellos que partieron, y que nos dejaron abrazando recuerdos que atesoraremos toda la vida.

DEDICATION

I dedicate this thesis work and all my efforts to my parents, who have always given me Love and have supported me through this long journey. Thank you for teaching me that achievements are possible through effort, and for being part of my joy. I thank God for my whole family and my dear friends, for protecting us during the pandemic, and for allowing me to fulfil my goals. I pray for the eternal peace of those who are no longer among us, and that left us hugging memories that we will treasure forever.

TABLE OF CONTENTS

1. INTRODUCTION

Mycobacterium abscessus (Mab) is a rapidly growing (RGM) nontuberculous mycobacterium (NTM) and an opportunistic human pathogen. In recent years, increasing rates of infections caused by Mab have been observed globally, mostly connected to patients with underlying pulmonary conditions such as cystic fibrosis or bronchiectasis [1, 2]. In addition to local and disseminated pulmonary disease, Mab has been reported as a causative agent for skin and soft tissue infections (SSTIs), ocular infections and, occasionally, infections of the central nervous system [1, 2].

Mab is believed to utilize environmental waters and soil as reservoirs and can also be found colonizing household and hospital water systems. It is resistant to many disinfectants and is able to form biofilms and resist temperatures of up to 50°C [3]. Contamination of medical devices that come in contact with the patient's soft tissue, contaminated water reservoirs of surgical air conditioning units, and insufficient disinfection of surgical instruments are also discussed as fomites for nosocomial infections [1, 2]. In addition, aerosol transmission among vulnerable hosts is under debate [4].

A hallmark of Mab is its extensive innate antibiotic resistance which has been extensively reviewed elsewhere [5, 6]. In addition, acquired resistance, for example to macrolides and aminoglycosides, can further complicate treatment. With standard therapy, consisting of four to five drugs administered over at least 12 months [7], cure rates for Mab pulmonary infections are only 30-50% [8, 9]. This is partially explained by the fact that all standard drugs prescribed to treat Mab infections are only bacteriostatic and not bactericidal against this mycobacterium and insufficiently cover bacteria contained in biofilms or host phagocytes [10, 11].

Mab can be found in two different phenotypes, smooth (S) and rough (R). The S variant is characterized by the presence of a glycopeptidolipid (GPL) layer on top of the outer layer of the bacterial cell wall and is associated with biofilm formation and colonization of the respiratory tract. GPL masks the mycobacterial surface and has been found to play an important role in persistence of Mab inside host phagocytes [12, 13]. The R variant, on the contrary, lacks a GPL layer due to mutations in the GPL biosynthetic pathway [14], shows a strong tendency to form cord-like structures, and upon phagocytosis triggers apoptosis. The R variant is also a strong inducer of inflammatory pathways and can cause extensive tissue damage [12, 13]. While the S variant is considered the "infecting" variant, R morphotypes are considered the most virulent form and are most frequently isolated from patients with chronic Mab infections following a S-to-R phenotype switch whose exact triggers are poorly understood [5].

Mab comprises three subspecies: *M. abscessus* subsp. *abscessus* (Mab_A)*; M. abscessus* subsp. *bolletii* (Mab_B), and *M. abscessus* subsp. *massiliense* (Mab_M). Mab_A, Mab_B, and Mab_M show differences in drug susceptibility and invasiveness [15]. Most importantly, all Mab_M but only some Mab_A and Mab_B isolates are susceptible to macrolides, which represent cornerstone drugs in treatment of Mab infections together with the aminoglycoside antibiotic amikacin [7]. Nevertheless, with low treatment success rates, more research on the factors that govern virulence, host persistence, and antimicrobial resistance of Mab are clearly needed.

Upon infection, Mab induces the production of inflammatory cytokines, such as tumour necrosis factor (TNF), which recruit neutrophils and macrophages to the site of infection [16]. These

immune cells gradually form an organized and dynamic structure called granuloma that matures through the recruitment of B and T cells, and only breaks down when Mab S variant transitions into its R morphotype, which forms massive extracellular cords [17]. Granulomas shield bacteria from the environment, and their low vascularization significantly reduces the possibility of drug delivery to the inside [18].

The combination of Mab resistance mechanisms, limited treatment options, weak anti-mycobacterial agents, and the presence of gradients of exposure to drug cocktails within the granuloma, create an environment for potential emergence of additional, acquired drug resistance [19].

The mycobacterial envelope protects the cell from hostile environments, offers mechanical resistance, and is the platform of many crucial processes such as the uptake and secretion of substances required for cell survival and interaction with other mycobacteria, and the adhesion to receptors [20]. Furthermore, it plays important roles in antibiotic resistance (due to its low permeability) [21], autoaggregation or cell-cell adhesion [22], pathogenicity [23] and aerosolization (associated to its hydrophobicity and interaction with water droplets) [24]. This complex structure owes its high hydrophobicity to its high content of lipids (up to 60% in the cell wall) [25] and is organized in different layers. The inner layer is the cytoplasmic membrane, on top of which a covalently linked structure of peptidoglycan and arabinogalactan rests. The mycomembrane or mycobacterial outer membrane (MOM) is covalently linked to the arabinogalactan and is composed of mycolic acids and extractable lipids and glycolipids. In the case of Mab these lipids include trehalose mono- and dimycolates, phosphatidyl inositol mannosides (PIM), phospholipids and GPL (Mab S) [5, 23].

Mycolic acids (MAs) are the longest fatty acids found in nature and are major components of the outer membrane of mycobacteria, playing a crucial role in its architecture. Most MAs known to date mycobacterial present oxygen-containing functional groups located in the distal part of the meromycolic chain. These oxygenated MAs are absent from Mab. Furthermore, mycobacterial MAs can be found in a variety of lengths (C60-C90), classified in α-mycolates (~C70–C90) and α'-mycolates (C66-C68) [26]. It has been shown that α- and α'-MA in Mab are present in comparable amounts in the S and R morphotypes, with no difference in structure [27]. In addition, it has also been shown that the mycobacterial envelope owes its hydrophobicity mostly to the presence of mycolic acids. [28].

Trehalose Polyphleates (TPPs) are large non-polar lipids of unknown role located in the outer membrane. Previously, Llorens-Fons et al. found that TPP molecules localized to the external surfaces of cords in Mab R morphotype, but not in the S variant and proposed that they have a function in the formation of clumps and cords in Mab rough variants [27].

Glycopeptidolipids (GPLs) contain mostly polar lipids. In the S variant, GPL is distributed in hydrophilic nanodomains, masking the mycolic acids and reducing Mab hydrophobicity. Due to irreversible mutations in the genome, GPL can be reduced or even lost (S-to-R conversion). It is suggested that as the hydrophilic nanodomains disappear, Mab ability to aggregate and form cord-like structures increases [28].

To facilitate the exchange with the environment despite their complicated envelope, four secretion systems have evolved in mycobacteria: the Sec pathway for unfolded proteins with an N-terminal signal peptide; the SecA2 pathway (associated with the ability of *M. tuberculosis* to

replicate inside macrophages and the secretion of factors that can arrest phagosome maturation [29]); the Tat pathway for prefolded proteins, some of which have a known N-terminal signal peptide; and the Type VII Secretion Systems (T7SS, also known as ESX systems), all reviewed in [30]. The first two secretion systems translocate proteins across the inner membrane, while T7SS represent the first mechanism proposed for the secretion of proteins into and across the mycobacterial envelope [31], aiding also in nutrient intake and virulence factors export. These systems are present in *Actinobacteria* and in *Firmicutes* [32], and have been widely found in pathogenic and non-pathogenic Gram-positive bacteria. For example, in *Firmicutes*, ESX-homologous systems have been found in *Staphylococcus aureus* [33], *Bacillus subtilis* [34], and *Listeria monocytogenes* [35]. In actinomycetes, several species like *Rhodococcus equi* [36], *Corynebacterium diphtheriae* [37], *Streptomyces coelicolor* [38], *Catenulispora Acidiphila* [39], *Kribbella flavida* [40], among others [35] contain ESX-4 systems. T7SS are present in all mycobacterial species, either non-pathogenic, opportunistic pathogens, or specific human pathogens [41].

T7SS have two main characteristics: the presence of genes that encode transmembrane proteins of the FtsK–SpoIIIE-like ATPase family, and the presence of genes that encode small secreted proteins of approximately 100 amino acids that have a conserved Trp-X-Gly motif (WXG100 superfamily) [42]. Structurally, T7SS are composed of a complex formed by at least four ESX-conserved-components (EccB, EccC, EccD, EccE), ESX-type-specific associated proteins (Esp), and secreted/exported proteins (Esx and/or PE and PPE proteins) organized in an operonic arrangement [43]. In addition, a conserved membrane-bound mycosin protease, MycP, is also found in the loci and has been shown to process some ESX substrates [44] and to stabilize the core membrane complex [45] [46]. Research on the T7SS in *M. xenopi* [47] and *M. smegmatis* [48] has revealed that Ecc proteins and MycP organize to form a structure that spans the mycobacterial inner membrane (Figure 1), and orchestrate the secretion of different substrates upon recognition. A recent study on the ESX-1 T7SS from *Mycobacterium tuberculosis* (Mtb) showed that ESX-dependent secretion was abolished and expression of other ESX-1 structural components was lowered upon deletion of *eccE*$_1$, and concluded that EccE$_1$ aids in the stabilization and function of the full membrane complex [49]. However, further research is needed to better understand the specific role of individual ESX structural components and substrates.

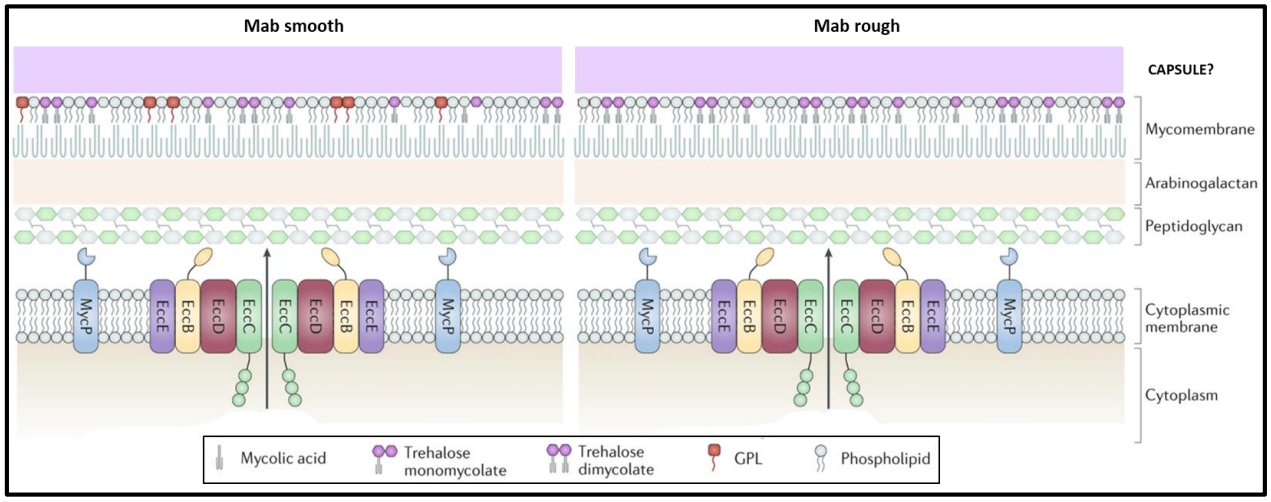

Figure 1. Mab ESX-4 and cell envelope structure in variants S and R. Adapted from Figure 3 in [5].

In addition, there is a gap of knowledge as to how T7SS substrates reach the external environment of the cell. As mentioned, it appears that T7SS only span the inner membrane and a structure facilitating T7SS substrate translocation across the outer membrane is not yet known.

Differences in the genetic organization within ESX systems have given rise to five known T7SS subtypes: ESX-1 to ESX-5 (reviewed in [23] and [41]). ESX-3 has been shown to be essential for iron homeostasis and viability, while ESX-1 (reviewed in more detail in [50]) and ESX-5 have been associated with virulence. Less is known about the roles of ESX-2 and ESX-4 and the substrates they secrete, particularly in NTM. For example, it has been shown that *Mycobacterium smegmatis* ESX-4 is required in the recipient strains for chromosomal DNA conjugation [51] and that its expression could be controlled by ESX-1 [52]. Also, it has been shown that ESX-4 is functional and plays a critical role in virulence in Mab as it is involved in phagosomal rupture [53]. However, a recent study showed that ESX-4 is not required for phagosomal rupture in *Mycobacterium marinum* (Mma), giving rise to the possibility of different roles of this system between SGM and RGM [54]. This same study showed that intact ESX-1 and ESX-4 were required for successful ESX-5-mediated secretion of CpnT, the only known toxin secreted by Mtb, giving ESX-4 an indirect role. To date, no other studies have addressed the function of this system in mycobacteria.

T7SS are highly diverse among mycobacterial species and phylogenetic research has helped us to understand their evolution. In 2015, a study by Dumas et al. revealed the existence of two main types of ESX systems in mycobacteria: the ancestral types (ESX-4 and ESX-4-like systems) and the mycobacteria-specific ESX systems (ESX-1, ESX-2, ESX-3, ESX-5 and the plasmid-encoded ESX types (ESX-P)) [31]. The study concluded that these ESX-P systems, found in some mycobacterial species, may have acted as gene-exchange vectors and accelerated the adaptation and evolution process within the genus through horizontal gene transfer (HGT). In 2016 another study suggested something similar, showing that the FtsK-WXG cluster present in the *Firmicutes* evolved to form the ESX-4 gene cluster resulting in the presence of ESX-4 in the genomes of various actinobacterial species and *Mycobacterium abscessus* [35]. From then on and through a series of events including gene duplication, re-arrangement, plasmid-mediated evolution, HGT and insertion into the mycobacterial chromosome, ESX-4 gave rise to all other ESX types (Figure 2). The ancestral ESX-4 and ESX-4-bis (presenting differences only in gene order and gene orientation) are short operons lacking pe/ppe and espG genes. Originally, ESX-4 included components EccB-E, but during evolution *eccE* was lost from the chromosomal ESX-4. To date, *eccE* is found only in Mab ESX-4 and in the ESX-4-bis of *M. mageritense* and one isolate from *M. aubagnense*, all RGM [31]. It is important to highlight that due to the absence of $eccE_4$ in most mycobacterial genomes, it was thought that ESX-4 in general was non-functional. However, a recent study showed that this system in Mab was not only functional but also associated with its virulence [53].

All mycobacteria contain ESX-4 and ESX-3, with the exception of *M. leprae* which has lost ESX-4. ESX-1 appeared after the divergence of Mab and has been found in both RGM and slow-growing mycobacteria (SGM). The presence of ESX-2 and ESX-5 marks the emergence of the SGM [31] [35]. RGM were clearly separated from SGM with the *M. terrae* complex occupying an intermediate position [55].

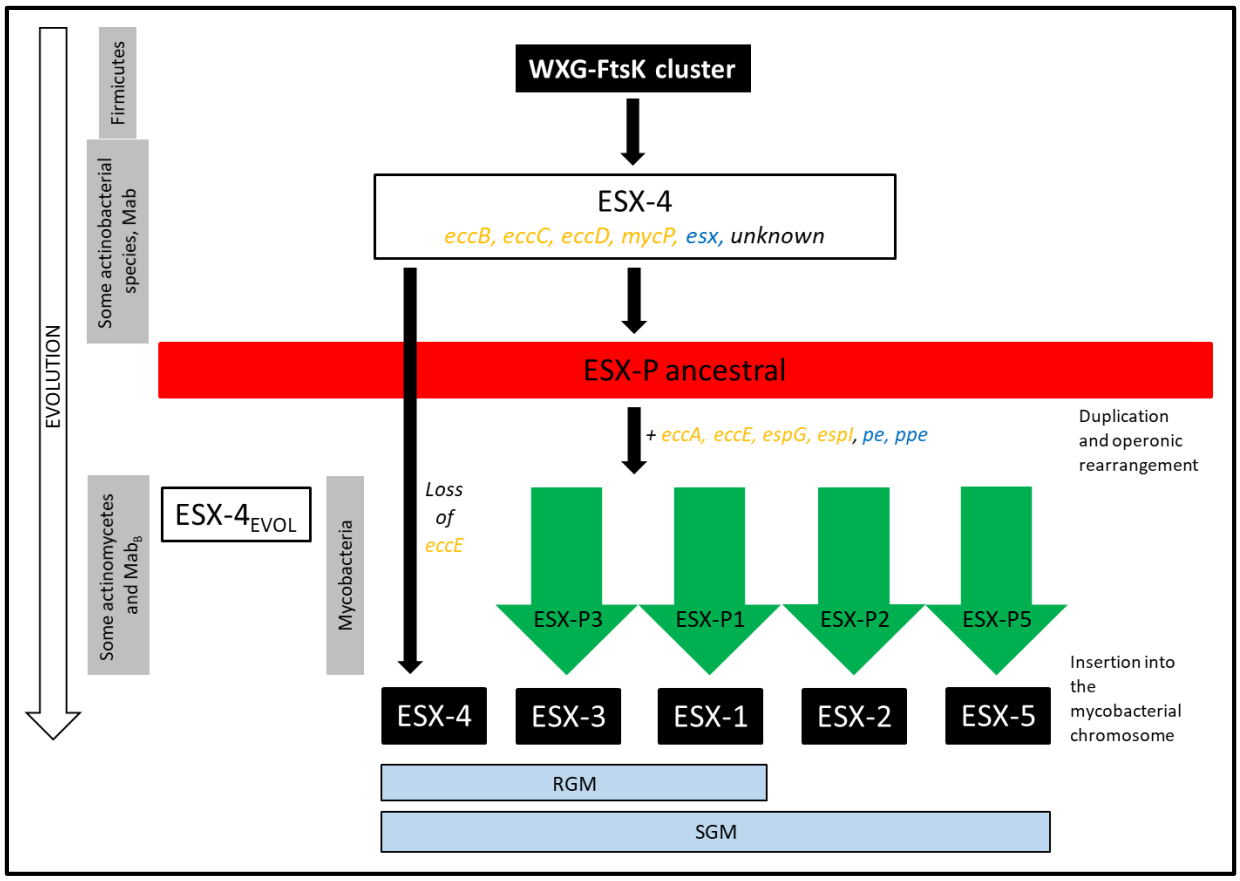

Figure 2. Evolution of ESX systems (based on [35]). ESX-4 is the ancestral ESX, present in some actinobacterial species and Mab. After duplication into plasmid ESX-P ancestral and acquisition of *eccB, eccC, eccD, mycP, esx* genes, it underwent several operon rearrangements giving rise to plasmids ESX-P3, ESX-P1, ESX-P2 and ESX-P5, which upon insertion into the mycobacterial chromosome gave rise to ESX-3, ESX-1, ESX-2 and ESX-5 respectively. ESX-4_{EVOL} also arose from ESX-P ancestral, after acquisition of genes, and was inserted into the chromosome of some actinomycetes and Mab_B. The ESX-4 system present in a mycobacteria does not contain *eccE*, due to its loss during evolution.

Current knowledge on substrates of mycobacterial T7SS is incomplete, particularly in NTM [41]. However, their structural features have been elucidated based on the most studied mycobacterial Esx proteins: Mtb EsxA and EsxB (previously known as ESAT-6 and CFP-10, respectively). Considering the structure homology, Esx proteins can be classified as part of three subfamilies, EsxA-like, EsxB-like and the *sag*EsxA-like [56]. The first two subfamilies group proteins with bicistronic expression, which upon pairing form an anti-parallel heterodimeric four-helix bundle. The EsxA-like WXG proteins subfamily presents a C-terminal secretion signal, three highly conserved residues (K/P38, Y51 and Q55) and a WXG motif, while the EsxB-like WXG proteins subfamily presents a C-terminal secretion signal and a WXG motif. The secretion signal is composed of sequence HxxxD/ExxhxxxH, where 'H' stands for highly conserved hydrophobic residue, 'h' for less conserved hydrophobic residues, and 'x' for any amino acid. The third subfamily is the *sag*EsxA-like for Esx proteins with monocistronic expression, that form homodimeric complexes, found within the ancient version of T7SS (T7SSb) in *Firmicutes* [56].

Up to now, studies have shown that EsxA/EsxB is secreted in Mtb [57] and Mma [58]. In biophysical studies, EsxA has been found to insert within membranes via its WXG motif and to

form a pore [59, 60]. Based on this evidence, it has been suggested that upon phagocytosis, EsxA could form a pore in the phagosome membrane, leading to disruption followed by bacterial escape [61]. In the diagnostic field, EsxA and EsxB have great importance in assessing previous patient exposure to *M. tuberculosis* complex (MTBC). The fact that these proteins trigger a strong IFN-γ response in sensitized T-cells led to the development of EsxA/EsxB-based IFN-γ Release Assay (IGRA) (Figure 3) (reviewed in [62]). A similar quantitative assay would be highly desirable for infections caused by Mab, not only to assess previous exposure of vulnerable host populations such as patients suffering from cystic fibrosis, but also to serve as a biomarker to rationalize induction and, importantly, cessation of months-long, toxic, multidrug antibiotic therapies.

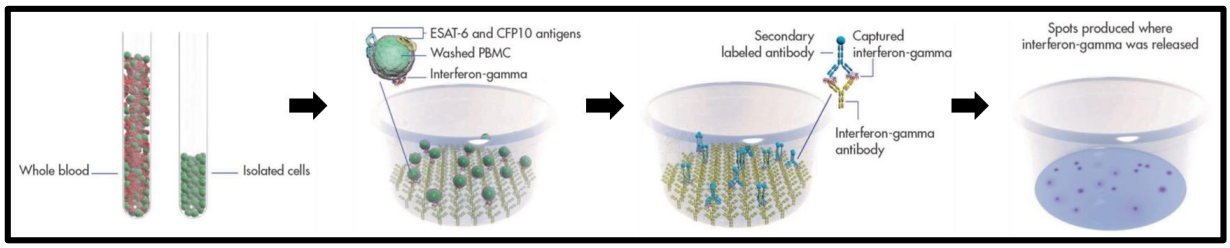

Figure 3. Principle of IFN-γ release assays. A blood sample is collected, after which peripheral blood mononuclear cells (PBMC) are isolated. The cells are washed, counted, transferred to plates and stimulated with TB-specific antigens (EsxA and EsxB). Cells responding to these antigens release IFN-γ, which is captured by IFN-γ antibodies. A secondary enzyme labelled antibody is added to bind to the first antibody. A detection reagent is added and reacts with the enzyme labelled antibody. This reaction produces spots that can be quantified, indicating the release of IFN-γ and therefore, previous exposure to MTBC. Images taken from the T-SPOT.*TB* website (https://www.tspot.com/why-the-t-spot-tb-test/technology/)

Mab contains a circular chromosome, whose complete sequence was first reported in 2009 [63]. Among all systems encoded in its genome, two T7SS can be found: ESX-3 and ESX-4. The Mab ESX-4 locus contains 8 genes, 5 of which encode membrane-bound components ($EccB_4$-$EccE_4$ and $MycP_4$), 2 encode for hypothetical secreted substrates (EsxU and EsxT, uncharacterized) and one gene has an unknown product (Figure 4).

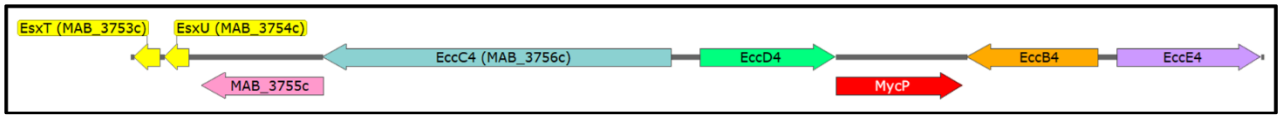

Figure 4. Mab ATCC 19977 ESX-4 locus. There are 3 genes in the forward DNA strand and 5 in the reverse strand, coding for the 8 components of the locus.

As mentioned before, Laencina et al. showed through experiments performed with THP-1 cells that Mab ESX-4 is functional and associated with virulence [53]. Using transposon mutagenesis, the authors could introduce mutations in most structural components of the ESX-4 operon but not in the putative ESX-4 substrates EsxU or EsxT. This pointed us to further investigate if EsxU and EsxT play a critical role in Mab homeostasis or fulfil a function similar to EsxA/EsxB from Mtb.

In the present work, we hence aimed to further characterize the organisation and function of the Mab ESX-4 system with a particular focus on the expression, structure and function of EsxU and EsxT as putative ESX-4 substrates. To that end, we expressed and purified the Mab ESX-4 operon in *M. smegmatis*. In addition, we expressed and purified EsxU and EsxT both individually and bicistronically, and studied their interaction with host cells using a broad spectrum of molecular techniques. Lastly, we investigated the interaction of the EsxU/EsxT heterodimer with lipid bilayers aiming to propose a function of the EsxU/EsxT heterodimer in Mab virulence and pathogenicity.

This work was conducted in close collaboration between the Institute for Medical Microbiology, Virology and Hygiene (UKE), the National and WHO Supranational Reference Laboratory for Mycobacteria at Research Center Borstel (FZB) and the European Molecular Biology Laboratory Hamburg site (EMBL) as part of the collaborative initiative that aimed at connecting innovative biophysical methods with research questions in infection biology and medicine (www.infectophysics,org). Two collaborating groups led by Prof. Jean-Louis Herrmann at Université Versailles Saint-Quentin-en-Yvelines (UVSQ) and Prof. Laurent Kremer at Institut de Recherche en Infectiologie de Montpellier (IRIM) joined our research as external partners.

2. MATERIALS AND METHODS

2.1 Cloning, Expression and Purification of Mab ESX-4 locus and EsxU/EsxT proteins

Cloning

All the primers used for cloning and for sequencing the inserts are shown on Tables 1 and 2, respectively.

Primers for pKB87					
Name	**Sequence (5'-3')**	**bp**	**%GC**	**Annealed bases**	**Fragment size**
pMVMabs_1	GTCAGTACGCGAAGAACCACTTAATCTAGTGGTGGTGGTGGTGCTGCGCGAAGGCCTGT	62	56	16	4.804 kb
Esx4I_F	GCGATGTCATCACAGCTGGC	20	60	20	
Esx4I_R	CCATTACGTGCATCGAGCCC	20	60	20	5.914 kb
pMVMabs_4	GAACTGCGGGTGGCTCCAAGCGCTATGTGGTTCACTCCAAGCGACCTG	48	60	24	
Primers for pKB89					
Name	**Sequence (5'-3')**	**bp**	**%GC**	**Annealed bases**	**Fragment size**
MabsUT_F	ACTACGTCGACATCGATATCAGTGGTGCCAGGCG	34	56	16	657 bp
MabsUT_R	GTACTTCCAGGGCGCAGTGGCTGTTTTTCAGAATGACCT	39	51	23	
Primers for pFV01					
Name	**Sequence (5'-3')**	**bp**	**%GC**	**Annealed bases**	**Fragment size**
MabsEsxU_R	ACTACGTCGACATCGATATTAGAAGGTCTGGCTCTCG	37	49	19	313 bp
MabsUT_R	GTACTTCCAGGGCGCAGTGGCTGTTTTTCAGAATGACCT	39	51	23	
Primers for pFV02					
Name	**Sequence (5'-3')**	**bp**	**%GC**	**Annealed bases**	**Fragment size**
MabsEsxT_F	GTACTTCCAGGGCGCAATGAGCCAGATTACTTACAACC	38	50	22	325 bp
MabsUT_F	ACTACGTCGACATCGATATCAGTGGTGCCAGGCG	34	56	16	

Table 1. Primers used for cloning

Sequencing Primers for pKB86			
Name	**Sequence (5'-3')**	**bp**	**%GC**
pMVseqF	TCGTGCGACTGTCCTCGTT	19	58
pMVseqR	GGCTAGAACTAGCTGATCAC	20	50
Sequencing Primers for pKB87			
Name	**Sequence (5'-3')**	**bp**	**%GC**
EccC seq F	AACTCTGGTCATGCGCTC	18	56
EccC4seqF2	CTTGTTCCGGATGGGCGTC	19	63
EccC4seqF3	CAGATGCGACCCGCCGAG	18	72
EccC4seqF4	GAGGTGGTGTGGCGCAATC	19	63
EccC4seqF5	CCGGCGATAGTGACTACTGC	20	60
EccC4seqR5	GAACCAGCGAGTGAGTGC	18	61
EccD4seqF6	CAGCGCCAGGTCTACCTG	18	67
EccD4seqF7	CGTCGTCACCCTCGGTATC	19	63
EccMseqF8	GATGAGGGGTGGCAGTCG	18	67
EccB4seqF9	GAGATCGTCGCTGACCGC	18	67
EccB4seqF10	CATCAAGATGAGCCGGGC	18	61
EccE4seqF11	CCGCAACCTATCGTGGTTG	19	58
EccE4seqF12	GGCCACGTTGTACGAATCG	19	58
pMVseq F	TCGTGCGACTGTCCTCGTT	19	58
Sequencing Primers for pKB89, pFV01 and pFV02			
Name	**Sequence (5'-3')**	**bp**	**%GC**
AP328	CGCAGTTGTTCTCGCATACC	20	55
pMyNT-R	GTACGCTAGTTAACTACGTCG	21	48

Table 2. Primers used for sequencing of pKB86, pKB87, pKB89, pFV01 and pFV02.

A synthetic DNA sequence containing a twin-streptavidin tag with its stop codon, followed by the sequence of Mab *esxU* and *esxT* (as found in ATCC 19977) was ordered (GeneScript,

Piscataway, NJ, USA). The *esxT* gene was designed to contain a C-terminal HA-tag. The vector used was pMV-ESX-5 (described in [47]). pMV-ESX-5 and the GeneScript insert were both digested with *PacI* and *HpaI* (New England Biolabs (NEB), Ipswich, MA, USA) and ligated with T4 DNA ligase (NEB), obtaining **pKB86**. *E. coli* DH5α cells were transformed with pKB86, plated in LB agar plates supplemented with Streptomycin (Roth, Karlsruhe, Germany, Cat. # HP66.2), and the construct was extracted using QIAprep™ Spin Miniprep Kit (Qiagen, Venlo, Netherlands) and sequenced to verify the inserted sequence (Eurofins Genomics).

Mycobacterium abscessus reference strain (ATCC 19977 / DSM 44196 / CIP 104536 / JCM 13569 / NCTC 13031 / TMC 1543) ESX-4 locus (without *Mab_3755c*) was amplified in 2 fragments (4.8 and 5.9 kb) and inserted in pKB86, previously digested with NEB *HindIII* and *PacI*, using SLiCE [64]. The final construct (**pKB87**) contained three tags: a C-terminal twin-streptavidin tag on $EccC_4$, a C-terminal His tag on $EccE_4$ and a C-terminal HA tag on EsxT. *E. coli* DH5α cells were then transformed with construct pKB87, plated in LB agar plates supplemented with Streptomycin, and the construct was extracted using QIAprep™ Spin Miniprep Kit (Qiagen) and sequenced to verify the inserted sequence (Eurofins Genomics).

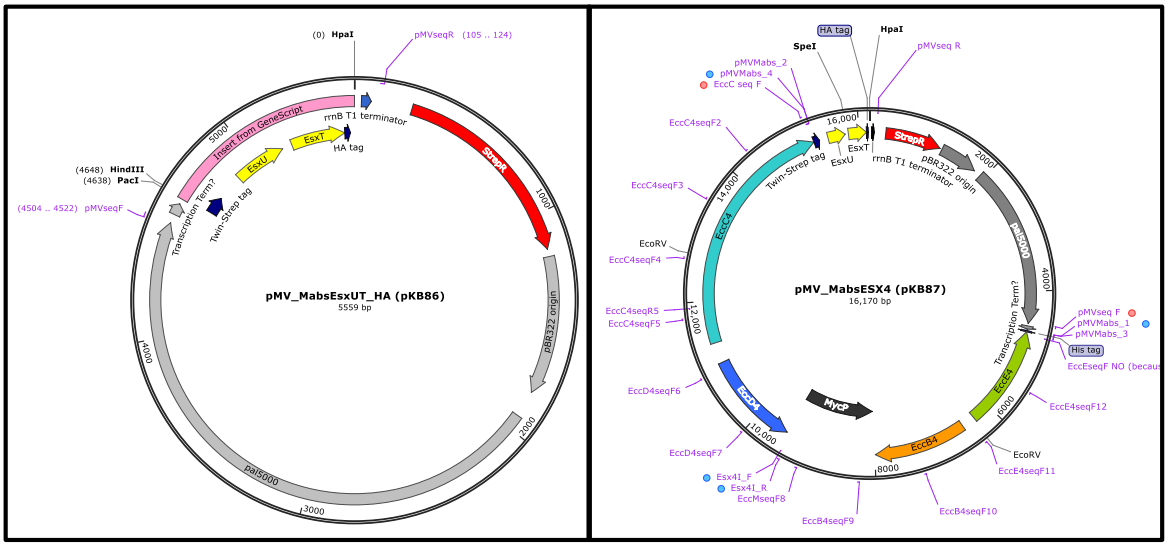

Figure 5: Map of constructs pKB86 and pKB87. Maps were constructed using SnapGene version 5.2.4.

Mab_3755c has not been previously characterized. In the present plasmid design this gene was underestimated and not considered. Structure prediction programs indicate that the product of this gene contains a transmembrane domain, but in the present study we have not investigated its structure nor its role in the ESX-4 locus.

Mab *esxU* and *esxT* were amplified from Mab ATCC 19977 and inserted into pMyNT vector, previously digested with NEB *NcoI* and *HindIII*, using SLiCE cloning. The final construct (**pKB89**) had an insert coding for two main proteins: EsxU with an N-terminal His-tag (with a TEV sequence between the tag and the protein) and EsxT, both under the control of an acetamidase promoter. It is important to highlight that for this cloning, the first residue of EsxU was changed from a methionine to a valine, and a methionine codon was placed upstream of the histidine tag to make sure that the protein would be expressed with its N-terminal tag. The *esxT* sequence remained as in the original strain. *E. coli* DH5α cells were then transformed with construct pKB89, plated in LB agar plates supplemented with hygromycin, and the

construct was extracted using QIAprep™ Spin Miniprep Kit (Qiagen) and sequenced to verify the inserted sequence.

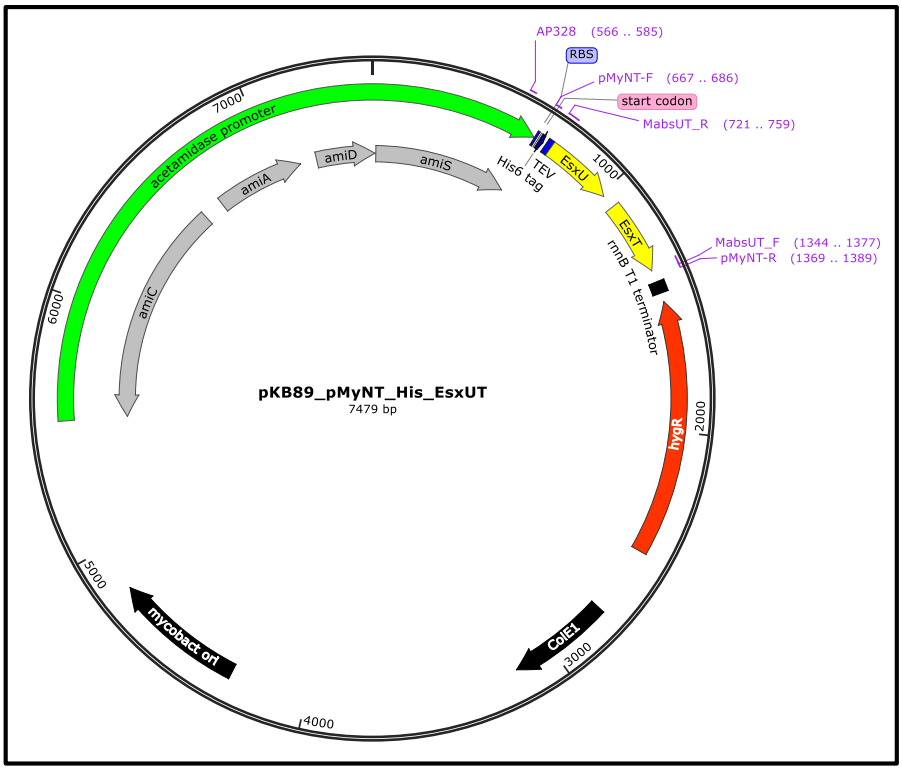

Figure 6: Map of construct pKB89 and pKB87. Map was constructed using SnapGene version 5.2.4.

Additionally, gene blocks of genomic *esxUT* were ordered from GeneScript. Those gene blocks contained mutations, either in the signal sequence at the C-terminus of EsxT (D87L and D87N) or a mutation in the predicted WXG motif of EsxT (A43W). Those were inserted within pMyNT using NEB *BamHI* and *HindIII*.

esxU and *esxT* were cloned separately from Mab ATCC 19977 into the pMyNT vector to obtain plasmids **pFV01** and **pFV02**, respectively. Both constructs coded for EsxU or EsxT with an N-terminal His-tag and a TEV sequence between the tag and the protein. As per in pKB89, the first residue of EsxU in pFV01 and EsxT in pFV02 was changed from a methionine to a valine, and a start codon was placed upstream of the histidine tag to make sure that the proteins would be expressed with its N-terminal tag. *E. coli* DH5α cells were then transformed with the new constructs, plated in LB agar plates supplemented with hygromycin, and the construct was extracted using QIAprep™ Spin Miniprep Kit (Qiagen) and sequenced to verify the inserted sequence.

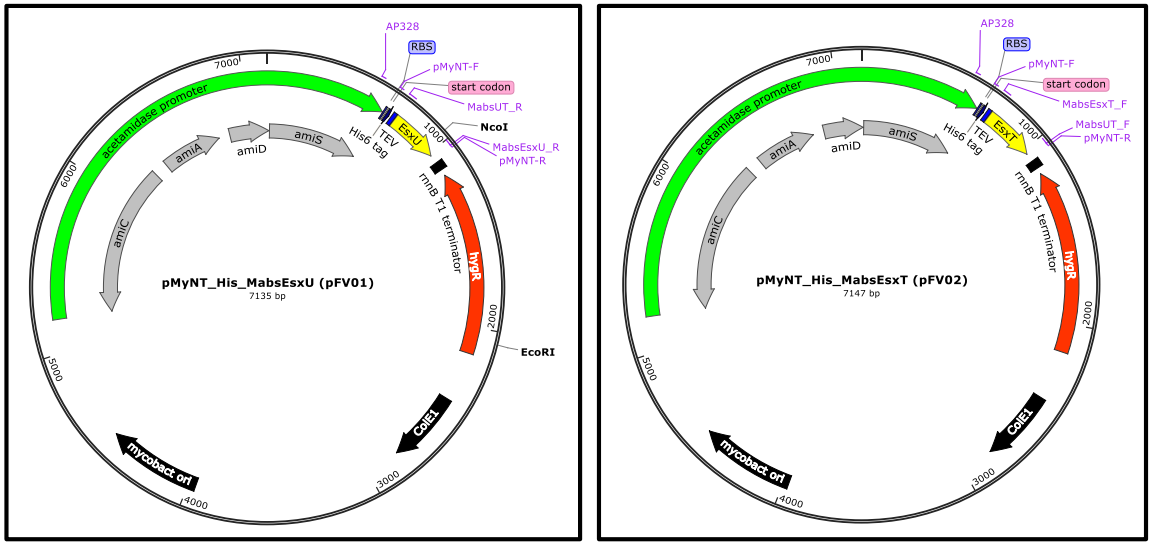

Figure 7: Map of constructs pFV01 and pFV02. Maps were constructed using SnapGene version 5.2.4.

Transformation in *M. smegmatis*

Once all sequences were checked, *M. smegmatis* mc^2155 groEL1ΔC was transformed with the relevant plasmids via electroporation on a Bio-Rad Micropulser at 2.7 kV. Cells were plated in LB agar plates supplemented with the appropriate antibiotic and incubated at 37°C for 3-4 days. Colonies were checked for plasmid presence via colony PCR or via restriction enzyme digestion. Successful colonies were cultured in complete media (Middlebrook 7H9 medium (BD Biosciences, New Jersey, USA) supplemented with 0.2% (vol/vol) glycerol (Roth, Cat. # 378.1), 10% albumin–dextrose saline (5% (wt/vol) BSA, 2% (wt/vol) glucose, 342 mM NaCl) and 0.05% (vol/vol) Tween-80 (Roth, Cat. # 9139.1)) at 120 r.p.m. Glycerol stocks were made for all *M. smegmatis* transformed with the new plasmids and stored at -80°C.

Small Scale Expression for pKB89, pFV01 and pFV02:

A starter culture was set up by placing the inoculum from the glycerol stock into 5 ml of complete media supplemented with 5 µl hygromycin B solution (Roth, Cat. # CP12.2) and incubated at 37°C for 2-3 days with shaking at 120 r.p.m. This starter culture was then used to inoculate a 100 ml culture of expression media (Middlebrook 7H9 medium (BD Biosciences) supplemented with 0.2% (vol/vol) glycerol (Roth, Cat. # 378.1), 0.2% (wt/vol) glucose (Roth, Cat. # X997.2) and 0.05% (vol/vol) Tween-80) containing 100 µl hygromycin and incubated at 37°C x 24 h. Protein expression was induced by adding 220X acetamide solution and incubating the culture at 37°C for 24 h more.

Fractionation of bacterial cells

All steps were carried out at 4°C. Cultures were harvested by centrifugation at 4,000 r.p.m. for 15 min. The supernatant was collected and filtered using a 0.2µm filter. 10-50 ml of filtered supernatant were concentrated using a 3K concentrator (Amicon® Ultra 15 Centrifugal Filter, Merck KGaA, Germany) to a final volume of 0.5-2 ml (final concentration = 20-25X). The pellet was resuspended in 20 ml lysis buffer (300 mM NaCl, 50 mM HEPES pH 8.0, 20 mM Imidazole) containing protease inhibitors and DNaseI. Cells were disrupted by three cycles of 3 min each through a sonicator (Bandelin, Ultrasonic Homogenizer HD 2200) at 45% power amplitude. At this point, a 100 µl sample for whole cell extract (WC) was taken. Intact cells and debris (insoluble fraction) were removed by centrifugation at 8,000 x g for 15 min. The

supernatant, containing the soluble proteins (soluble fraction), was transferred to a different tube.

Purification of proteins

The soluble fraction was purified in a Nickel column (CV=50µl) using extraction buffer (300 mM NaCl, 50 mM HEPES pH 8.0, 20mM Imidazole) to equilibrate and wash the column. The proteins of interest were eluted in 3 x 1CV elution buffer (300 mM NaCl, 50 mM HEPES pH 8.0, 500mM Imidazole).

Large Scale Expression for pKB89, pFV01, pFV02 and EsxU/EsxT mutants

A starter culture was set up by placing the inoculum from the glycerol stock into 8 ml of 7H9 complete media supplemented with 50 µg/ml Hygromycin and incubated at 37°C for 2-3 days with shaking at 120 r.p.m. This starter culture was then used to inoculate a culture of 6 L of expression media supplemented with hygromycin and incubated at 37°C for 24 h with shaking at 120 r.p.m. Protein expression was induced by adding 220X acetamide solution and then incubating at 37°C for 24 h more.

Fractionation of bacterial cells

All steps were carried out at 4°C. Cultures were harvested by centrifugation at 4,000 r.p.m for 15 min. 50 ml of supernatant was collected, filtered using a 0.2µm filter and concentrated using a 3K concentrator (Amicon®) to a final volume of 2-3 ml (final concentration = 25X). The pellets were resuspended in lysis buffer (300 mM NaCl, 50 mM HEPES pH 8.0, 20 mM Imidazole) containing protease inhibitors and DNaseI and stirred for at least 1 h until the solution was homogeneous. Cells were lysed by high-pressure emulsification (3 times at 10000-15000 psi). At this point, a 100µl sample for whole cell extract (WC) was taken. Intact cells and debris (insoluble fraction) were removed by centrifugation at 19,000 r.p.m for 1 hour at 4°C (Beckmann centrifuge, rotor JA 25.50). The supernatant was filtered through a 0.45µm filter and kept at 4°C until purification. A 100µl sample for soluble fraction (SOL) was taken.

Purification of proteins

Purification was carried out in 3 steps. On the first step immobilized metal affinity chromatography (IMAC) was performed using 5 mL HiTrap™ TALON® Crude (GE Healthcare, Illinois, USA) and the eluate fractions were collected. Following cleavage of the his-tag by TEV protease, a second IMAC was performed using the same column and the fractions of the washing steps were collected. The protein was concentrated and injected onto a S75 preparative column (GE Healthcare) pre-equilibrated with SEC buffer (300 mM NaCl, 50 mM HEPES, pH 7.5) for size exclusion chromatography (SEC), the last purification step. A western blot with an anti-his antibody was performed to check if the final purified complex had histidine tags left. The expression and purification yield of EsxU/EsxT wild-type protein was high (60 mg of complex from 20 g of cell pellet). However, the yields for EsxT and EsxU purified from cells transformed with pFV01 and pFV02 were much lower, being EsxU the most problematic to purify.

To analyse the oligomeric state of the purified EsxU/EsxT complex and EsxT (there was not enough quantity of EsxU to do this analysis) multi-angle light scattering coupled with size exclusion chromatography (SEC-MALLS) was performed. Samples were processed under supervision of Dr. Cy Jeffries at EMBL Hamburg (for details of the instrument and setup please refer to [65]). Data were processed using ASTRA software and graphed using Microsoft Excel.

For Mass Fingerprinting, samples were sent to the Proteomics Core Facility at EMBL Heidelberg.

Small Scale Expression for pKB87

A starter culture was set up by placing the inoculum from the glycerol stock into 5 ml of complete media supplemented with 5 µl Streptomycin and incubated at 37ºC for 2-3 days with shaking at 120 r.p.m. This starter culture was then used to inoculate a 100 ml of expression media containing 100 µl Streptomycin and incubated at 37°C for 24 h with shaking at 120 r.p.m.

Fractionation of bacterial cells

Cultures of 100 ml were harvested by centrifugation at 4,000 r.p.m. for 15 min. The supernatant was collected and filtered using a 0.2 µm filter. 50ml of filtered supernatant were concentrated using a 3K concentrator (Amicon®) to a final volume of 2 ml (final concentration = 20-25X). The pellet was resuspended in 20 ml lysis buffer (300 mM NaCl, 50 mM HEPES pH 8.0, 20 mM Imidazole) containing protease inhibitors and DNaseI. Cells were disrupted by three cycles of 3 min each through a sonicator (Bandelin, Ultrasonic Homogenizer HD 2200) at 45% power amplitude. At this point, a 100 µl sample for whole cell extract (WC) was taken. Intact cells and debris (insoluble fraction) were removed by centrifugation at 8,000 g for 15 min (Beckmann centrifuge, rotor JA 14.50). The supernatant, containing the soluble proteins (soluble fraction), was transferred to an ultracentrifuge tube and centrifuged at 35,000 r.p.m, 4ºC for 1 h. The pellet was resuspended in less than 200 µl of lysis buffer. 10 ml of solubilisation buffer (300 mM NaCl, 50 mM HEPES pH 8.0) was added and the sample's concentration was measured using NanoDrop 2000c (Thermo Fischer Scientific, Massachusetts, USA). ANATRACE detergent was added to a concentration of 0.25% and the solution was homogenized at 4°C for 1 hour, after which it was ultracentrifuged at 30,000 r.p.m, 4ºC for 30 min. The supernatant containing the membrane proteins was carefully transferred to a different tube. The pellet was resuspended in 80 µl of solubilisation buffer (insoluble fraction).

Purification of proteins

The soluble fraction was purified in a column containing StrepTactin beads (IBA). Solubilisation buffer (300 mM NaCl, 50 mM HEPES pH 8.0) was used to equilibrate and wash the column. The proteins of interest were eluted in 2x100µl elution buffer (20 mM Tris, 150 mM NaCl, 10 mM desthiobiotin (IBA Lifesciences, Göttingen, Germany), 0.03% DDM).

Large Scale Expression for pKB87

A starter culture was set up by placing the inoculum from the glycerol stock into 80 ml of complete media supplemented with 80 µl Streptomycin and incubated at 37°C for 48 h with shaking at 120 r.p.m. Then, big cultures were set up in 12 x 2 L flasks: 500 ml of expression media, 500µl Streptomycin and 5 ml of starter culture were added into each flask and incubated at 37°C for 24 h with shaking at 120 r.p.m.

Fractionation of bacterial cells

All steps were carried out at 4ºC. Cultures were harvested by centrifugation @ 4,000 r.p.m for 15 min. 50 ml of supernatant was collected, filtered using a 0.2 µm filter and concentrated using a 3K concentrator (Amicon®) to a final volume of 2-3 ml (final concentration = 25X). The pellets were resuspended in lysis buffer (300 mM NaCl, 50 mM HEPES pH 8.0, 20 mM Imidazole) containing protease inhibitors and DNaseI and stirred for at least 1 h until the

solution was homogeneous. Cells were lysed by high-pressure emulsification (3 times at 10,000-15,000 psi). At this point, a 100 µl sample for whole cell extract (WC) was taken. Intact cells and debris (insoluble fraction) were removed by centrifugation at 8,000 r.p.m for 15 min at 4°C (Beckmann centrifuge, rotor JA 14.50). The supernatant, containing the soluble proteins, was transferred to ultracentrifuge tubes and centrifuged at 35,000 r.p.m., 4°C for 1 h. After discarding the supernatant, pellets were removed, placed in a glass homogenizer with a few ml of lysis buffer and homogenized. The final volume was adjusted to 10-20 ml with cold lysis buffer. At this point, a 50 µl sample (MEM) was taken. 100 ml of solubilisation buffer (300 mM NaCl, 50 mM HEPES, pH 8.0) was added and the sample's concentration was measured using NanoDrop 2000c. ANATRACE detergent was added to a concentration of 0.25% and the solution was homogenized at 4°C for 1 h, after which it was ultracentrifuged at 30,000 r.p.m., 4°C for 30 min. The supernatant containing the membrane proteins was carefully transferred to a different tube. The pellet was resuspended in 500 µl of solubilisation buffer (insoluble fraction).

Purification of membrane proteins

StrepTactin beads (IBA Lifesciences) were added to the fraction previously collected and mixed at 4°C for 20 min after which the solution was poured into a 20 ml column. Wash steps were performed with solubilisation buffer and the proteins of interest were eluted in 0.5, 1 and 0.5 ml of elution buffer (20mM Tris, 150mM NaCl, 10 mM desthiobiotin (IBA Lifesciences), 0.03 % DDM).

Protein Analysis

Proteins were routinely analysed by SDS-PAGE on Bis-Tris gels and Coomasie staining. For analysis by Western blotting, proteins were transferred onto 0.2 µm nitrocellulose membranes (Trans-Blot ® Turbo ™ Mini nitrocellulose transfer packs) using the Trans- Blot® Turbo ™ Transfer System (Bio-Rad, California, USA). Antibody binding was detected using SuperSignal™ West Pico PLUS Chemiluminescent Substrate (Thermo Fisher Scientific, Waltham, USA). Imaging was performed with the ChemiDoc™ XRS+ System (Bio-Rad) and the Image Lab Software. The antibodies used were: penta·His HRP conjugate (Qiagen) in dilution 1:2000, Strep-Tactin® HRP conjugate (IBA Lifesciences) in dilution 1:2000, and mouse anti-HA (Abcam, Cambridge, UK, Cat. # ab130275) in dilution 1:1000.

For Mass Spectrometry, samples were sent to the Proteomics Core Facility at EMBL Heidelberg.

2.2 Cellular and Molecular Experiments

Mab culture conditions

Two different media were used depending on the experiment: Middlebrook 7H9 medium supplemented with 10% OADC (BD Middlebrook OADC Enrichment) and 0.05% of Tween-80 (Sigma-Aldrich, Missouri, USA) or with no detergent added, or RPMI red-free (PAN-Biotech, Aidenbach, Germany, Cat. # P04-16516) with 0.05% of Tween-80 (Sigma-Aldrich) or with no detergent added. All strains used in the present study were grown in T25 flasks (Sarstedt, Lower Saxony, Germany, Cat. # 83.3911.002) with 12-15 ml of media and incubated without shaking, at 37°C for 3-4 days, and with 5% CO_2 in the case of cell growing in RPMI. For harvesting, the cultures were transferred to 15ml and centrifuged at 5000 r.p.m., 4°C for 10 min (Thermo Scientific ™ Heraeus ™ Multifuge ™ X1). After discarding the supernatant, or transferring it to a different tube for future analysis of the "secreted fraction", the pellet was

washed with 10 ml of 1X DPBS (PAN-Biotech), centrifuged at 5000 r.p.m., 4°C for 10 min, and resuspended in 1X DPBS. The suspension was then syringed approximately 10 times with a 1 ml syringe and a 20G x 1 ½" needle to get rid of clumps.

Hydrophobicity of Mab

To study Mab hydrophobicity, a microbial adhesion to hydrocarbons (MATH) test was performed as described in [66], using n-dodecane as the nonpolar solvent. Mab cells were cultured in RPMI with no detergent, harvested by centrifugation, resuspended in DPBS and syringed. The OD_{600} was measured and 4 ml of culture were added to 1 ml of n-dodecane. Following 2 min of vortexing, the suspension was left undisturbed for 15-30 min to allow the separation of phases, after which the OD_{600} of the lower phase (close to the bottom of the tube) was measured. The percentage of cell surface hydrophobicity (CSH) was calculated as:

$$\mathrm{CSH}\ (\%) = 100 \times \frac{A_{control} - A_{MATH}}{A_{control}}$$

where, $A_{control}$ is the absorbance of the control culture not subjected to the MATH test and A_{MATH} is the aqueous phase absorbance of the cell culture subjected to the MATH test.

Lewis acid–base properties of Mab

The microbial adherence to solvents (MATS) method was used to investigate the Lewis acid–base properties of Mab surface, as described in [67]. Briefly, Mab cells were cultured in Middlebrook 7H9 medium supplemented with OADC (no detergent), harvested by centrifugation and resuspended in DPBS. The OD_{600} was measured and 1ml of solvent (chloroform or ethyl acetate) were added to 5ml of culture. Following vortexing, the suspension was left undisturbed for 30 min to allow the separation of phases, after which the OD_{600} of the solvent phase was measured. The hydrophobicity index (HI) or percentage of adhesion was calculated as:

$$\mathrm{HI} = 100 - \frac{E \times 100}{E_0}$$

where E_0 is the initial OD_{600} of the cell suspension, and E is the OD_{600} of the aqueous phase after its separation from the solvent phase.

Percoll Gradient Centrifugation for the Density Fractionation of Mab Cells

This protocol was based on one previously published [68]. For the size fractionation of Mab cells, discontinuous gradients of 85, 92 and 100% of Percoll were set up. Stock Isotonic Percoll (SIP) was prepared by mixing nine parts of Percoll (Sigma Aldrich) with one part of sterile 10X DPBS (PAN-Biotech). In order to obtain the different percent Percoll fractions, the SIP was further diluted by adding 1X DPBS to obtain a final volume of 10 ml for each fraction. 1.5-1.7 ml of 100% Percoll was poured into 15 ml tubes (Sarstedt). 1ml of the correspondent Percoll percentages was carefully layered on top so the gradient would go from highest percentage at the bottom to the lowest percentage at the top.

12 ml of Mab cells were grown in T25 flasks in Middlebrook 7H9 medium supplemented with OADC (no detergent). After a 3-day incubation @ 37°C (OD_{600}=1-1,5) the cells were transferred to 15 ml tubes and harvested by centrifugation. The cell pellet was washed once

with 10 ml of sterile DPBS and then centrifuged at 5,000 r.p.m., 4°C for 10 min. The cell pellet was resuspended in 3 ml of sterile DPBS and syringed forcefully to remove clumps, and 1-2 ml were layered onto the top of the gradient. The cells were fractionated by centrifugation in Thermo Scientific ™ Heraeus ™ Multifuge ™ 3S-R centrifuge at 800 × g for 20 min at 20°C.

Phenotypic drug susceptibility testing (pDST)

pDST was conducted at the National and WHO Supranational Reference Centre for Mycobacteria (NRZ) using the Sensititre Myco RAPMYCOI assay (Thermo Fisher Scientific) as recommended by the manufacturer and following CLSI guidelines (Clinical Laboratory Standards Institute, 2018). Time points for plate reading were days 3, 5, and 7. *M. peregrinum* ATCC 700686 was used as quality control and inoculated with each run of pDST. Plates were read by two investigators independently, and in case of disagreement, a consensus MIC was obtained. The assay allows MIC testing for the following antibiotics (abbreviations and MIC ranges in brackets): Cotrimoxazol (SXT 0.25/4.75–8/152 mg/ml), Linezolid (LZD 1–32 mg/ml), Ciprofloxacin (CIP 0.12–4 mg/ml), Iminiperem (IMI 2–64 mg/ml), Moxifloxacin (MXF 0.25–8 mg/ml), Cefoxitin (FOX 4–128 mg/ml), Amikacin (AMI 1–64 mg/ml), Tigecyclin (TGC 0.015–4 mg/ml), Tobramycin (TOB 1–16 mg/ml), Clarithromycin (CLA 0.06–16 mg/ml), Cefepim (FEP 1–32 mg/ml), Cefriaxon (AXO 4–64 mg/ml), Doxycyclin (DOX 0.12–16 mg/ml), Amoxicilin/clavulanic acid (AUD 2/1-64/32 mg/ml) and Minocyclin (MIN 1–8 mg/ml).

Ex Vivo Red Blood Cell Hemolysis Assay for the Evaluation of pH-response to EsxU/EsxT

This protocol is based on [69]. Briefly, erythrocytes were isolated from 25 ml of blood from different human donors and were suspended in buffers with pH values that mimic extracellular (7.4), early endosomal (6.8), and late endo-lysosomal (6.2) environments. Erythrocytes incubated at pH<5 lysed in the media due to the low pH and were therefore not suited for analysis. 10 µl of EsxU/EsxT purified complex was added to final concentrations of 5, 50 and 500 µg/ml in 96-well plates and topped up with 190 µl of diluted erythrocytes in different pH buffers. 10 µl of 20% Triton X-100 (0.1 % final concentration) was added to the positive control wells, 10 µl of buffer was added to the negative control wells, and 10 µl of SEC buffer was added to the protein buffer control wells. The plates were incubated at 37°C for 1 h. Intact erythrocytes were pelleted at 500 x g for 5 min (Thermo Scientific ™ Heraeus ™ Multifuge ™ 3S-R centrifuge), and 100 µl of supernatants (containing hemoglobin released from lysed erythrocytes) were transferred into a clear, flat-bottomed 96-well plates, which were then read in a plate reader at 405 nm (characteristic absorbance wavelength of hemoglobin). The following formula was used to calculate the percentage of hemolysis for each well:

$$\% \text{ Hemolysis} = \frac{\text{A405 sample} - \text{A405 negative control}}{\text{A405 positive control} - \text{A405 negative control}} \text{ x } 100$$

Isolation and Infection of Human PMN

Human polymorphonuclear neutrophils (PMN) were isolated from heparinized whole blood of healthy volunteers. PMN were purified by density centrifugation at 800 x g for 20 min using Histopaque 1199 (Sigma Aldrich). Collection of the granulocytes fraction was followed by a discontinuous Percoll (Sigma Aldrich) density gradient (85%, 80%, 75%, 70%, 65%) and centrifugation at 800 x g for 25 min as described before [70]. PMN were resuspended in RPMI medium (PAN-Biotech) supplemented with 10 mM HEPES buffer (PAN-Biotech) and 1% (vol/vol) L-glutamine (PAA Laboratories, Pasching, Austria) and plated in 6-well plates at 2

million cells per well. 10 ng of EsxU, EsxT or EsxU/EsxT was added to the treated wells. Media was added to the untreated and lysis (LDH) control wells, Triton X-100 to a final concentration of 1% was added to the lysis positive control wells, and 100 ng/ml LPS (Invivogen) with 5 µM Nigericin (Merck) were added to the control wells for cytokine secretion. Nigericin was added 3 hours after the addition of LPS, and Triton X-100 was added 5 min before finishing incubation. Plates were incubated at 37°C and 5% CO_2 for 6 and 21 hours.

Lactate-Dehydrogenase Activity Assay

To assess the extent of necrotic cell death, a Lactate-Dehydrogenase (LDH) Activity Assay was performed using Cytotoxicity Detection Kit (Roche Diagnostics, Mannheim, Germany) and according to manufacturer's protocol. Supernatant was collected and measured at 490 nm using an ELISA reader.

Cytokine secretion

Supernatant was collected and cytokine secretion was assessed using DuoSet ELISA kits (R&D Systems, Minnesota, USA) for cytokines hIL-1β, hIL-18, hIL-8 and hTNFα, and according to manufacturer's protocol. Finally, the samples were measured at 490 nm using an ELISA reader.

Isolation, differentiation and cultivation of human monocyte derived macrophages

Mononuclear cells were isolated from peripheral blood mononuclear cells (PBMC) of healthy volunteers by density gradient centrifugation. Heparinised peripheral blood was collected and diluted in PBS (1:1), slowly transferred on top of a polysucrose solution (Pancoll, 10 ml) and centrifuged in a swing bucket rotor (403 x g, 40 min, room temperature, without break). The upper layer was discarded and the interface transferred to a new 50 ml tube. Cells were washed with PBS (50 ml) and re-suspended in Hank's Balanced Salt Solution (HBSS) containing 0.1% BSA. Cell numbers were adjusted ($5x10^6$ cells/ml) using a cell counter (Casy2, Schärfe System). Isolated PBMCs, containing lymphocytes, monocytes and thrombocytes, were separated by counterflow elutriation using a centrifuge equipped with an elutriation rotor (Beckman, JE 5 B rotor), tubing systems and a peristaltic pump (RTC) (purity consistently greater than 92%). Prior to elutriation, the rotor was disinfected with ethanol (70%), washed twice with dH_2O and equilibrated (BSA (0.1%) in HBSS). PBMCs were loaded and separated under centrifugation by stepwise increase of the flow rate (24 up to 44 ml/min, Table 3). Received fractions were analysed with a cell counter (Casy2, Schärfe System). Isolated monocytes were centrifuged (258 x g, 10 min, 4°C) and cell density was adjusted to $2x10^7$ cells/ml by addition of RPMI 1640 containing human serum (2%) and recombinant human macrophage colony-stimulating factor (M-CSF, 10 ng/ml). For differentiation of monocytes into macrophage, cells were seeded into teflon-coated cell culture bags (VueLifeTM 72, Celgenix) and incubated for 7 d at 37°C in a 5% humidified CO_2 atmosphere. To detach macrophages, cell culture bags were placed on ice for 1 h and subsequently pulled over the edge of a bench. Cells were counted in a counting chamber (Neubauer, Brand) using trypan blue vital staining.

Flow rate (ml/min)	Volume (ml)	Fraction
24	200	Loading of PBMC
26	50	Thrombocytes
28	50	Washing
30	50	Small lymphocytes
32	50	Lymphocytes

33	50	Lymphocytes
34	50	Lymphocytes
35	50	Lymphocytes
36	50	Large lymphocytes
37	50	Washing
38	50	Washing
39	50	Washing
40	50	Washing
41	50	Washing
42	50	Washing
43	50	Monocytes
44 (stop)	50	Pure Monocytes

Table 3. Elutriation protocol

Infection of macrophages and analysis by RT-PCR:

Prior to stimulation experiments, 2 x 10^5 monocyte derived macrophages were incubated in 500 µl HMM (RPMI 1640, 4 mM L-Glutamine, 10% FCS) in 48-well flat-bottom microtiter plates (NUNC, Roskilde, Denmark). Cells were allowed to attach for 2 h at 37°C in a humidified atmosphere with 5% CO_2. Macrophages were infected with Mab strains at the indicated MOI for 4 and 24 h. Mtb H37Rv bacteria [71] provided by Prof. N. Reiling served as positive control. Supernatants were removed and cytokine mRNA formation (TNF-α, IFNβ, CCL3 and CCL4) was analysed by quantitative real-time PCR.

Total RNA was isolated from human macrophages (2 x 10^5) using the DirectZol® RNA MiniPrep kit (Zymo Research, Irvine, CA, USA) according to the manufacturer´s instructions. Notably, this procedure included an in-column DNase I treatment (5 units/column, 20 min, room temperature). Concentration and purity of isolated nucleic acids were determined with a NanoDrop ND-1000 spectrometer (Thermo Fisher Scientific). For reverse transcription of isolated RNA the Maxima® First Strand cDNA Synthesis Kit for RT-qPCR (Thermo Fisher Scientific) was used. 7 µl of isolated RNA were mixed with 2 µl Master Mix, 1 µl Enzyme Mix and subjected to a thermal cycler (Gene Touch®, BIOER, China) with following program: 10 min RT, 30 min 55°C, 5 min 85°C. After dilution of samples with DNase-free water, samples were stored at -20°C until further usage. For quantitative real-time PCR analysis a hydrolysis probe based assay system was used (TaqMan® assay, Roche Diagnostics). Gene-specific primer pairs and matching TaqMan® probes were generated with the Universal ProbeLibrary Assay Design Center (Version 2.50 and earlier; http://lifescience.roche.com/shop/en/mx/overviews/brand/universal-probe-library). Primer pairs were obtained from Eurofins MWG Operon (Ebersberg, Germany) and the sequences are given in table 4.

Primer Name	Forward 5'-3'	Reverse 5'-3'
hCCL3	CAGAATCATGCAGGTCTCCAC	GCGTGTCAGCAGCAAGTG
hCCL4	CTTCCTCGCAACTTTGTGGT	CAGCACAGACTTGCTTGCTT
hIFNB1	CTTTGCTATTTTCAGACAAGATTCA	GCCAGGAGGTTCTCAACAAT
hTNFα	CAGCCTCTTCTCCTTCCTGAT	GCCAGAGGGCTGATTAGAGA

Table 4: Primers used for human cytokine expression

For RT-PCR sample preparation the LightCycler® 480 Probe Master Kit was used (Roche Diagnostics, 1 µl cDNA, 5 µl MasterMix, 1.6 µl Primer-Mix (sense + antisense, 3,125 µM), 0.1

µl TaqMan® probe, 2.3 µl dH20). Samples were transferred to the provided 96-well plates, which were sealed and centrifuged (180 x g, 2 min, 4°C). Amplification was conducted during an initial incubation at 95°C for 10 min, and then 55 cycles at 95°C for 10 seconds and 60°C for 5 seconds using a LightCycler® 480 Instrument (LC480) (Roche Diagnostics). Crossing points of target and reference gene (hypoxanthine-guanine phosphoribosyltransferase, *HPRT*) were determined by the second derivative maximum algorithm. Relative gene expression values were calculated with the E-method, which considers the amplification efficiency of the individual PCR reaction by means of a relative standard curve (LightCycler Software Version 1.4 or earlier, Roche Diagnostics).

RNA isolation and reverse transcription from Mab clinical strains

Bacterial cells were resuspended in TRIzol (Thermo Fisher Scientific) reagent, stored at -80°C for 24 h and then lysed with the Fast Prep instrument (MP Biomedicals, Solon, OH) using 5 cycles of 50 seconds each at 6.5 m/s. RNA extraction was performed using the Zymo Research Direct-Zol RNA MiniPrep Plus kit (Zymo Research) followed by the One Step PCR Inhibitor Removal kit (Zymo Research), according to manufacturer's protocol. The purity and concentration of RNA were estimated using a NanoDrop spectrophotometer. The synthesis of complementary DNA (cDNA) was carried out using the Maxima First Strand cDNA Synthesis Kit with dsDNase (Thermo Fisher Scientific) following the manufacturer's instructions.

Mab ESX-4 Gene expression by RT-PCR

Relative expressions of *eccB4, eccC4, eccD4, eccE4, mycP4, Mab_3755c*, *esxU* and *esxT* were quantified by real-time PCR (RT-PCR) using *sigA* as the reference gene. Mab ATCC 19977 strain and 20 Mab clinical isolates were analysed using the primers listed in Table 5. The sequences of primers for *esxU*, *esxT* and *sigA* were obtained from Prof. J. Herrmann's team. RT-PCRs were carried out on the LightCycler® 480 Instrument (LC480) (Roche Diagnostics) using the LightCycler® 480 SYBR Green I Master Mix (Roche) and 2 µL of cDNA (total reaction volume: 10 µL) in 96-well plates. Amplification was conducted during an initial incubation at 95°C for 10 min, and then 45 cycles at 95°C for 10 seconds and 57°C for 10 seconds using a LightCycler® 480 Instrument (LC480) (Roche Diagnostics). Each reaction was conducted with technical triplicates. Crossing points of target and reference gene were determined by the second derivative maximum algorithm. Relative gene expression values were calculated with the E-method, which considers the amplification efficiency of the individual PCR reaction by means of a relative standard curve (LightCycler Software Version 1.5.1, Roche Diagnostics). Data were graphed using GraphPad Prism software version 9.0 (GraphPad Software, California, USA). Pearson's correlation test was performed to correlate the genetic expression between the genes.

Primer Name	Sequence 5'-3'	Efficiency	Error
Mab_EccB4_F_qPCR$_2$	CAACGAGCTACCCATCAAG	2.077	0.00492
Mab_EccB4_R_qPCR$_2$	CTCAATCTACTTGCCGTTCA		
Mab_EccC4_F_qPCR	GACACCAGGTTTGCCTCTTC	1.757	0.0136
Mab_EccC4_R_qPCR	CAGAATTCCTGCGCACCTTG		
Mab_EccD4_F_qPCR	TCGTCGACATCATCAACCAG	1.899	0.00142
Mab_EccD4_R_qPCR	GGGTGAGAATCAGCAGATCG		
Mab_EccE4_F_qPCR	TCATGGTGATCTCGCAGTTG	1.998	0.0082
Mab_EccE4_R_qPCR	AATCCGGTAACTGCCCAATG		
Mab_MycP4_F_qPCR	CATCAAGAACACGGCGCATC	1.812	0.0316

Mab_MycP4_R_qPCR	GTGGCAGTACGAGCTTCTTG		
Mab_3755_F_qPCR$_2$	CATGCGCTGTGTGAATTGC	2.009	0.00382
Mab_3755_R_qPCR$_2$	CGGTTACTTACACCGAGGT		
Mab_EsxU_F_qPCR	CTCCATGGTGTCGTGAATAC	1.711	0.00682
Mab_EsxU_R_qPCR	GCAAGTACCAGGAGTTCACG		
Mab_EsxT_F_qPCR	GTCAGGATCTGGTTCAGGTC	1.732	0.00672
Mab_EsxT_R_qPCR	CGCTGGTTGCTGATGTCAAG		
Mab_SigA_F_qPCR	TCCGAGAAAGACAAGGCTTC	1.893	0.00515
Mab_SigA_R_qPCR	CCAGCTCAACTTCCTCTTCG		

Table 5: Mab ESX-4 RT-PCR primer sequences and efficiencies.

Isolation of lipids from Mab outer and inner membranes

M. abscessus ATCC 19977 was cultured in Middlebrook 7H9 medium (BD Biosciences) supplemented with 0.2% (wt/vol) glucose (Roth, Cat. # X997.2), 0.05% (vol/vol) Tween-80 and 1 g/L L-arginine at 37°C for 2 days. Cells were harvested by centrifugation and the pellet was resuspended in methanol. Lipids from membranes were extracted as previously described [72]. Briefly, samples were taken up into $CHCl_3/CH_3OH$ (2:1, vol/vol) and bacteria extracted at 56°C for 15 min under sonication. After centrifugation at 3,800 x g, supernatant was taken, filtered through a 0.22 µm PFTE filter and dried with N_2. This extraction was repeated once. A third extraction was performed at 4°C overnight. Insoluble material from the extracts was removed by (repeated) centrifugation and filtration through a 0.22 µm PFTE filter. Extracts were then subjected to biphasic partitioning in $CHCl_3/CH_3OH/H_2O$ (4:2:1, by vol.). $CHCl_3$ phases were combined and dried with N_2. Lipids in the organic phase were stored at -20°C until analysed by thin liquid chromatography (TLC) and by SDS-PAGE. This fraction contained the total lipids from Mab inner (IM) and outer membranes (OM).

To separate the lipids of the IM from the ones of the OM, new Mab cultures were set up as described before. After harvesting the cells, the pellet was resuspended in heptane and 1,4-bis (2-ethylhexyl) ester sodium salt (AOT) and steered at 4°C for 24 h, after which it was centrifuged to pellet the cells. The supernatant (heptane fraction) was filtered through a 0.22 µm PFTE filter and stored at -20°C until extraction. The AOT fraction and pellet were resuspended in methanol and stored at -20°C until extraction. Both fractions were centrifuged at 3,800 x g, supernatant was taken, filtered through a 0.22 µm PFTE filter and dried with N_2. This extraction was repeated once. A third extraction was performed at 4°C overnight. Insoluble material from the extracts was removed by (repeated) centrifugation and filtration through a 0.22 µm PFTE. Samples were dried separately under a stream of N_2 and extracted twice with $CHCl_3/CH_3OH/H_2O$ (4:2:1, by vol.). $CHCl_3$ phases were combined and dried with N_2. Finally, the samples were resuspended in $CHCl_3/CH_3OH$ (2:1). The extract from the heptane fraction contained the IM lipids and the extract of the second fraction (AOT) contained the OM lipids.

2.3 Techniques to characterize EsxU/EsxT-membrane interaction

For the biophysical experiments we used dioleoyl-phosphatidylcholine (DOPC, Avanti Polar Lipids, Alabama, USA, Cat # 850375P) or Mab membrane extracted lipids from the outer membrane (OM), inner membrane (IM) or a combination of both (full membrane).

The buffers used were: SEC buffer (300 mM NaCl, 50 mM HEPES, pH 7.5), Hepes buffer (100mM NaCl, 10mM Hepes, pH 5.0-7.0), Citrate buffer (100 mM NaCl, 10 mM Citrate, pH 3.0 and 4.0), and 10mM Sodium Phosphate Buffer (pH 4.0 and pH 7.0 for OCD experiments).

Pore spanning lipid bilayer (NanoSpot assay)

Indium tin oxide (ITO)-coated glass slides were used for the electroformation of giant unilamellar vesicles (GUVs), as described before [73, 74]. Briefly, solutions of DOPC at a concentration of 2 mg/mL were prepared in chloroform, dried by a N_2 stream and then resuspended in ethanol. ITO-coated glass slides (2.5 × 4 cm) were placed on a hot plate (Stuart CB162) set to 50°C. Drops of lipid solution were deposited onto each ITO electrode surface using a needle to spread carefully back and forth. Finally, the lipid coated ITO electrodes were dried in a plasma cleaner (Diener electronics GmbH&Co.KG, PlasmaCleaner Zepto, Ebhausen, Germany) for 1.5 h. Two slides of ITO electrodes, both coated with lipid thin films, were separated by a thick spacer with a 1.5 x 2.3 cm hole. The electroformation cell was filled with 2 ml of 1 mM sucrose solution. The assembled sample block was placed on a sand bath for temperature maintenance at 55°C and connected to a sinusoidal AC electric field applied with a signal generator (Voltcraft 6 MHz Seep / Function Generator FG-506, England) at 10.x Hz and 3V to generate GUVs. The temperature was maintained for at least 5 h.

For the preparation of lipid bilayers, a Si/SiO_2 chip-based protocol based on the one described in [75], was previously developed and tested in the laboratory. The chips were prepared “in house” using silicon wafer with pre-cut and pre-etched chips (Micromotive GmbH, Mainz, Germany). Each chip contained approximately 250,000 single cavities and was glued into the wells of 8-well chamber slides (IBIDI GmbH, Bayern, Germany). These chambers were then plasma cleaned (intensity 6, air flow 0.4-0.6 mbar) for one minute. 250 µl of SEC buffer was added to each well and the chamber was sonicated for 2 min to remove air bubbles trapped in the cavities. 5µl of Atto488 carboxy fluorescence dye (ATTO-TEC GmbH, North Rhine-Westphalia, Germany, Cat # AD 488-21) was added to each well (final concentration of 5 nM), followed by 50 µl of previously harvested GUVs. Chambers were centrifuged at 400xg for 10 min at room temperature (Heraeus® Megafuge® 1.0, Germany) to allow rupture of GUVs and formation of lipid bilayers on top of the cavities, after which the remaining dye was washed off with SEC buffer. The chamber was placed in a dark camera kept at 37°C connected to a fluorescence inverted microscope (MORE integrated Life Cell Imaging System, Thermo Fisher Scientific FEI Munich formerly Till Photonics, Planegg, Germany) equipped with a 10×/0.45 objective (planapochromat 420640−9900−000, Zeiss, Jena, Germany), a FITC filterset (ET480_40x/ET535_50m/T510LPXRXT, Chroma, Rockingham, USA) and LED (transmitted light) and oligochrome (fluorescence) light sources (Thermo Fisher Scientific). 16-bit images were taken with a Andor clara low light imaging interline CCD camera (Andor Technology plc, Belfast, Northern Ireland) using Live Acquisition Software (LAS V. 2.2.2, Thermo Fisher Scientific). 20µl of EsxU/EsxT was added to the well to initiate the experiment. Membrane permeabilization was detected in terms of fluorescence dye-efflux. In some experiments, 10µl of 10mg/ml TexasRed®-labeled dextran molecules (Life technologies, Carlsbad, CA, USA) of 40 000 MW were added before the complex. Monitoring of this dye-influx allowed estimation of the diameter of the pore formed by EsxU/EsxT.

Image analysis (drift correction, identification of fluorescent areas, and extraction of time series) was done with ImageJ 1.52p (USA). Final data analysis and graphs were done with and GraphPad Prism software version 9.0.

Oriented Circular Dichroism (OCD)

To study the membrane alignment and conformation of the EsxU/EsxT complex, OCD experiments were conducted at Karlsruhe Institute of Technology (KIT), using their own home-built cell previously described in [76], which allows for fully automated measurements. EsxU/EsxT complex was prepared in phosphate buffer at pH 4.0 and pH 7.0. DOPC and Mab total membrane lipids were prepared in chloroform at 2 mg/ml. 75 µl of different peptide/lipid (P/L) molar ratios were prepared and deposited onto circular quartz glass plates, dried at room temperature, and rehydrated inside the OCD cell at 20°C for at least 6 h. This process achieves spontaneous alignment of the lipids into lamellar multibilayers. OCD spectra of EsxU/EsxT in oriented DOPC and Mab total lipids bilayers were acquired between 270 and 180 nm at 0.1-nm intervals, for every cell rotation of 45.0°, generating eight successive spectra in a total acquisition time of approximately 47 min per sample. The eight spectra were averaged for the final analysis. Background spectra of pure lipid bilayers were measured in a separate experiment as a control, and were subtracted from the corresponding spectra of the peptide-containing samples. All data were acquired and analysed with a proprietary software from the laboratory at KIT but final graphs were obtained using GraphPad Prism software version 9.0.

Tethered bilayer setup

We used the TethaPod system (SDX Tethered Membranes, New South Wales, Australia) to determine the impedance properties of lipid bilayers. We used the T10 electrode chips which had a pattern of gold electrodes that were supplied with a pre-coating of a stable monolayer that comprised a mixture of ester-free DLP ($C_{49}H_{92}O_{11}S_2$) and BnSS TEG ($C_{15}H_{24}O_4S_2$) molecules in the molar ratio of 10:90. The gold electrodes had an area of 2.1 mm^2. The tethered bilayer was formed by adding 8 µl of either 3 mM DOPC, 3 mg/ml of OM lipids, or 3 mg/ml of IM lipids, all resuspended in ethanol (96%), to each of the 6 wells of the chip previously described. Different pH values were obtained using Hepes buffer for pH 5-7, and citrate buffer for pH 3.0 and 4.0. The bilayer formation occurred when 100 µl of corresponding buffer was flushed through the test chamber. Electrical data was processed using SDx® TETHAQUICK Software. After 20 min of measurements (time given for the membrane to stabilize) the EsxU/EsxT complex in SEC buffer was added every 30 min to achieve final concentrations of 0.1, 0.5, 1, 5, 10 and 50 µM. Information about time, conductance and capacitance was acquired throughout the experiment and the analysis was performed using GraphPad Prism software version 9.0.

Unsupported Planar membranes

Single channel currents from EsxU/EsxT (10 mg/mL in SEC buffer) were recorded using the Orbit Mini (Nanion Technologies, Munich, Germany) with EDR3 software (Elements SRL, Cesena, Italy). Briefly, a four-electrode recording chip (MECA4) (100 µm; Ionera Technologies, Germany) was mounted in the Orbit Mini apparatus and recording buffer was applied to the chip. Planar lipid bilayers consisting of 10 mM DOPC dissolved in octane were painted on the recording wells. 5.3 µL of EsxU/EsxT in recoding buffer (SEC buffer for pH 7.5 and citrate buffer for pH 4.0) was added to the cis-side of the bilayer. Subsequently, alternating voltages were applied to facilitate insertion of the channels. Recordings were carried out at a sampling rate of 1.25 kHz with no filter applied. Mean current amplitudes were plotted as a function of tested voltages. Single channel conductances were determined as the slope factor of a linear regression to the current-voltage (IV) plot. Elements Data Analyzer (EDA) v1.3.8 (Elements SRL) and GraphPad Prism software version 9.0 were used for data analysis.

3. RESULTS

3.1 Characterization of the *M. abscessus* ESX-4 locus

First, we studied the expression levels of the genes contained in the Mab ESX-4 locus to gain insight into the stoichiometry of the components encoded by the ESX-4 operon. Moreover, we wanted to investigate if the expression of any of the genes within this locus was different in clinical Mab isolates as compared to the type strain, for which we used clinical isolates obtained from pulmonary and extra-pulmonary samples of patients suffering from Mab infections. To further study the organization of the ESX-4 secretion system, we designed, cloned and overexpressed the Mab ESX-4 modified operon (tags were added on the C-terminal of some genes) in *Mycobacterium smegmatis*, a non-pathogenic and rapidly growing NTM. After corroborating this method of expression was successful, we isolated the membrane fraction from *M. smegmatis* and used the tags to purify and identify the membrane-bound ESX-4 structural components. Following a similar approach, we cloned the putative Mab ESX-4 substrates, *esxU* and *esxT,* and produce high yields of the proteins to study their solubility and interaction.

3.1.1 *esxU* and *esxT* show high expression levels and are strongly expressed in *M. abscessus* clinical isolates

To investigate the expression levels of *esxU* and *esxT* in comparison to the other genes encoded in the ESX-4 operon, quantitative real-time PCR (RT-PCR) was performed targeting the eight genes present in the Mab ESX-4 locus and using *sigA*, a mycobacterial transcription initiation factor, as a reference gene [77]. In the Mab ATCC 19977 type strain, the expression levels of *Mab_3755c* and the ESX-4 structural components *eccB$_4$, eccD$_4$, eccE$_4$,* and *mycP$_4$*, were lower or equal to those of *sigA.* On the contrary, expression of *esxU* and *esxT* was over ten times higher than expression of *sigA* (Figure 8).

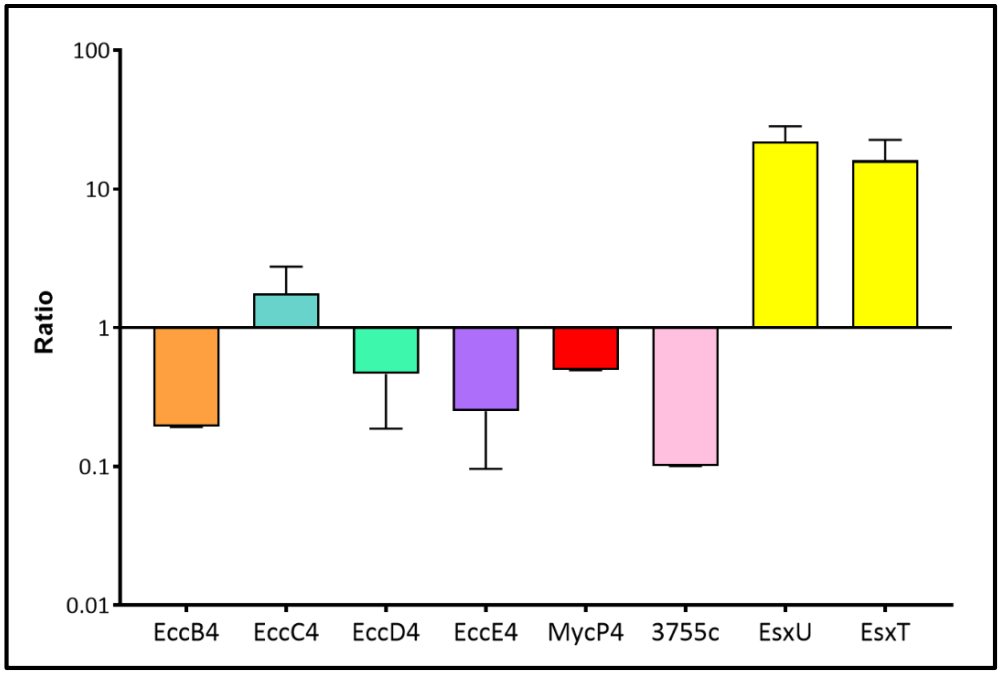

Figure 8. Relative Quantification of Mab ATCC 19977 ESX-4 locus transcripts. *sigA* was used as the reference gene and the ratio for each gene was calculated using the LightCycler 480 software. Results are a compilation of 3 different experiments.

Next, twenty clinical isolates representing all three Mab subspecies and both S and R phenotypes were assessed for ESX-4 genes expression levels. All isolates showed up to five times higher *esxU* and *esxT* expression levels as compared to the reference strain, independent of the sample origin (pulmonary versus extra-pulmonary, Figure 9). Moreover, correlation of expression of *esxU* and *esxT* clearly demonstrated equal expression levels in all investigated isolates (Pearson's correlation, $p < 0.0001$, Figure 10). Taken together, these findings strengthen the hypothesis that *esxU* and *esxT* are clinically relevant for Mab virulence or pathogenicity and support a 1:1 heterodimer conformation model.

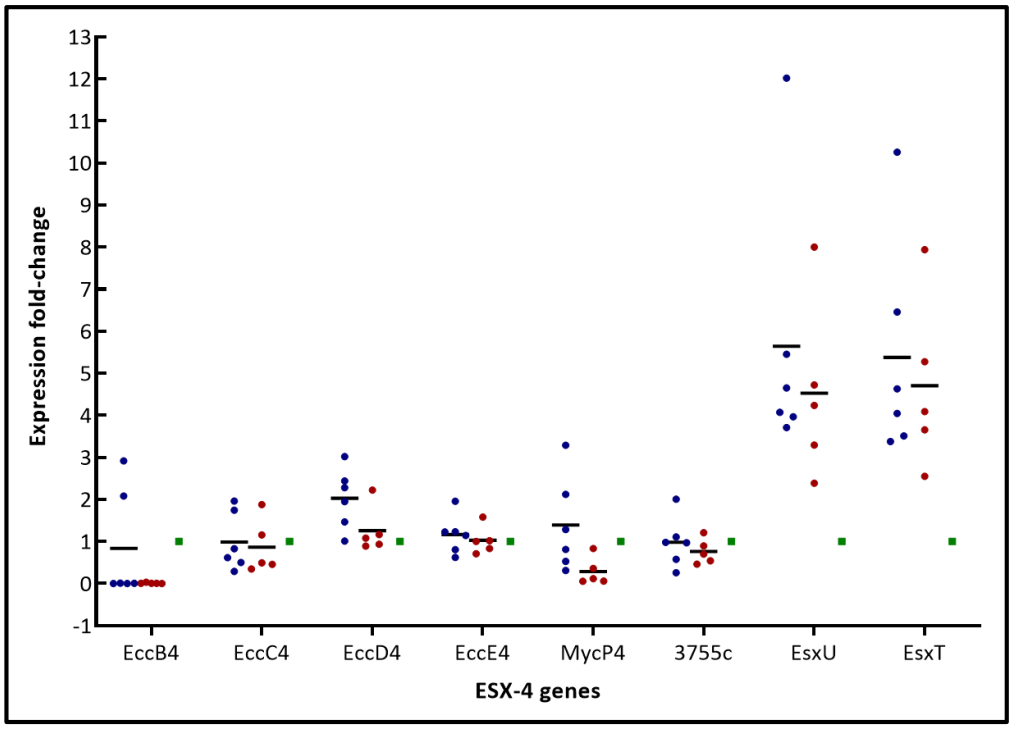

Figure 9. Expression of ESX-4 genes in eleven Mab_A and Mab_M smooth clinical isolates. The fold-change was calculated using Mab ATCC 19977 as the reference strain (shown in the graph with green dots). Blue dots: pulmonary samples. Red dots: extra-pulmonary samples.

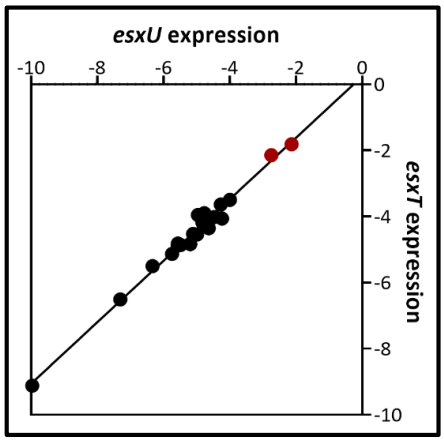

Figure 10. Correlation of *esxU* and *esxT* expression in Mab ATCC 19977 (red dots) and clinical isolates (black dots). Using Pearson's correlation test an $R^2 = 0.9845$ ($p < 0.0001$) was obtained, with a linear approximation expressed as: $y=0.9302x+0.2434$.

3.1.2 EsxT is a substrate of Mab ESX-4

To further study the organization of the Mab ESX-4 secretion system and elucidate the relationship between EsxU/EsxT and the structural components of the secretion machinery, we expressed the Mab ESX-4 operon in *M. smegmatis*. 7 of the 8 genes of the locus were cloned in a 2-step process (see Materials and Methods). In brief, a synthetic construct containing *esxU* and *esxT* with a C-terminal HA tag was first cloned into the vector, giving rise to the plasmid pKB86. Then, the 10.5 kb fragment containing *eccC$_4$-eccE$_4$* was cloned from Mab ATCC 19977 into pKB86. The final construct (pKB87) contained three tags: a twin-streptavidin tag on the C-terminal of EccC$_4$, a His tag on the C-terminal of EccE$_4$ and an HA tag on the C-terminal of EsxT, as shown in Figure 11.

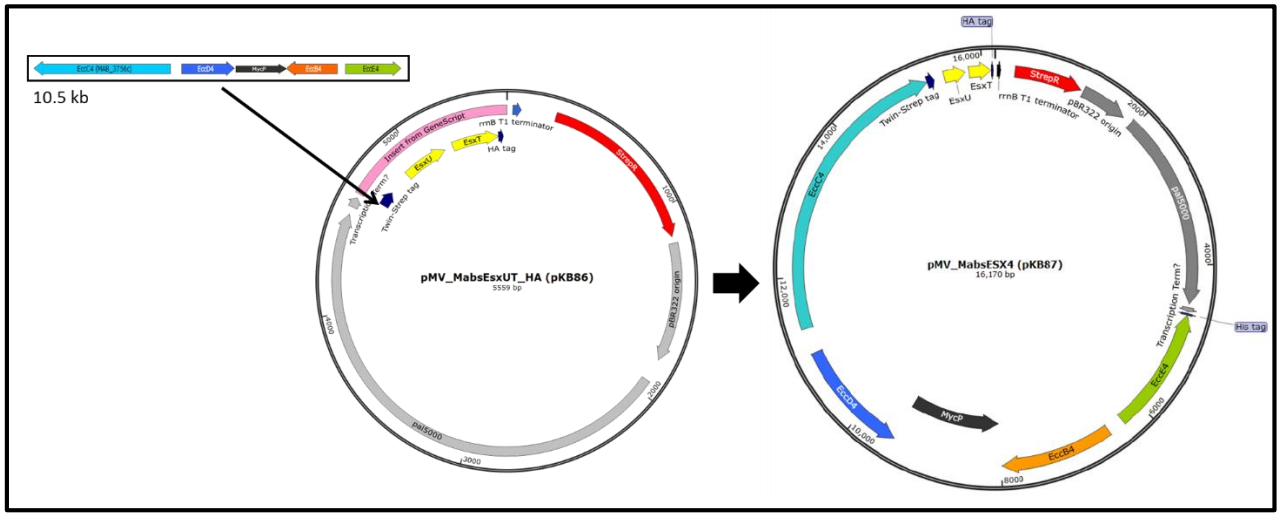

Figure 11. Schematic of the strategy followed to clone Mab ESX-4 into pMV-ESX-5 and genetic map of plasmid pKB87 (right).

Large scale fractionation was carried out and the EccB$_4$-E$_4$ complex was purified from the membrane fraction using streptavidin beads. Fractions were loaded onto a SDS-PAGE gel and then analysed by Coomasie staining and western blot as shown in Figure 12. The Coomasie-stained SDS-PAGE gel showed the presence of 4-5 bands in the eluted fraction, at weights expected for components EccB$_4$-E$_4$ and MycP$_4$. The western blots confirmed the presence of EccC$_4$ and EccE$_4$ at the expected weights (145.4 and 59.54 kDa, respectively) in all fractions (Figure 13). In addition, in the anti-streptavidin blot a second band was observed at approximately 70 kDa. This band likely represents a typical degradation product due to the instability of the ATPase domains in EccC, as observed for the *M. xenopi* ESX-5 (Beckham, personal communication, unpublished).

In analogy with Mtb secreted substrates EsxA and EsxB, Mab EsxT was expected to be found mostly in the whole cell extract as it would be secreted to the exterior of the cell. Surprisingly, the anti-HA blot showed strong signals for EsxT in the whole cell but also in the membrane fraction (Figure 13, far right), suggesting that the protein was interacting with the mycomembrane. Moreover, after incubation with a substrate that enables femtogram detection, a band corresponding to EsxT could also be seen in the eluted fraction. This suggests an association of EsxT with the structural components of the ESX-4 secretion machinery that, though minimal, was sufficiently strong to allow the pull-down of small quantities of EsxT when the purification aimed to retain EccC$_4$. Taken together,

these results show that EsxT was present in the mycomembrane at an unexpectedly high concentration and that it was also weakly associated with the structural components of the ESX-4 complex located in the inner membrane.

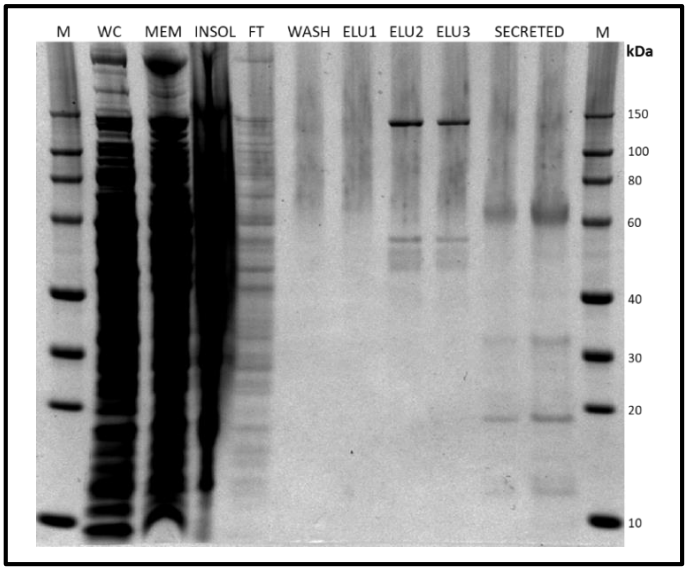

Figure 12. Coomasie-stained 4-12% SDS-PAGE gel with samples collected throughout the purification process. The eluate was collected using 3 different volumes of elution buffer (ELU1-ELU3). The secreted fraction was concentrated to 25X and loaded in 2 different volumes. WC=whole cell extract; MEM=membrane; INSOL=insoluble fraction; FT=flow-through; ELU=elution; *=typical degradation product (ATPase domains).

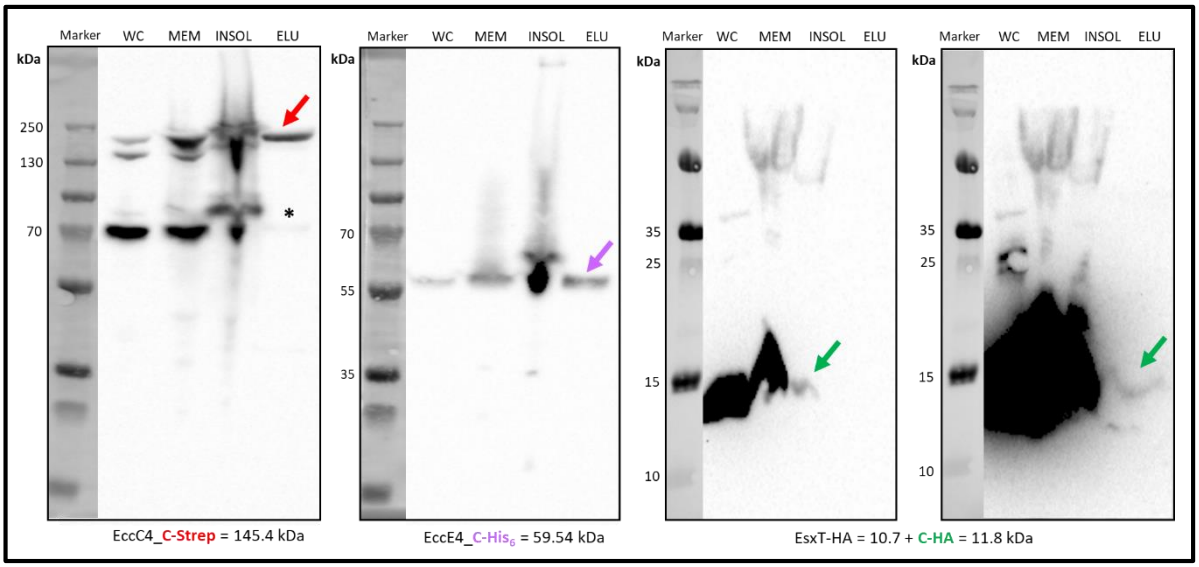

Figure 13. Western blots in 0.2 µm nitrocellulose membranes show the presence of $EccC_4$_Streptavidin, $EccE_4$_His and EsxT_HA in all fractions loaded (expected products indicated by arrows). The second EsxT_HA membrane (far right) was incubated with a substrate that enables femtogram detection. Below each figure is the expected size of the respective fusion protein. WC=whole cell extract; MEM=membrane; INSOL=insoluble; ELU=elution; *=typical degradation product (ATPase domains).

Another SDS-PAGE was run for a longer time to increase the separation between the bands so they could be analysed by mass spectrometry and all proteins in the eluted fraction could be identified. Proteins were compared to their homologs in *M. xenopi* and *M. smegmatis*, as well as checked for contaminants, and were found to match best to the protein sequence of Mab ESX-4 locus components $EccB_4$, $EccC_4$, $EccD_4$, $EccE_4$ and $MycP_4$ (Figure 14), confirming successful expression and purification, and tight association between the structural components. Interestingly, $MycP_4$ was also identified in the purified complex making this the first time this component was eluted and identified alongside other ESX structural components. Notably, copurification of MycP has recently also been reported by Bunduc et al. when the Mtb ESX-5 membrane complex was expressed in *M. smegmatis* [78].

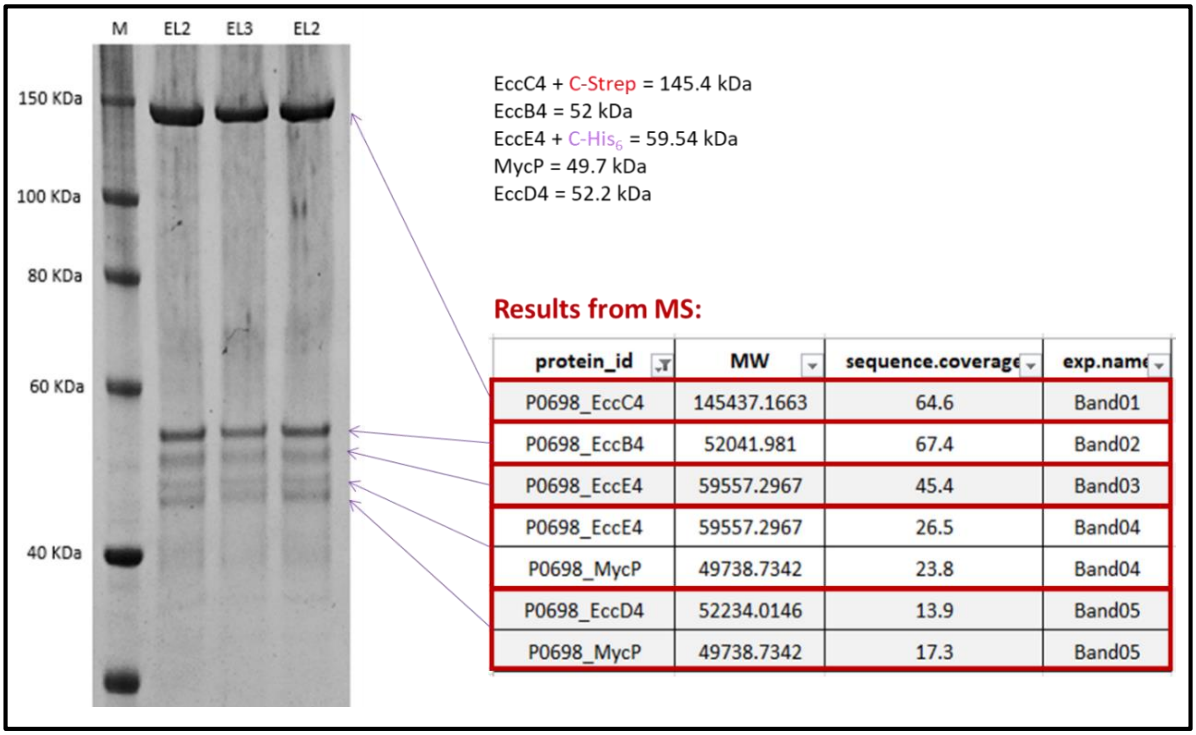

protein_id	MW	sequence.coverage	exp.name
P0698_EccC4	145437.1663	64.6	Band01
P0698_EccB4	52041.981	67.4	Band02
P0698_EccE4	59557.2967	45.4	Band03
P0698_EccE4	59557.2967	26.5	Band04
P0698_MycP	49738.7342	23.8	Band04
P0698_EccD4	52234.0146	13.9	Band05
P0698_MycP	49738.7342	17.3	Band05

Figure 14. Coomasie-stained 4-12% SDS-PAGE gel. The bands were analysed by mass spectrometry and found to correspond to Mab $EccB_4$, $EccC_4$, $EccD_4$, $EccE_4$ and $MycP_4$ protein sequences. The eluted fraction was collected in consecutive and different volumes of elution buffer (EL2 and EL3) as specified in the Materials and Methods section.

M. smegmatis possesses three endogenous T7SS, ESX-1, ESX-3 and ESX-4 (which lacks *eccC*$_4$). To investigate if translocation of Mab EsxT to the mycomembrane was also possible through the *M.smegmatis* ESX machinery or whether it specifically required the presence of ESX-4 from Mab, we obtained two strains: *M. smegmatis* transformed with pKB86 (containing only Mab *esxU* and *esxT_HA*) and *M. smegmatis* transformed with pKB87 (containing Mab ESX-4 structural genes, in addition to *esxU* and *esxT_HA*). Whole cell extracts, soluble fractions and secreted fractions from both strains were loaded onto SDS-PAGE gels. As shown in Figure 15, the anti-HA western blot targeting EsxT_HA did not show a band in the secreted fraction of pKB86 culture, as opposed to pKB87 where a band could be identified in all 3 fractions (WC, SOL and SEC). This shows that trafficking of EsxT from the cytosol to the exterior of the cell is dependent on the presence of ESX-4

from Mab, and confirms that *M. smegmatis* ESX-4 was not involved in the translocation of Mab EsxT.

The low intensity of the band in the secreted fraction of pKB87 clearly indicates a lower quantity of EsxT reaching the exterior of the cell when compared to the band obtained for the whole cell extract or even the soluble fraction. Reasonably, the majority of EsxT must be remaining within the cell. In the case EsxT would be associated to the mycomembrane, the faint band in the secreted fraction of pKB87 probably suggests residual loss of the protein.

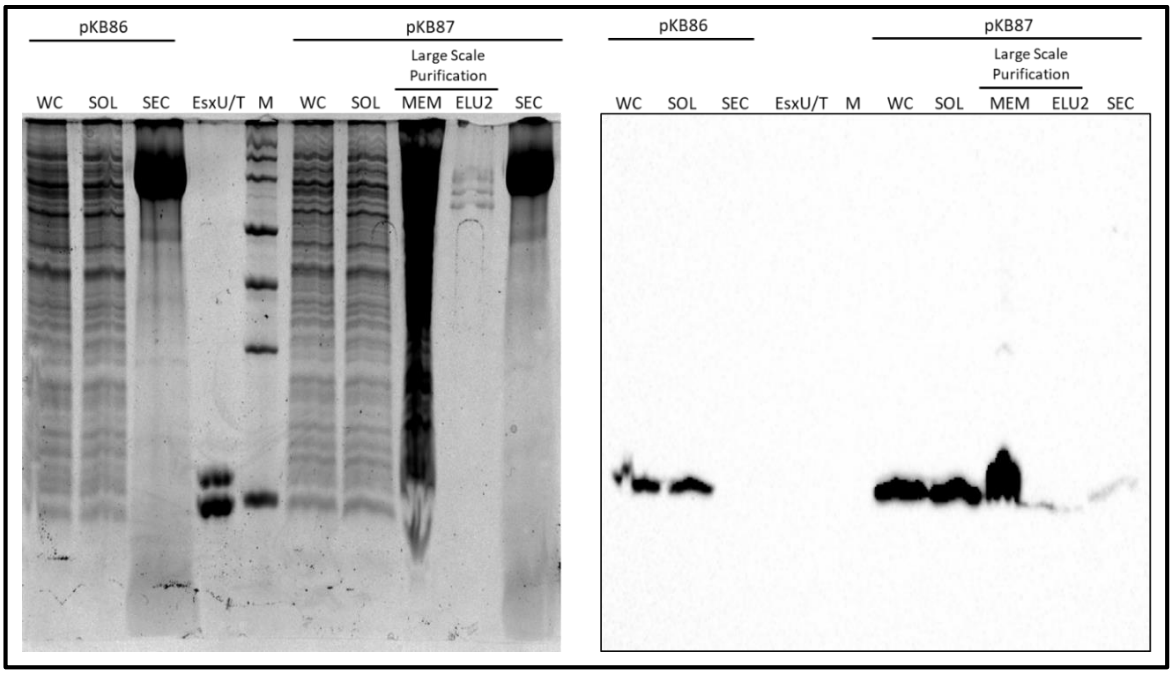

Figure 15. Small scale purification of pKB86 and pKB87 expressed in *M. smegmatis*. **Left:** Coomasie-stained 15% SDS-PAGE gel. The secreted fractions (filtered and concentrated to 40X) and the WC and soluble fractions (5X) were loaded into the gel in equal amounts. **Right:** Western blots in 0.2 µm nitrocellulose membranes, probed with anti-HA antibody, showing the presence of EsxT in all fractions except in the secreted fraction of pKB86. MEM and ELU2 fractions from previous pKB87 large scale purification were included as controls. EsxU/EsxT (not HA-tagged) from previous pKB89 large scale purification (addressed later) was also included as a control, showing bands at approximately 10 kDa. WC=whole cell extract, MEM=membrane, SOL=soluble fraction, ELU=elution, SEC=secreted.

In summary, we have successfully expressed and purified the Mab ESX-4 locus in *M. smegmatis*. Furthermore, we showed that EsxT is much more abundant in the membrane as compared to the culture supernatant. Lastly, we demonstrated that even though EsxT interacts with the inner membrane complex, it is not tightly bound to it. These results suggest that the Mab ESX-4 inner membrane complex is functional and that EsxT is a substrate of it. Our findings also argue against the assumption that EsxT is mostly secreted but rather point to a strong interaction of EsxT with biological membranes, including the Mab mycomembrane.

3.1.3 EsxU/EsxT is soluble and can be purified as a stable heterodimer

We next focused on further characterization of Mab EsxU (Rv3445c) and EsxT (Rv3444c). Mab EsxU (92 residues) and EsxT (96 residues) are Esx proteins that, based on their structural homology, can be easily aligned and recognized as part of the EsxA-like and EsxB-like WXG protein subfamilies (Figure 16). EsxT belongs to the EsxA-like WXG proteins subfamily, presenting a C-terminal secretion signal, three highly conserved residues (K/P38, Y51 and Q55) and a WXG-like motif (AEG sequence instead of WXG). Conversely, EsxU belongs to the EsxB-like WXG proteins subfamily. It contains a WXG motif and lacks a C-terminal secretion signal. Both EsxT and EsxU have an approximate weight of 10 kDa, and in analogy with the other Esx proteins within the subfamilies, EsxU and EsxT are thought to form a 1:1 heterodimer to be secreted as a complex through the ESX-4 membrane-bound structure.

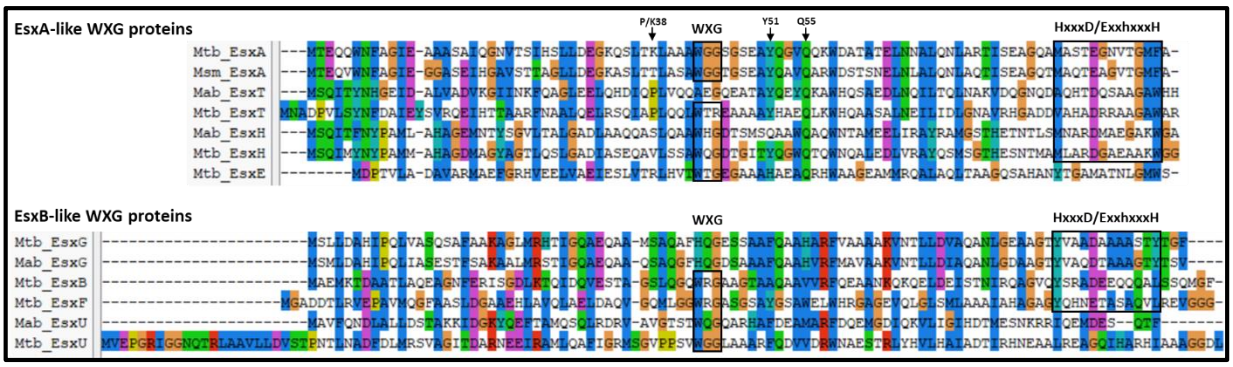

Figure 16. *In silico* homology analysis of WXG100 proteins from Mab and Mtb. The WXG motif and the secretion signal are shown in boxes [56]. The arrows indicate three highly conserved residues in the EsxA-like WXG proteins subfamily. Alignments were done using ClustalX 2.1.

Mab *esxU* and *esxT* were cloned from Mab ATCC 19977 into a pMyNT vector and transformed into *M. smegmatis* for subsequent overexpression of the construct. The final product had an N-terminal histidine tag in EsxU, which was used for purification following small scale expression. The purified compound was very soluble, rendering a thick band at around 10 kDa in a Coomassie-stained SDS-PAGE gel, as shown in Figure 17B. The gel was then analysed by peptide mass fingerprinting showing that the sequences of the purified substance corresponded to Mab EsxU and EsxT proteins, with a sequence coverage of 75.3% and 25.8%, respectively (Figure 17C).

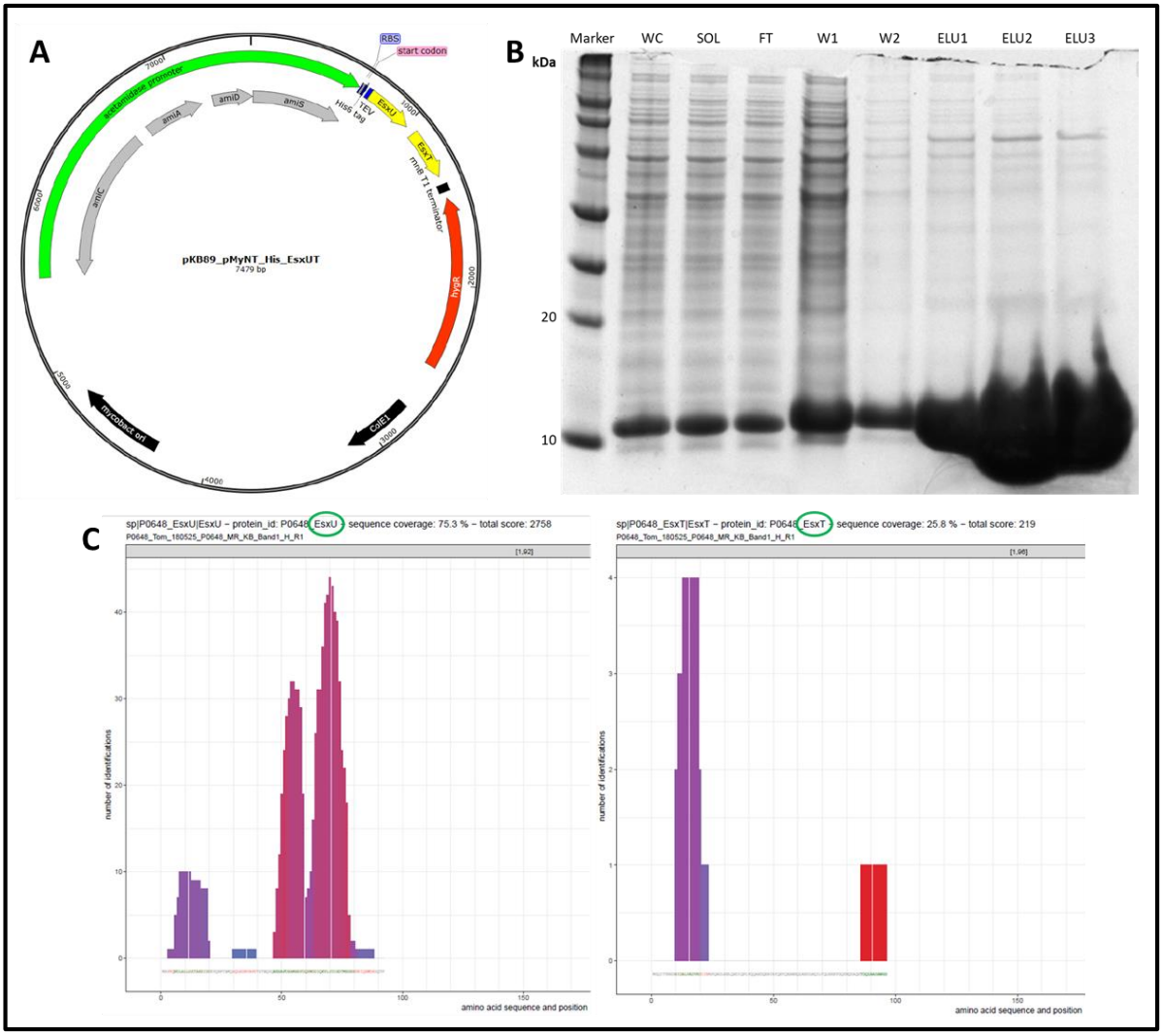

Figure 17. A: Map of plasmid pKB89 containing Mab *esxU* and *esxT* and a six-histidine tag in the N-terminal of EsxU. **B:** Coomassie-stained 10% SDS-PAGE gel showing different fractions of the small scale purification (Ni-NTa) of Mab EsxU/EsxT complex expressed in *M. smegmatis*. **C:** Peptide Mass Fingerprinting results of EsxU/EsxT complex. WC=whole cell extract, SOL=soluble fraction, FT=flow-through, W=wash, ELU=elution.

These results indicate that EsxU and EsxT indeed form a stable and soluble heterodimer that could be purified by “grabbing” only one of the proteins (in this case, EsxU via its His-tag). These observations are important as they allow us to expand the results obtained for EsxT in section 3.1.2 to the EsxU/EsxT heterodimer.

After large scale expression, EsxU/EsxT was purified by affinity purification and size exclusion chromatography (SEC), obtaining a relatively high yield (approximately 60 mg from 1.2 litres of culture). The final purified proteins were untagged (as confirmed by an anti-His western blot performed on the fractions collected from the SEC run, data not shown) and eluted in a buffer that contained no detergents. After running an SDS-PAGE gel, two distinctive bands were observed above 10 kDa, with the lower band being more intense than the upper band. No other bands were observed as shown in Figure 18.

The purified EsxU/EsxT complex was sent for production of antibodies. Accordingly, a polyclonal anti-EsxU/EsxT antibody raised in rabbit was successfully produced and delivered as both antiserum and affinity purified antibody.

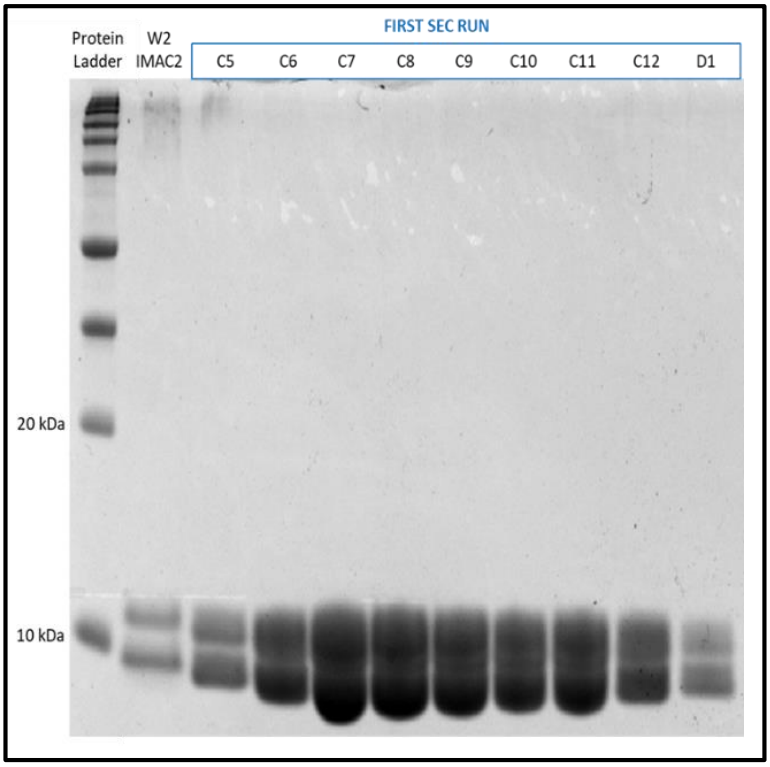

Figure 18. Coomassie-stained 15% SDS-PAGE gel showing different fractions collected from the SEC run. Two strong bands are observed in all fractions. These would correspond to EsxU and EsxT. No other bands were observed.

Similarly, Mab *esxU* and *esxT* were also separately cloned in a pMyNT vector to overexpress and purify the individual proteins. Two plasmids were generated: pFV01 (containing *esxU*) and pFV02 (containing *esxT*), both with an N-terminal histidine tag (Figure 19A and B). After small scale expression and purification, the Coomassie-stained SDS-PAGE indicated that both proteins were not very soluble, as the soluble fraction showed much less protein than the whole cell extract. In addition, EsxU seemed to be less soluble than EsxT, as shown in Figure 19C. Moreover, even though both proteins weighted just above 10 kDa, EsxU showed a band that ran at a lower weight than the one corresponding to EsxT, indicating a different interaction with SDS molecules.

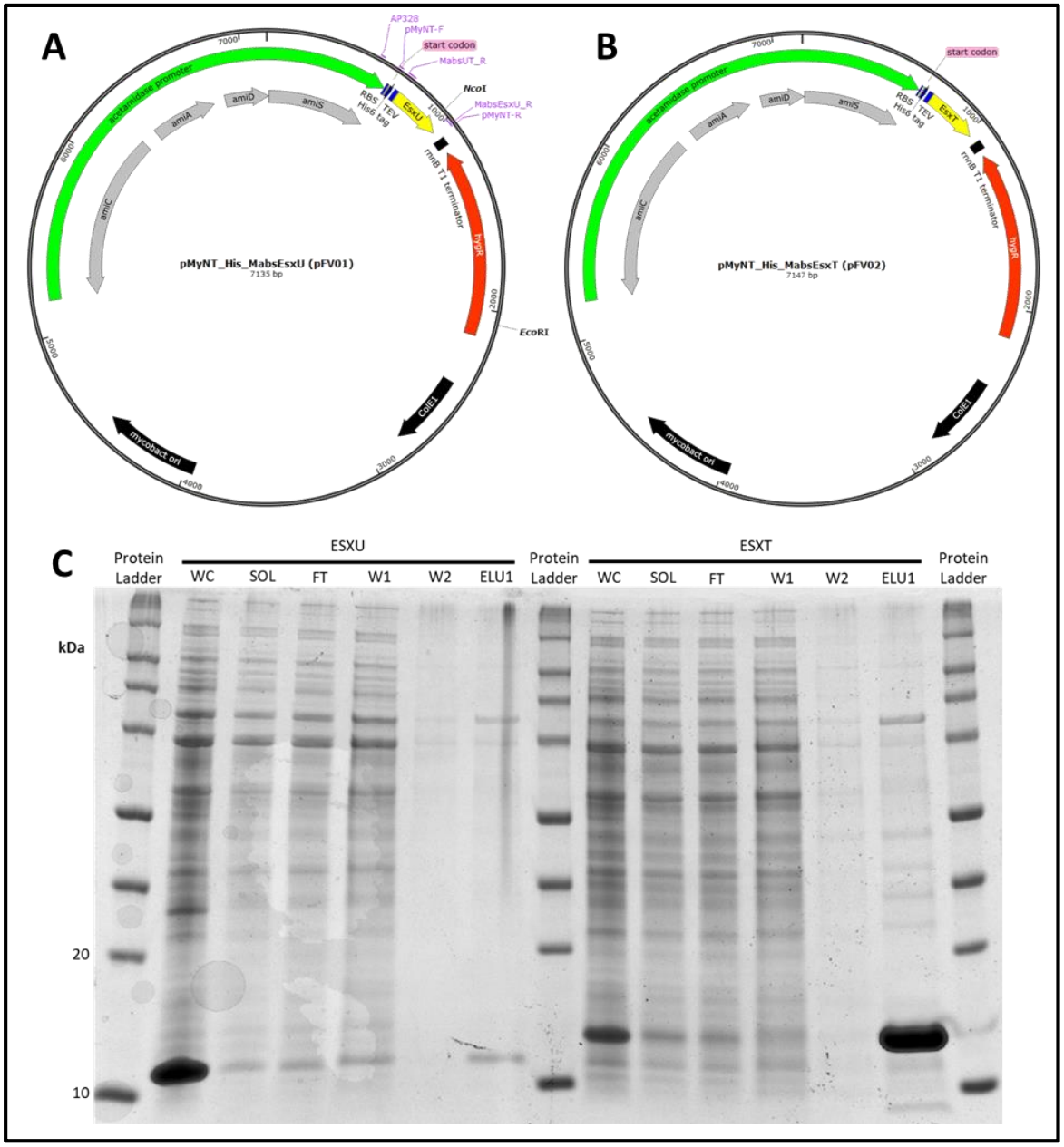

Figure 19. A: Map of plasmid pFV01 containing Mab *esxU* with an N-terminal six-histidine tag. **B:** Map of plasmid pFV02 containing Mab *esxT* with an N-terminal six-histidine tag. **C:** Coomassie-stained 10% SDS-PAGE gel showing different fractions of the small scale purification (Ni-NTa) of Mab EsxU and EsxT expressed in *M. smegmatis*. WC=whole cell extract; SOL=soluble fraction; FT=flow-through; W=wash; ELU=elution.

After large scale expression, the individual proteins were purified by affinity purification and size exclusion chromatography (SEC), and relatively low yields of EsxU (approximately 0.21mg from 3 litres of culture) and EsxT (approximately 6 mg from 2 litres of culture) were obtained. This is in line with previous studies that indicate that co-expression of Esx proteins leads to much higher yields than expression of the individual proteins as they are much more stable when together [56, 79]. The purified proteins were untagged (as confirmed by an anti-His western blot performed on the fractions collected from the SEC run, not shown) and eluted in a buffer that contained no detergents. For EsxT, one strong band at around 10 kDa and a lighter band at around 20 kDa (probably a homodimer) were

obtained (Figure 20A). For EsxU, one band at around 10 kDa was obtained from one of the SEC fractions (sample C7) However, the other fractions that were collected showed bands at higher molecular weights (samples B2, B5, B8, B12), suggesting the presence of possible oligomers in the eluate (Figure 20B).

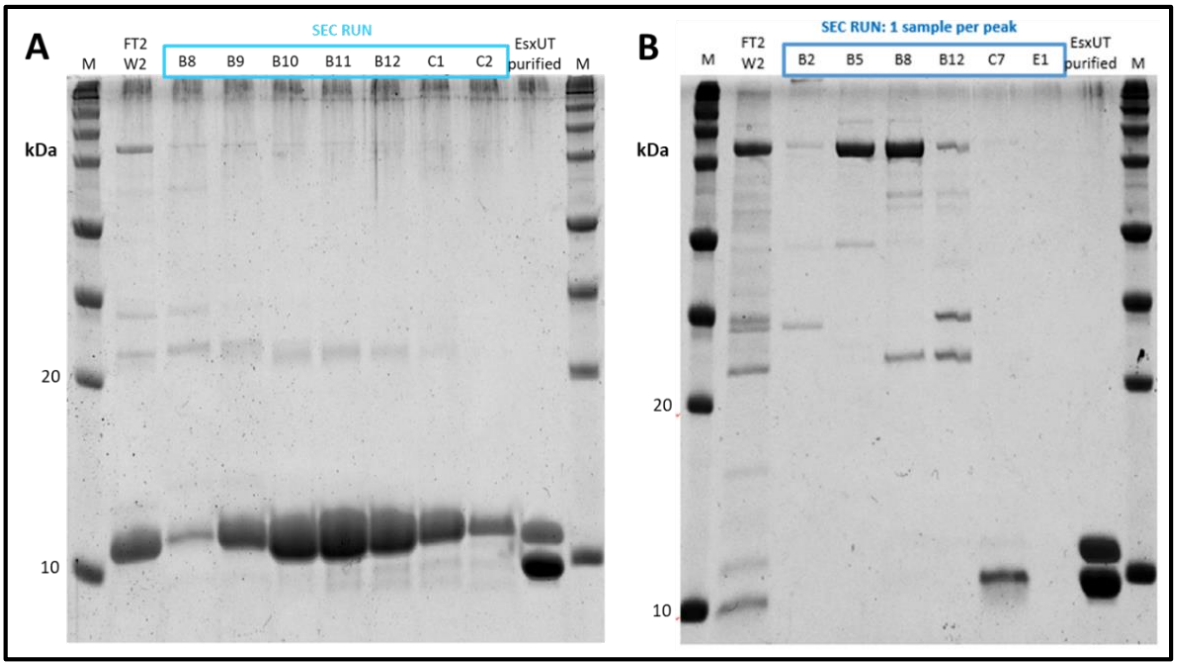

Figure 20. A: Coomassie-stained 15% SDS-PAGE gel showing different fractions collected from the SEC run for the purifications of Mab EsxT. **B:** Coomassie-stained 15% SDS-PAGE gel showing different fractions collected from the SEC run for the purifications of Mab EsxT. FT=flow-through; W=wash.

To analyse the oligomeric state of the purified proteins, SEC-MALLS was performed for the co-purified EsxU and EsxT, and for the individually purified EsxT. Due to the low amount obtained after purification of the individual protein, it was decided not to analyse EsxU by this technique. Both EsxU/EsxT and EsxT were found to be present as dimers of approximately 20 kDa (Figure 21).

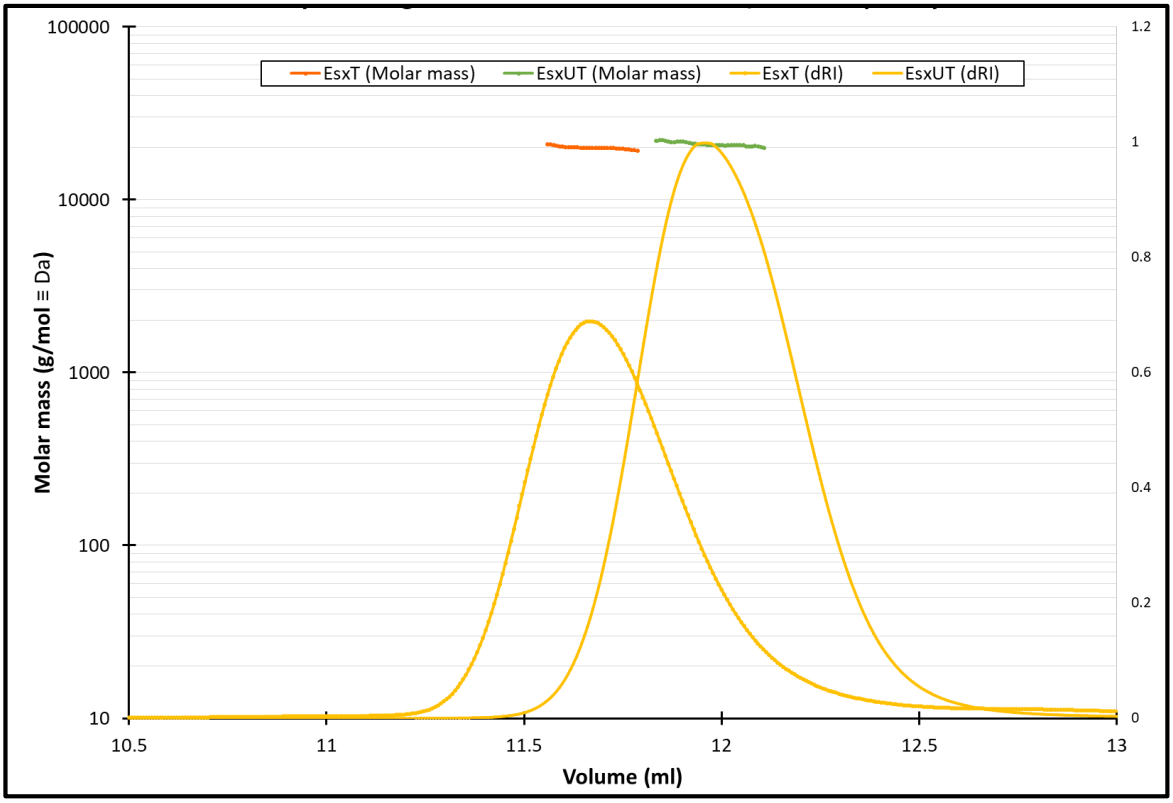

Figure 21. SEC-MALLS analysis of the EsxU/EsxT complex and the individually purified EsxT. Both samples were found to be present as dimers of approximately 20 kDa. GA=residues left after TEV cleavage during purification.

To find out if the purified EsxU/EsxT complex contained only heterodimers and not EsxT homodimers, the complex was analysed by intact mass measurement. As shown in Figure 22, three mayor peaks were found at 10.654, 10.589 and 21.259 kDa. The predicted weights after TEV cleavage and purification indicate that GA_EsxU (with V as the first residue) should weigh 10.65391 kDa; EsxT (without considering the first residue M) should weigh 10.58944 kDa; and the heterodimer in a 1:1 stoichiometry should weigh 21.24335 kDa. Results indicated that the masses of purified EsxU and EsxT were correct. However, for the heterodimer the value found by intact mass measurement exceeded the theoretical value by 15.65 Da. Furthermore, it did not match the theoretical mass for an EsxT homodimer (21.17888 kDa) or an EsxU homodimer (21.30782 kDa) either. Considering that the theoretical values for all dimers were very close together and bearing in mind the limitations of the technique, these results indicate that a minor fraction of homodimers was likely present among the purified EsxU/EsxT heterodimers.

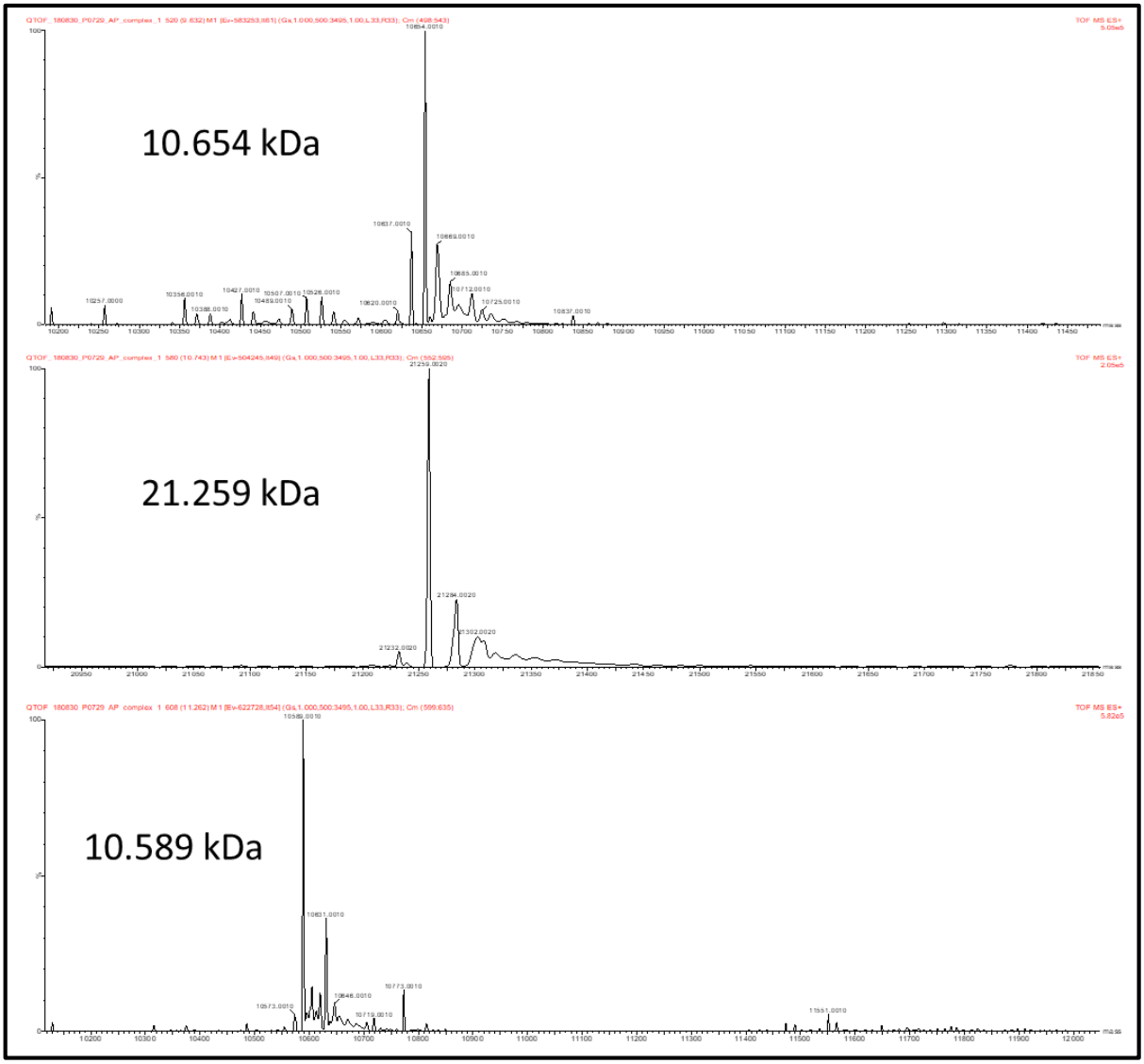

Figure 22. Purified Mab EsxU/EsxT analysed by intact mass measurement. Three mayor peaks were found at 10.654, 10.589 and 21.259 kDa. The peaks at approximately 10 kDa matched the theoretical masses of EsxU and EsxT. Analysis by Dominic Helm at EMBL Heidelberg and Dr. Annabel Parret at EMBL Hamburg.

3.1.4 EsxU/EsxT is membrane-bound

We tested three antibodies for detection of Mab EsxU/EsxT: a polyclonal anti-EsxU/EsxT raised in rabbit (affinity purified, see Chapter 3.1.3), and monoclonal anti-EsxU and anti-EsxT raised in mice (serum, provided by Dr. F. Misguich and Prof. J. Herrmann at UVSQ). The purified proteins (EsxU, EsxT, EsxU/EsxT) were run on a SDS-PAGE gel after which western blots were carried out. As shown in Figure 23, all three antibodies recognized their targets but anti-EsxU/EsxT seemed to need less exposure time to render stronger bands, probably as it was affinity purified. Interestingly, anti-EsxU/EsxT was able to recognize both EsxU and EsxT showing that it had epitopes in both proteins. In addition, purified EsxU seemed to be more on a monomeric state, while almost equal amounts of monomers and dimers were observed for the purified EsxT.

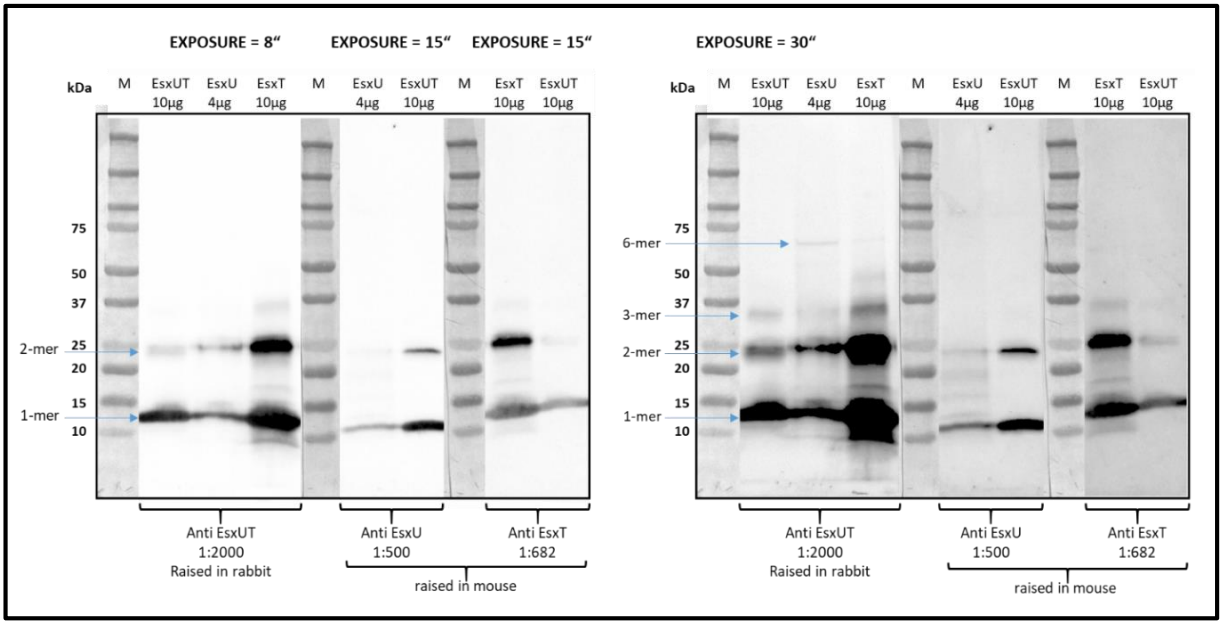

Figure 23. Western Blots to test the sensitivity of the antibodies. A polyclonal affinity purified rabbit anti-EsxU/EsxT, and monoclonal mouse anti-EsxU and mouse anti-EsxT were tested against purified Mab proteins EsxU, EsxT and EsxU/EsxT. Different exposure times are shown.

Our collaborators at Prof. Laurent Kremer's group at IRIM were able to produce different genetically modified Mab strains. They knocked-out *esxU* and *esxT* from the CIP 104536T type strain of Mab_A (MabsCIP), following a previously described protocol [80], demonstrating that these genes are not essential for bacterial survival. For each, S and R variants, they obtained 5 genotypes: wild-type (WT), *ΔesxUΔesxT* double knock-outs (DKO), *ΔesxUΔesxT* DKO complemented with *esxU* (c.EsxU), *ΔesxUΔesxT* DKO complemented with *esxT* (c.EsxT), and *ΔesxUΔesxT* DKO complemented with *esxU* and *esxT* (c.EsxUT). The WT and DKO strains were unmarked while the complemented strains needed to be supplemented with kanamycin. In addition, the complemented strains were constructed with genes containing a C-terminal HA tag for later identification.

To investigate the localization of the EsxU/EsxT heterodimer in Mab, a cell fractionation was performed to obtain different cell compartments (secreted, capsule, membranes, and cytoplasm). The samples were run in an SDS-PAGE gel and western blots were performed using the three antibodies tested previously. The samples were loaded so that the amount in each well would correspond to the same proportion of bacteria and in this way allow comparison of the quantity of EsxU/EsxT present in the different cell compartments. Unfortunately, unspecific binding was observed for all three antibodies in the membrane and cytoplasm fractions when analysing Mab ATCC 19977 and Mab_S_DKO (data not shown). However, only a very faint band was observed in the secreted fraction lane for all antibodies, further corroborating that none of the target proteins, including EsxU/EsxT, is strongly secreted.

In cooperation with the group of Prof. Kremer we then developed an experimental strategy to directly confirm localization of EsxU/EsxT in the Mab mycomembrane using Mab strains DKO_c.EsxUT and DKO_c.EsxT. After fractionation, compartment preparations corresponding to the same amount of bacteria were analysed by SDS-PAGE and anti-HA western blots, avoiding the unspecificity of the previously mentioned antibodies. As shown

in Figure 24, EsxU and EsxT were mainly found in the cytosol, with the second strongest band found in the plasma membrane fraction and the weakest band observed in the cell wall fraction, confirming our previous finding from expression experiments in *M. smegmatis* that EsxU/EsxT complex is highly abundant in the mycobacterial membrane.

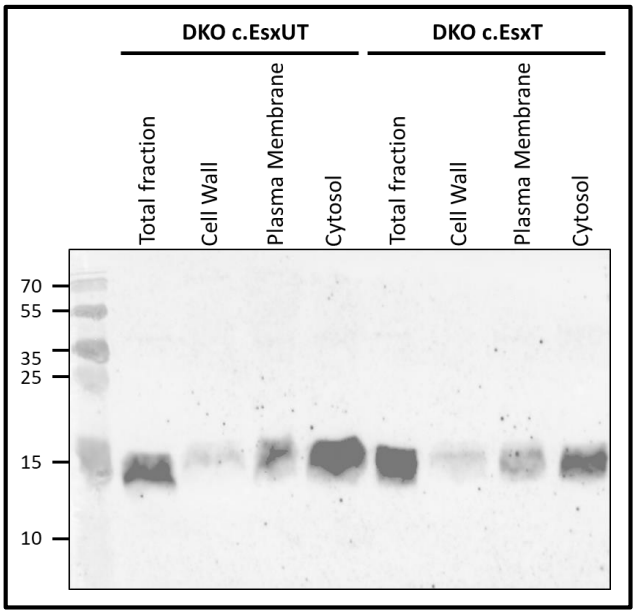

Figure 24. Western blots in Mab cell compartments of strains DKO_c.EsxUT and DKO_c.EsxT. The complemented strains had a C-terminal HA tag in EsxU and EsxT, respectively. Cultures were harvested at an OD_{600} of 0.8, and cells were fractionated and run in an 18% SDS-PAGE gel. Western blots were performed using a rat anti-HA antibody (1:2000). Experiments conducted by Dr. Wassim Daher at IRIM.

Finally, a plasmid containing Mab *esxU* and *esxT* with a C-terminal GFP tag (pVV16-EsxUT-GFP) was designed. After transformation and expression in MabsCIP, high resolution confocal microscopy images were acquired. As shown in Figure 25, GFP was found localized in the periphery of the bacilli, confirming the hypothesis that the EsxU/EsxT heterodimer is membrane-bound.

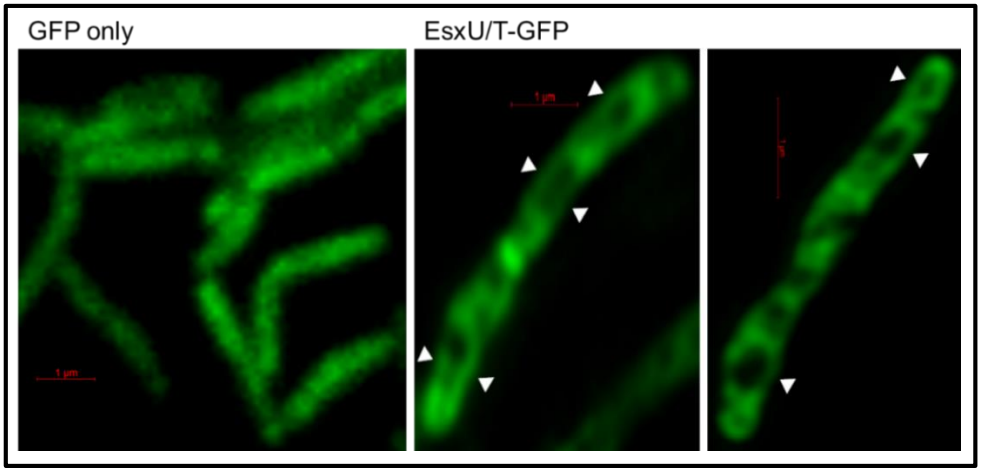

Figure 25. Mab expressing EsxU/EsxT with a C-terminal GFP tag. High resolution confocal microscopy images of Mab expressing either pVV16-GFP (left) as a control, or pVV16-EsxUT-GFP (right) were acquired. In the control, GFP was found in the cytoplasm, evenly distributed. In the samples, the distribution of GFP was constraint

to some areas. The arrows indicate regions where GFP can be seen only in the periphery of the bacilli. Experiments conducted by Dr. Wassim Daher at IRIM.

3.1.5 EsxU/EsxT affects the physiochemical properties of the cell

Since EsxU/EsxT is highly expressed and localized in the mycobacterial membrane, we wanted to investigate if its absence affected the physiochemical properties of the bacterial cell. Thus, we designed a set of experiments to study growth, hydrophobicity, sedimentation, Lewis acid–base properties, density and morphology using both the wild type and the EsxU/EsxT mutant strains described in Chapter 3.1.4.

Growth curves

Growth curves were obtained for the WT and DKO strains in both the S and R genetic background as shown in Figures 26A and C. Growth rates were similar between S and R variants and among WT, DKO and EsxU/EsxT complemented strains in both backgrounds (Figures 26B and D). This demonstrates that neither deletion of nor complementation with *esxU* and *esxT* affected bacterial growth in both S and R backgrounds.

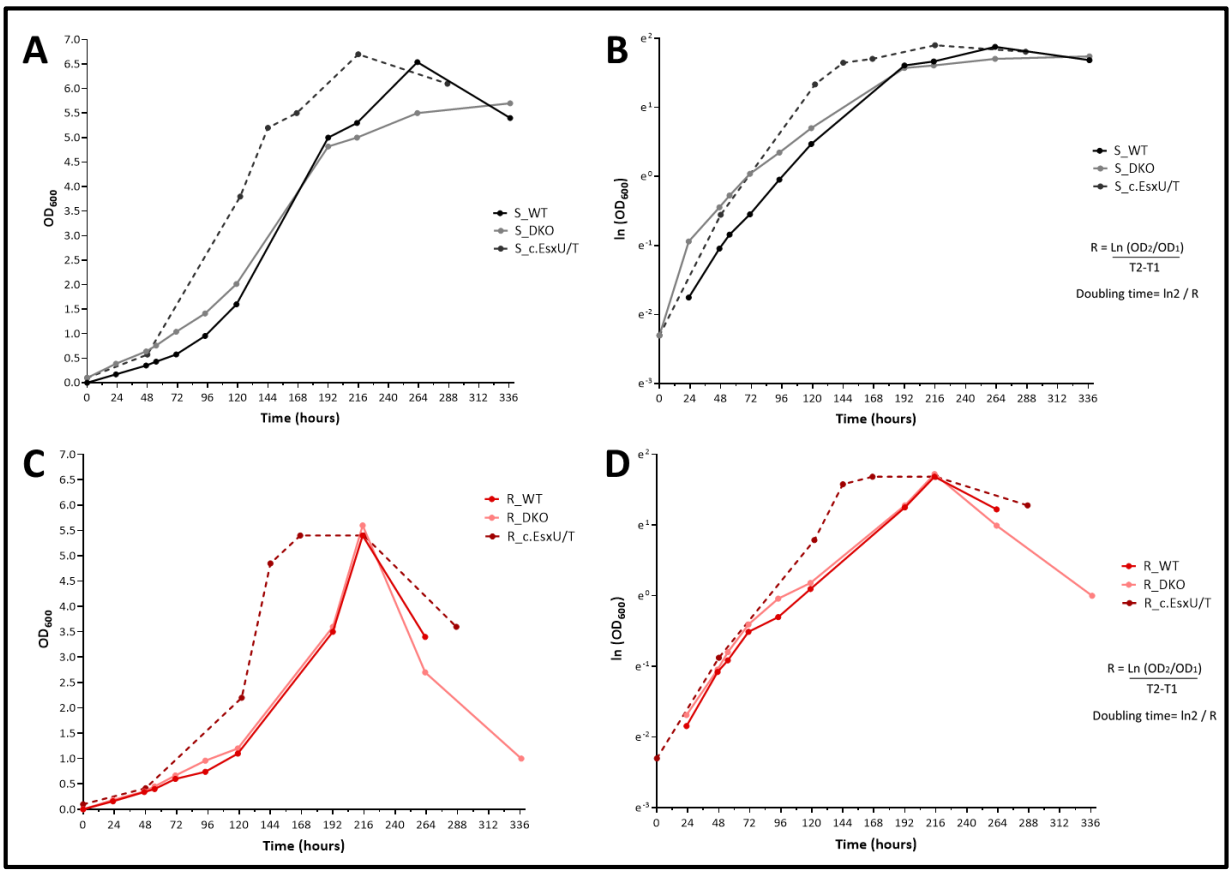

Figure 26. Mab growth curves. Bacterial strains were grown in 7H9 medium supplemented with OADC and Tween-80. The OD_{600} was measured for the S **(A)** and R **(C)** variants. To compare the growth of different strains, the slopes of the growth curves were calculated and plotted for the S **(B)** and R **(D)** variants.

Hydrophobicity of Mab

It is well known that the mycobacterial membrane is highly hydrophobic. To study if the lack of *esxU* and *esxT* affected Mab hydrophobicity, a microbial adhesion to hydrocarbons

(MATH) test was performed. As shown in Figure 27, all Mab strains showed high affinity to the hydrocarbon phase, confirming hydrophobicity. The percentage of cell surface hydrophobicity (CSH) was calculated and no differences were found between the WT and DKO strains, or between the S and R variants, indicating that the absence of *esxU* and *esxT* does not alter the hydrophobicity of the mycomembrane.

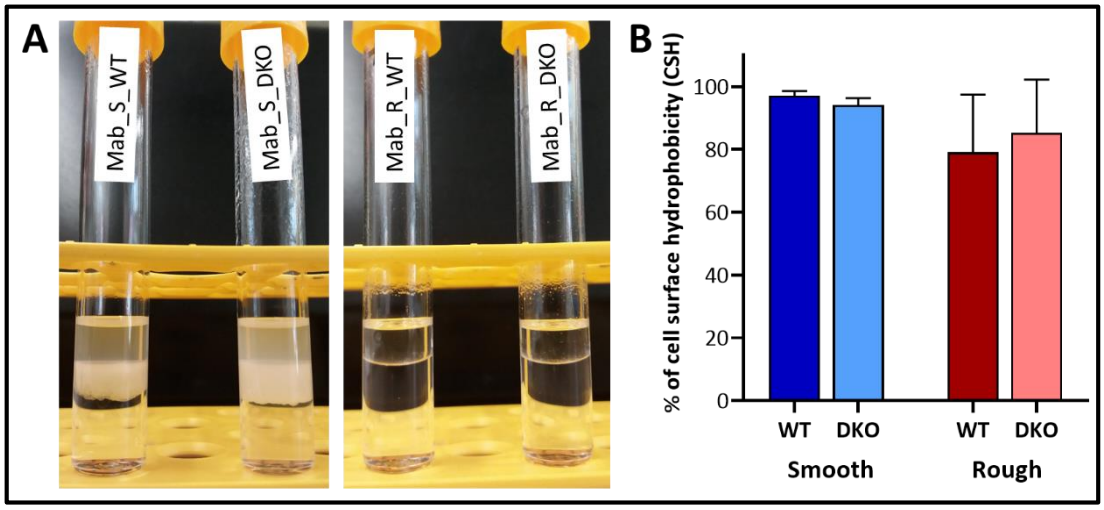

Figure 27: Hydrophobicity of Mab. **A:** Different strains of Mab were grown in RPMI media (no detergent) and MATH test was performed. Strong association of bacteria with the hydrocarbon phase was observed for all Mab strains. **B:** Cell surface hydrophobicity (CSH) of Mab S_WT, S_DKO, R_WT and R_DKO. Values shown are the average of 4-5 experiments.

Sedimentation of Mab

Mab cells aggregate, with the R variant forming much larger aggregates (cord-like structures) than the S variant. This characteristic, in addition to its strong hydrophobicity, causes Mab cells to sediment when suspended in medium or PBS. After growing Mab in medium without detergent, the cultures were centrifuged and the pellets were resuspended in DPBS. Cultures were left undisturbed at room temperature and the OD_{600} was measured from the top part of the culture at different time points. The percentage of non-sedimented culture was calculated using the OD_{600} at time zero as the reference, and graphed as shown in Figure 28. Results showed that the S and the R variants sedimented at different rates. After 90 minutes 91% of the R bacteria sedimented while only 24.3% of the S bacteria was at the bottom at the same time point, showing a difference of 66.7% between the variants. In addition, there was an approximately 14% difference between the sedimentation rate between the S_WT and the S_DKO, while there was no difference in the sedimentation between the R_WT and R_DKO. It is important to highlight that the S_DKO culture was most of the time resuspended and did not show aggregates. Taking these observations together, results suggest that the lack of EsxU and EsxT interferes with the aggregation properties of the S variant.

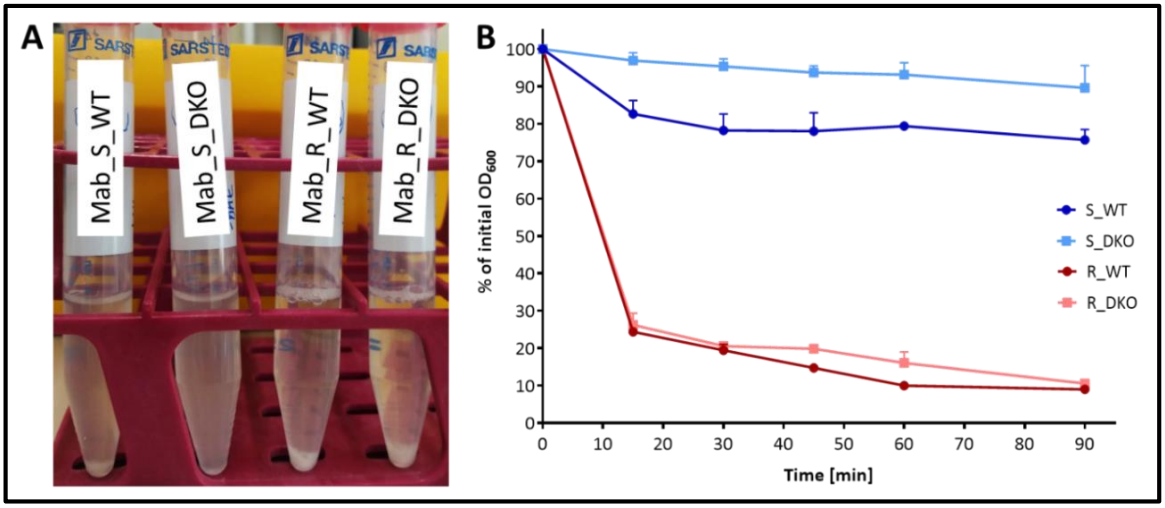

Figure 28. Sedimentation of Mab. **A:** Different strains of Mab were grown in Middlebrook 7H9 medium supplemented with OADC (no detergent), harvested, and the pellets were resuspended in DPBS. Cultures were left undisturbed at room temperature for 30 min. Pellets can be observed in Mab S_WT, R_WT and R_DKO. **B:** Variation of the percentage of initial OD_{600} at different time points. Values shown are the average of 3-5 experiments.

Lewis acid–base properties of Mab

Adhesion of bacterial cells is considered a virulence factor because the production of extracellular substances lead to the formation of a self-protecting environment (matrix) which shields the bacteria from external dangers, such as antibiotics [81]. One crucial determinant in bacterial adhesion is hydrophobicity. The other determinant is bacterial surface charge, which is influenced by environmental factors such as pH, medium, and ionic concentration [82].

The microbial adherence to solvents (MATS) method was used to investigate the Lewis acid–base properties of the Mab cell surface (see Materials and Methods). As shown in Figure 29A, all strains had a strong affinity for chloroform, a monopolar acidic solvent. Interestingly, the S strains (WT and DKO) were more distributed in the chloroform phase, while the R strains (WT and DKO) aggregated at the top of the chloroform phase forming a layer. There were no differences between the WT and DKO strains in both variants.

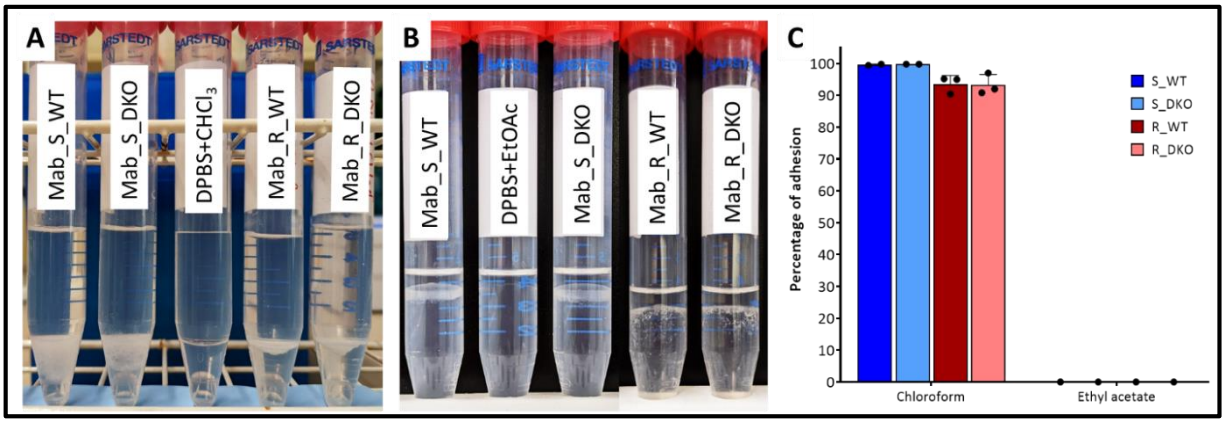

Figure 29: Lewis acid–base properties of Mab. Different strains of Mab were grown in 7H9 medium supplemented with OADC (no detergent), the cultures were centrifuged in 15 ml tubes and the pellets were resuspended in DPBS. **A:** Cultures

were mixed with 1 ml of chloroform and left undisturbed at room temperature. **B:** Cultures were mixed with 1ml of ethyl acetate and left undisturbed at room temperature. **C:** The percentage of adhesion, which represents the affinity of the bacteria to the solvents, was calculated for each strain. Values shown are the average of 2-3 experiments.

When tested with ethyl acetate, a monopolar basic solvent, the S strains localized at the top part of the aqueous phase, in a layer-conformation (Figure 29B). The R variant, however, showed distribution of the aggregates in the aqueous phase. All strains showed a very low affinity for ethyl acetate, with no differences between the WT and DKO strains.

These results showed that all strains displayed a higher affinity for acidic solvents and a lower affinity for basic solvents, which demonstrates that Mab is a strong electron donor and weak electron acceptor. In other words, the strains tested had a strong basic and a weak acidic character. This is the first time these characteristics are reported for Mab. Similar physicochemical properties are displayed by *Pseudomonas aeruginosa*, which is also a lung pathogen [83].

Density of Mab

To study if the absence of EsxU and EsxT would impact the density of the bacterial cells, a differential density centrifugation was performed. For the size fractionation of Mab cells, discontinuous gradients of 85, 92 and 100% of Percoll were set up. Briefly, Mab cells were grown in Middlebrook 7H9 medium supplemented with OADC (no detergent) for 3 days, harvested by centrifugation, washed, resuspended in DPBS, syringed and layered on top of the Percoll gradient. Then, the cells were fractionated by centrifugation at 800 × g for 20 min at 20◦C. As shown in Figure 30, no differences were observed in the R variants between the WT and DKO strains. However, in the S variants, the DKO population seemed to have a slightly bigger size than the WT strain, as the layer of bacteria appeared at a higher position.

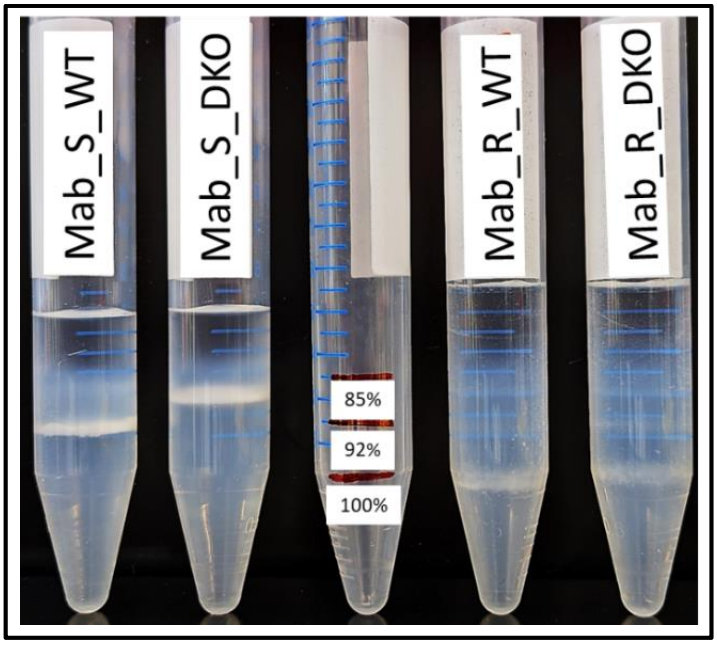

Figure 30. Density of Mab. Different strains of Mab were grown in 7H9 medium supplemented with OADC (no detergent). The cultures were centrifuged and the

pellets were resuspended in DPBS. Discontinuous gradients of 85, 92 and 100% of Percoll were set up and after Mab cells were layered on top they were fractionated by centrifugation. Figures shown are representative of 4 experiments.

The same difference in layer positions was observed when culturing Mab in medium containing Tween-80 (Figure 31).

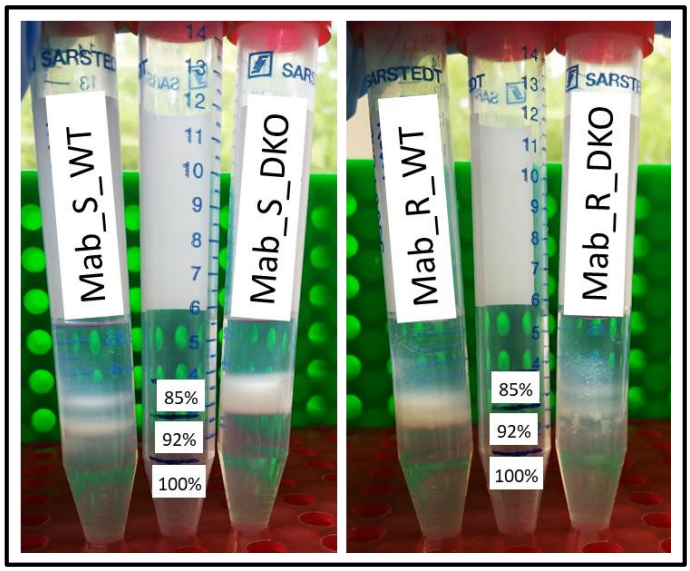

Figure 31. Density of Mab. Different strains of Mab were grown in Middlebrook 7H9 medium supplemented with OADC and Tween-80. The cultures were centrifuged and the pellets were resuspended in DPBS. Discontinuous gradients of 85, 92 and 100% of Percoll were set up and after Mab cells were layered on top, there were fractionated by centrifugation. Figures shown are representative of 2 experiments.

Morphology of Mab strains

Scanning electron microscopy (SEM) was performed to observe the morphology of Mab S and R strains and to detect if the absence of EsxU and EsxT caused changes in bacterial morphology. As shown in Figure 32, no observable difference was found between the WT and DKO strains of each variant. However, there was an important difference in the aggregation and consistency of the bacterial clumps between the bacteria cultured with and without detergent. Upon treatment with detergent, the matrix surrounding the bacteria is washed off, and this is particularly visible in the R variant.

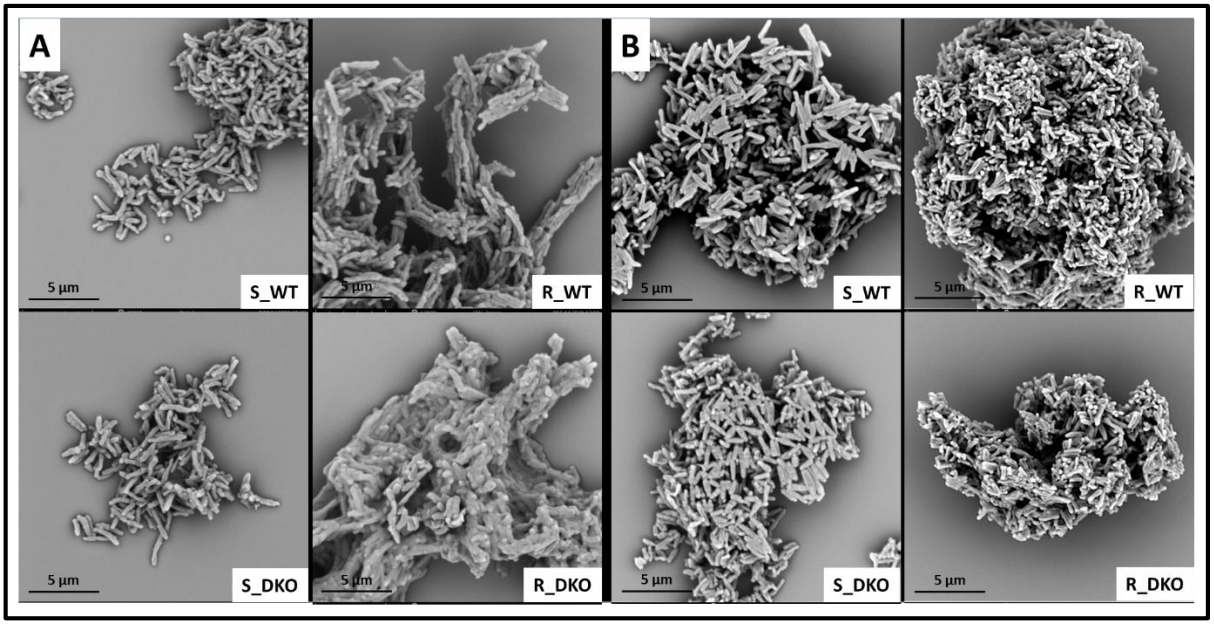

Figure 32. Scanning EM of different Mab strains harvested at OD_{600} of approximately 1. Bacteria were grown in Middlebrook 7H9 medium supplemented with OADC. **A:** without Tween-80. **B:** with Tween-80. Magnification: 13000X. Scale bar: 5 µm

The lack of the surrounding matrix could have some effects in the study of Mab in culture and may affect parameters like quorum sensing and their interaction with other cells (for example: host cells). Long established protocols in laboratories suggest to culture mycobacteria in media with detergent (Tween-80, Tyloxapol, Genapol), but the effects of these on mycobacterial morphology, biochemistry and host-interacting properties are diverse [84]. Even though none of the studies cited in that review analysed the particular effects of detergents on *Mycobacterium abscessus*, it is important to consider them when thinking about the context in which the bacteria will be used.

In summary, we have shown that *esxU* and *esxT* are clinically relevant for Mab virulence or pathogenicity as evidenced by their higher expression in clinical isolates. We have verified that Mab ESX-4 system can be successfully cloned, expressed and purified using *M. smegmatis* as an expression model. Moreover, the results indicated that the structural components ($EccB_4$-$EccE_4$ and $MycP_4$) are membrane-bound, and suggested that EsxT is weakly associated with them.

Similarly, we have shown that Mab EsxU/EsxT can be successfully cloned, overexpressed and purified using *M. smegmatis* as an expression model. The proteins form a 1:1 stable heterodimer that when expressed without the Mab ESX-4 structural components, remain in a soluble complex that can be purified as an untagged and detergent-free heterodimer. In contrast, when the same method was followed to purify the individual proteins, they were found to be much less soluble and tended to form aggregates with different number of monomers.

Using genetically modified Mab strains, and in collaboration with scientists at IRIM group, we have shown that EsxU/EsxT localizes to the mycobacterial membrane. Moreover, in the S variant, the absence of EsxU and EsxT affects the structure of the cell, decreasing its density and decreasing its auto aggregation. In the R variant, the absence of these proteins showed no visible effects in the physiochemical properties studied.

3.2 Functional characterization of the *M. abscessus* EsxU/EsxT heterodimer

With the EsxU/EsxT heterodimer strongly expressed in clinical Mab isolates and, unlike EsxA/EsxB from Mtb, localized in the mycobacterial membrane, we next investigated the role of EsxU and EsxT in Mab virulence and pathogenicity. We designed a set of experiments to test if Mab EsxU/EsxT complex is involved in the uptake of mycobacteria by host phagocytes and whether the heterodimer induced similar cytokine responses in host cells.

3.2.1 EsxU/EsxT plays a role in host-pathogen interaction and contributes to intra-phagosomal survival

Our collaborators at IRIM (Prof. Kremer) and UVSQ (Prof. Herrmann) generated genetically modified Mab strains (*ΔesxUΔesxT* DKO and complemented mutants) and investiged them with regard to differences in virulence, in particular in the Mab_S background. The team at IRIM found a higher percentage of infected THP-1 cells following exposure to S_DKO, in comparison to the WT (Figure 33A). Also, using a zebrafish model, they found a higher mortality in embryos infected with S_DKO, and a higher number of embryos with granulomas in zebrafish infected with S_DKO (Figure 33B). These results, part of a manuscript that is currently being written, suggested that the absence of *esxU* and *esxT* conferred an advantage to the bacteria during infection and predicted a worse outcome for the host, at least in the S Mab morphotype.

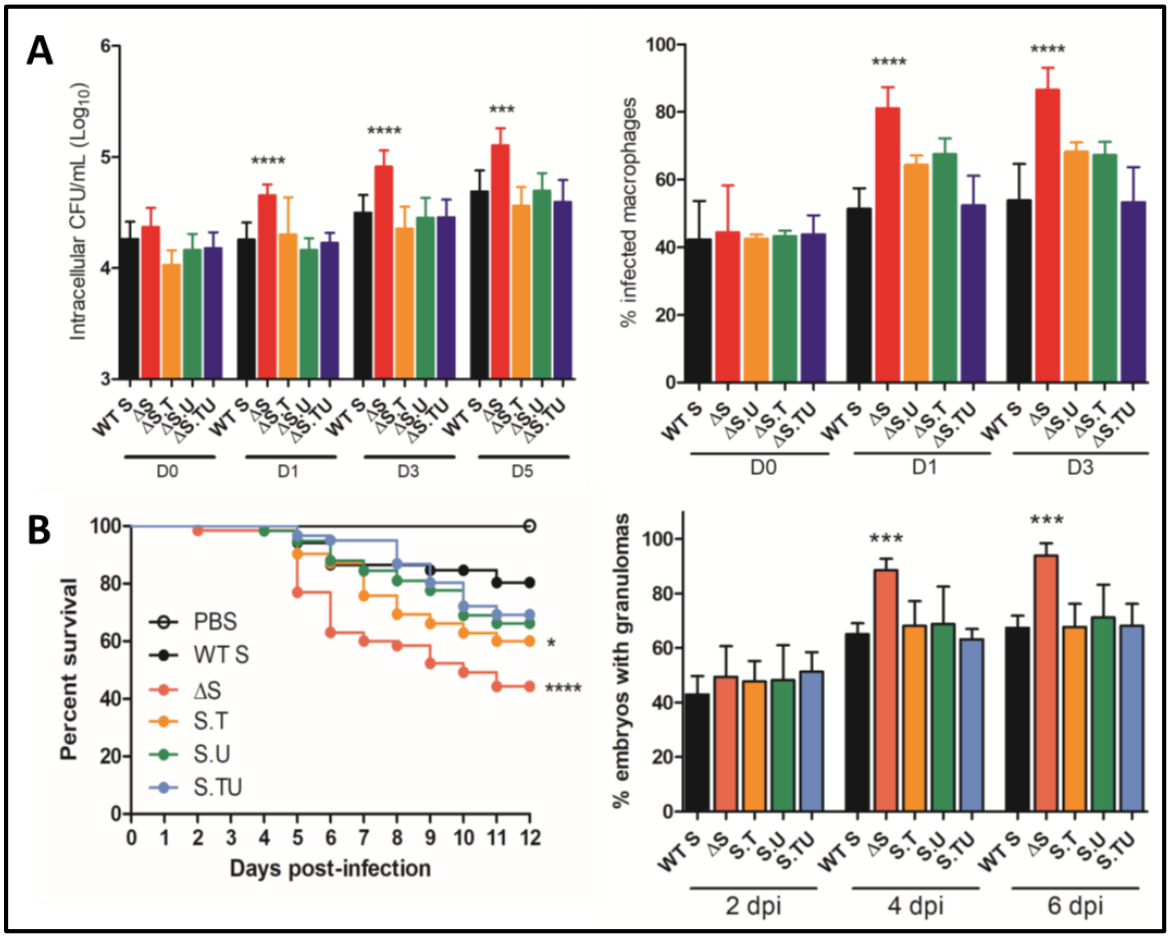

Figure 33. Host-pathogen interaction with Mab S mutants. **A:** Results of THP-1 macrophage infection with Mab S EsxU/EsxT mutants at MOI=2, after 0, 1, 3 and 5

days. **B:** Zebrafish embryos were infected via caudal vein injection at 30 h post-fertilisation with ~200 CFU of Mab strains. The embryo mortality was monitored over a 12 day period and the percentage of embryos with granulomas was assessed at 2, 4 and 6 dpi. Results from A and B are the compilation of at least 3 different experiments performed by Dr. Matt Johansen (IRIM).

At UVSQ, the role of EsxU/EsxT in Mab_S infected murine macrophages was studied, with a focus on phagosomal membrane damage. They found that S_DKO was unable to damage the phagosomal membrane, compared to the WT (Figure 34). These results suggested a role of EsxU/EsxT in phagosomal escape, through a mechanism yet unknown (Marion Lagune's PhD thesis, UVSQ PhD candidate, unpublished). Taken together, our collaborators' findings indicated a role of EsxU/EsxT in host-pathogen interaction and in the fate of the mycobacteria inside the phagosome.

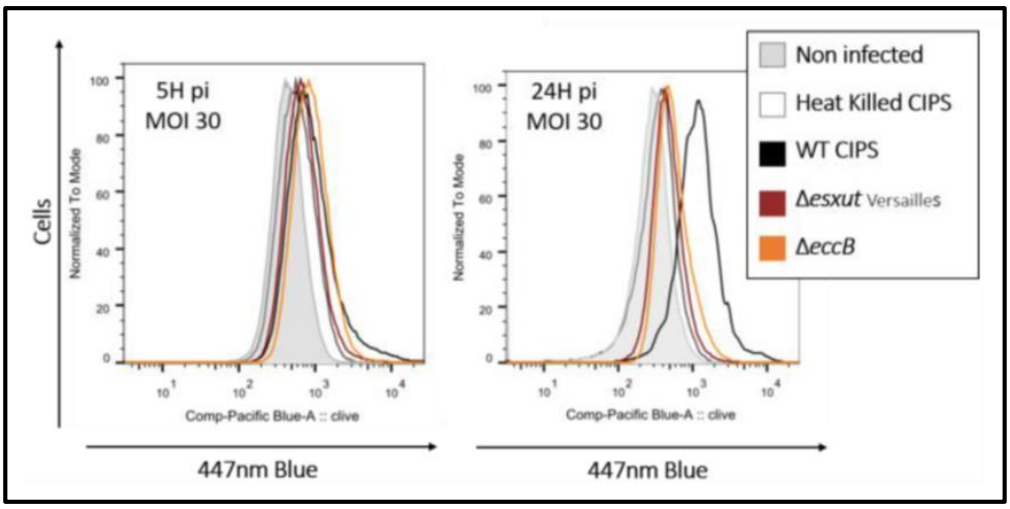

Figure 34. Phagosomal membrane damage assessment at 5 and 24 hpi in J774.2 murine macrophages. Experiments performed for the doctoral thesis of Marion Lagune (UVSQ).

3.2.2 EsxU/EsxT, EsxT and EsxU do not lyse human cells

While it was demonstrated that EsxU/EsxT plays a role in macrophage uptake and phagosomal escape (see Chapter 3.2.1), we investigated if EsxU/EsxT also showed direct membrane lysis activity, as it has been extensively reported for ESX-1 substrates (reviewed in [50]). To that end, human erythrocytes, macrophages and neutrophils were isolated and incubated with purified EsxU, EsxT and EsxU/EsxT. As shown in Figure 35, human neutrophils and macrophages incubated with Mab purified EsxU, EsxT and EsxU/EsxT at physiological pH for 6 and 21-22 hours, and subsequently analysed by LDH assay showed that there was no lysis effect. As it has been reported that the lysis activity of ESX-1 is dependent on pH (as it would help Mtb escape the phagosome in the middle of a low pH environment), incubations of freshly isolated human erythrocytes with Mab purified proteins at 3 different pH were carried out. No lysis effect was observed in all three pH conditions

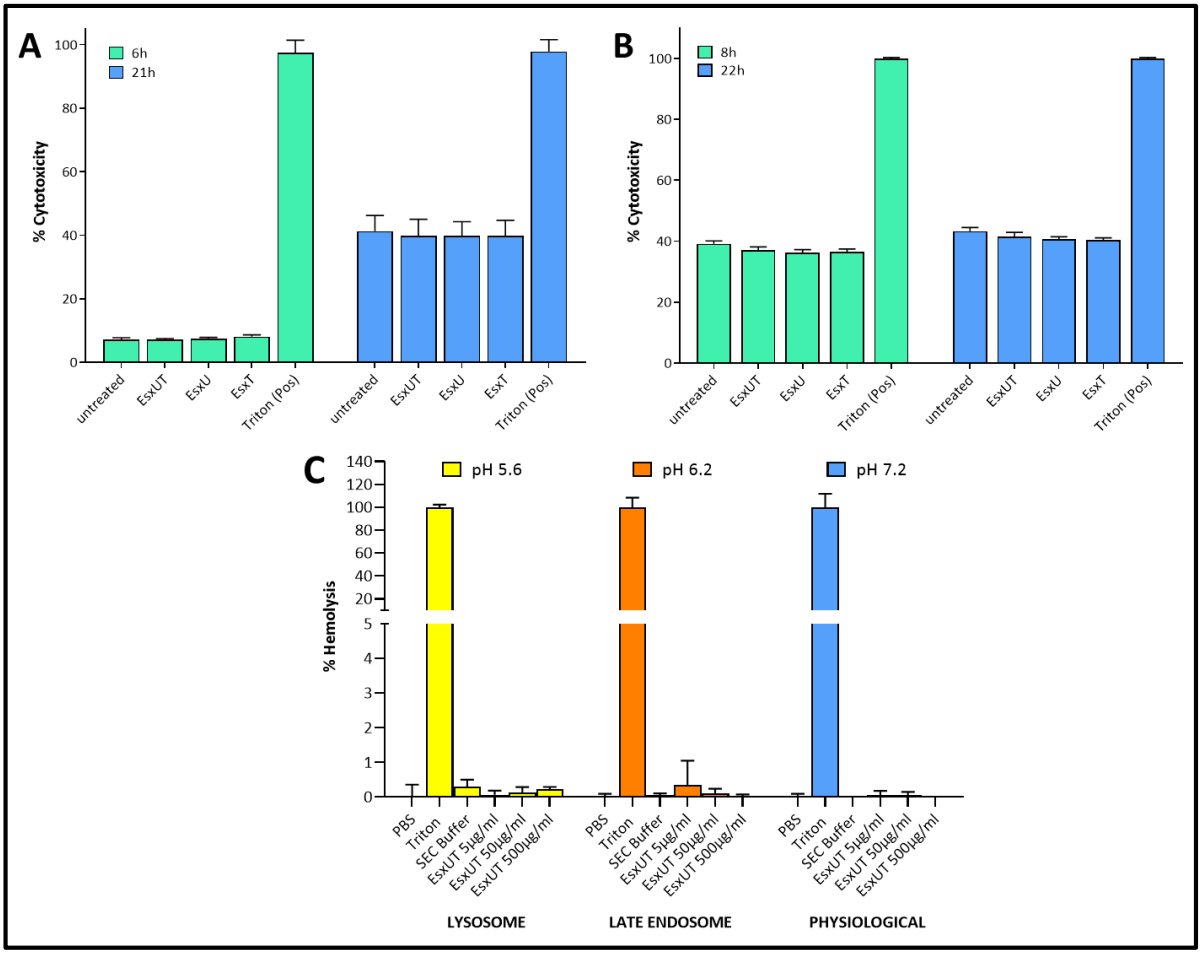

Figure 35. Lysis Potential of Mab purified proteins in human cells. Human neutrophils **(A)** and human macrophages **(B)** were incubated with Mab purified proteins EsxU/EsxT, EsxU and EsxT at a concentration of 5 ng/million cells for 6 and 21/22 hours. Results are the summary of 2 different experiments (2 different blood donors). **C:** Haemolysis assay in human red blood cells incubated with 5, 50 and 500 µg/ml EsxU/EsxT complex for one hour at pH correspondent to the lysosome, late endosome and physiological. For all experiments, Triton X-100 was used as a positive control.

3.2.3 EsxU/EsxT, EsxT and EsxU do not activate the inflammasome in human phagocytes

Proteins associated with the membrane of pathogenic bacteria could act as pathogen-associated molecular patterns (PAMPs) which activate the host's innate immune responses after being recognized by toll-like receptors (TLRs) and other pattern recognition receptors (PRRs). To explore the possibility of Mab EsxU/EsxT complex acting as a PAMP, different cytokine release experiments were performed. We checked for inflammasome NLRP3 activation by measuring cytokine secretion of IL-1β and IL-18. TNF-α secretion was also measured as it has been reported that Mtb EsxU/EsxT induce high levels of this cytokine in PBMCs of tuberculosis patients [85]. Moreover, tuberculosis progression and granuloma formation are highly dependent on TNF-α [86]. Therefore, neutrophils and monocyte-derived macrophages from different human donors were incubated with 5 ng/million cells of purified EsxU/EsxT, EsxU and EsxT proteins. The supernatants were collected at two different time points, filtered, and ELISAs were run to quantify the IL-18,

IL-1β and IL-8 (neutrophils) and IL-18, IL-1β and TNF-α (macrophages) released by the cells. Results are shown in Figure 36.

In none of the samples incubated with the purified proteins, the release of the analysed cytokines was different than in the untreated cells. Also, TNF-α release did not seem to be induced by any of the purified proteins.

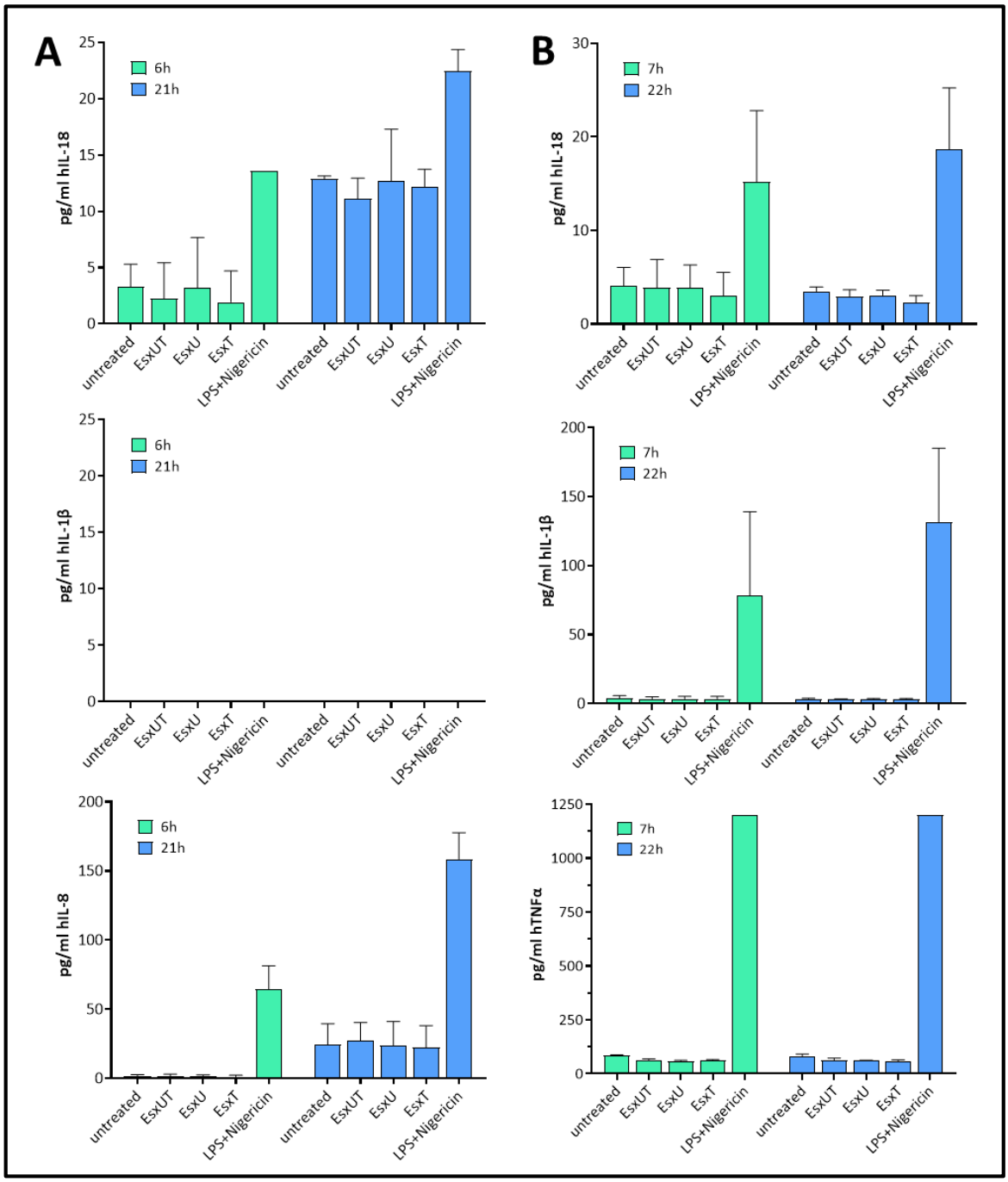

Figure 36. Cytokine secretion in human phagocytes. **A:** IL-18, IL-1β and IL-8 secreted from human neutrophils after 6 and 21 hours of incubation with Mab purified proteins EsxU/EsxT, EsxU and EsxT at a concentration of 5 ng/million cells. Results are the compilation of 3 different experiments (3 different blood donors). **B:** TNF-α, IL-1β and IL-8 secreted from human macrophages after 7 and 22 hours of incubation with Mab purified proteins EsxU/EsxT, EsxU and EsxT at a concentration of

5ng/million cells. Results are the compilation of 2 different experiments (2 different donors). Cells primed with LPS and incubated with nigericin were used as a positive control for the activation of the NLRP3 inflammasome.

The same experiments were run after priming the samples with LPS to test if the proteins needed a second signal to activate the inflammasome, but no difference in the results was observed (data not shown). These findings suggest that if Mab would secrete EsxU/EsxT before being phagocytized, the protein complex alone is not sufficient to activate a NLRP3 inflammasome response, nor TNF-α secretion, in human neutrophils and macrophages. Together with the results shown in Figure 35, these results also suggest that exposure of human neutrophils to Mab EsxU/EsxT complex may not contribute to the recruitment of neutrophils, as it does not cause apoptosis nor release of IL-8, an important chemoattractant for these cells.

Human PBMCs isolated from blood of a patient previously exposed to Mtb produce IFN-γ upon stimulation with Mtb proteins EsxA and EsxB. This response is orchestrated by mycobacteria-specific CD4 and CD8 T cells and can be quantified by an IFN-γ ELISpot test [87]. To investigate if Mab proteins EsxU/EsxT and EsxT induce a similar effect, cells from a cystic fibrosis patient who suffered from Mab infection were isolated, incubated with Mab EsxU/EsxT and EsxT at concentrations of 2.5 and 5 µg/ml, and analysed via an IGRA. No IFN-γ production was detected. This result also supports the idea that the EsxU/EsxT complex on its own is not capable of producing a cytokine response in phagocytes, and indicates that both EsxT and the heterodimer are not recognized as antigens.

3.2.4 Infection with different Mab mutant strains does not trigger different cytokine expression profiles in human macrophages

Mtb, upon phagocytosis, has the ability to induce host type I interferon expression (IFN-α, IFN-β, IFN-κ, IFN-δ, IFN-ε, IFN-τ, IFN-ω, and IFN-ζ) [88]. To investigate if Mab could induce a similar response, human macrophages were infected with Mab strains (S_WT, S_DKO, R_WT and R_DKO) at different MOI and analysed at two different timepoints for expression of human cytokines IFN-β and TNF-α and chemokines CCL3 and CCL4. No IFN-β expression was observed in any of the conditions assessed. For TNFα, CCL3 and CCL4, expression was higher at 4 hpi than at 24 hpi, but at both timepoints there was no difference in the expression between the WT and DKO strains, as shown in Figure 37. These results corroborate our previous findings using purified EsxU/EsxT that this heterodimer does not fulfil a role in activating the host cytokine response.

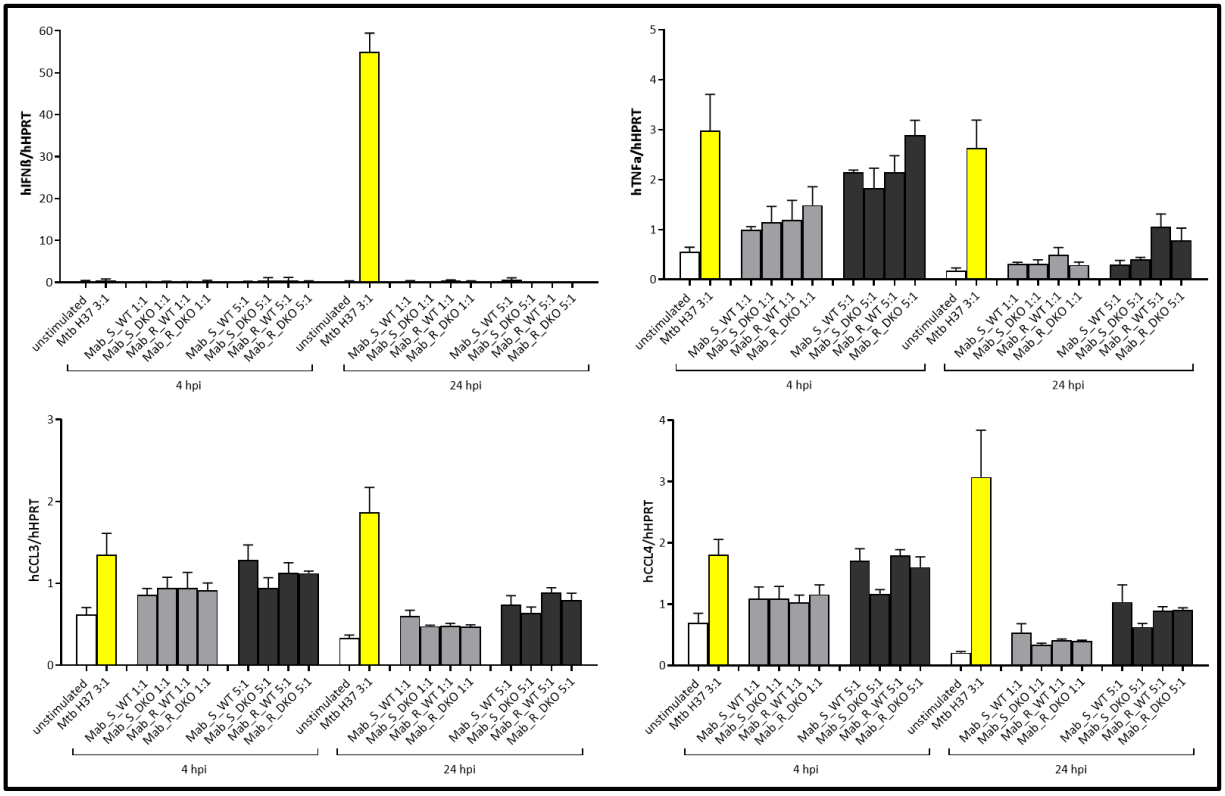

Figure 37. Cytokine expression (IFN-β, TNF-α, CCL3, CCL4) in human macrophages infected with Mab strains S_WT, S_DKO, R_WT and R_DKO at MOI of 1 and 5, for 4 and 24 hours. Bacteria were cultured in Middlebrook 7H9 medium supplemented with OADC and Tween-80. Mtb H37Rv strain was used as a positive control and the expression for all samples was normalized to the housekeeping gene HPRT. Values are the average of 3 different experiments.

3.2.5 No drug susceptibility difference in Mab mutant strains

Phenotypic drug susceptibility testing (pDST) is a routine diagnostic assay for assessing the susceptibility of mycobacterial strains against different compounds. For this test, the Minimal Inhibitory Concentration (MIC) is obtained for each strain treated with different kinds and doses of antibiotics. To investigate if the absence of EsxU/EsxT affected the susceptibility profile of Mab, DST was performed in Mab strains S_WT, S_DKO, R_WT and R_DKO and in Mab reference strain ATCC 19977. The results, shown in Figure 38, showed no or only minor differences among the strains that do not extend beyond the method-intrinsic variability of the assay, i.e. +/- one two-fold dilution step, suggesting that the absence of EsxU/EsxT has no effect on the MIC values of the mutated strains when compared to their respective WT strains and the Mab ATCC19977 reference strain.

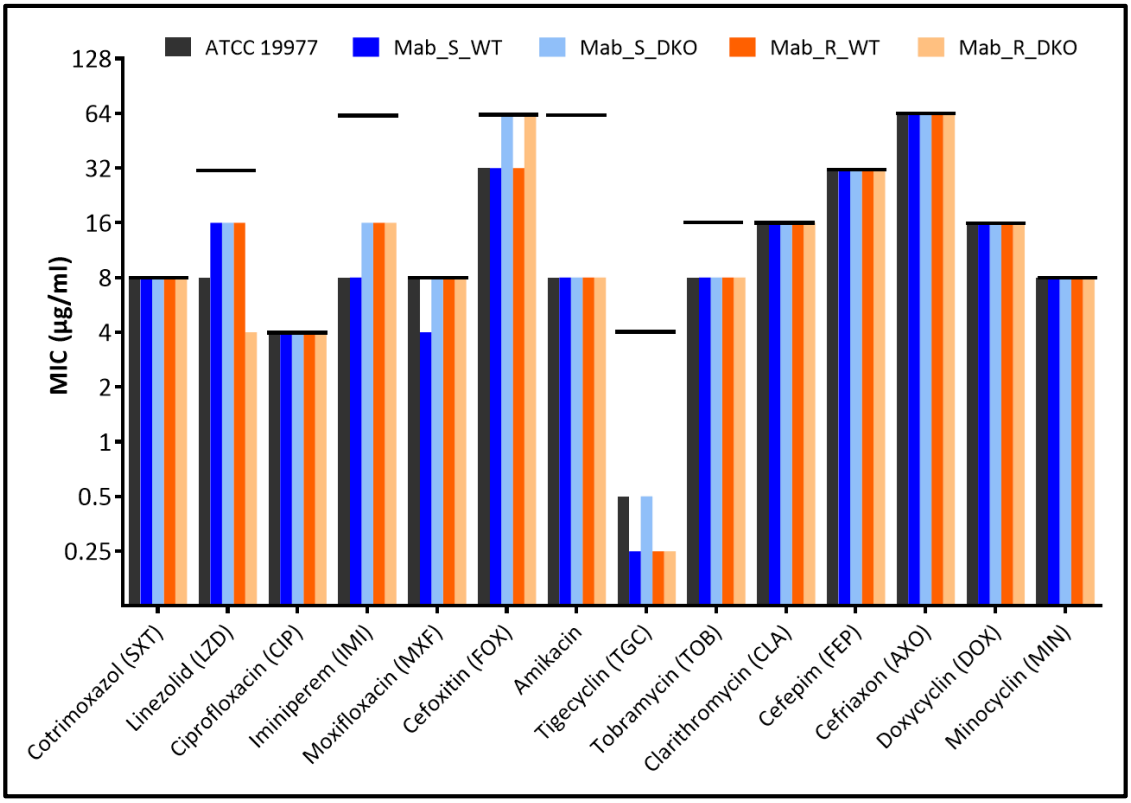

Figure 38. pDST in Mab mutant strains. pDST was performed in Mab strains S_WT, S_DKO, R_WT and R_DKO and in Mab reference strain ATCC 19977 using the Sensititre Myco RAPMYCOI assay. The results shown correspond to a reading at day 3. The black horizontal bars represent the highest antibiotic concentrations available in the test.

In summary, our results showed that the purified EsxU/EsxT complex itself does not lyse human cells or activate a cytokine-driven immune response in human macrophages. Furthermore, there was no difference in cytokine expression between human macrophages infected with Mab WT or DKO strains. This indicates that even if present in the mycomembrane, the EsxU/EsxT heterodimer may not directly interact with host receptors that could activate an inflammasome response or a host type I/II interferon response. Moreover, these results suggest that an Interferon-Gamma Release Assay (IGRA) for patients previously exposed to Mab cannot be developed using EsxU/EsxT as an antigen, as it does not induce IFN-γ secretion. However, the findings generated at IRIM and UVSQ clearly indicate a role of EsxU/EsxT in host-pathogen interaction and in the fate of the mycobacteria inside the phagosome, though the exact mechanisms require further investigation. Taken together, the observations indicate that despite its similarities in terms of protein sequence homology, the Mab EsxU/EsxT heterodimer differs from Mtb EsxA/EsxB in its localization and function.

3.3 Biophysical characterization of the EsxT/EsxU heterodimer

To better understand the interaction of the EsxU/EsxT complex with biological membranes, biophysical experiments were conducted in cooperation with Prof. Dr. Thomas Gutsmann and team at FZB. As a model of eukaryotic membranes, dioleoyl-phosphatidylcholine (DOPC) was used.

3.3.1 EsxU/EsxT interacts with DOPC membranes

NanoSpot approach

First, we performed several experiments using the **NanoSpot** approach. Using this technique, lipid bilayers are built over cavities filled with a fluorescent dye. On top of the membrane, the protein is added and if it inserts into the bilayer it would allow the dye to be released. The fluorescent signal is constantly measured to monitor the interaction between the protein and the membrane. Results of all experiments showed decreased fluorescence in the cavities upon addition of the EsxU/EsxT heterodimer, suggesting that it interacts with DOPC membranes, allowing the dye to escape and the fluorescence to decrease (Figure 39A).

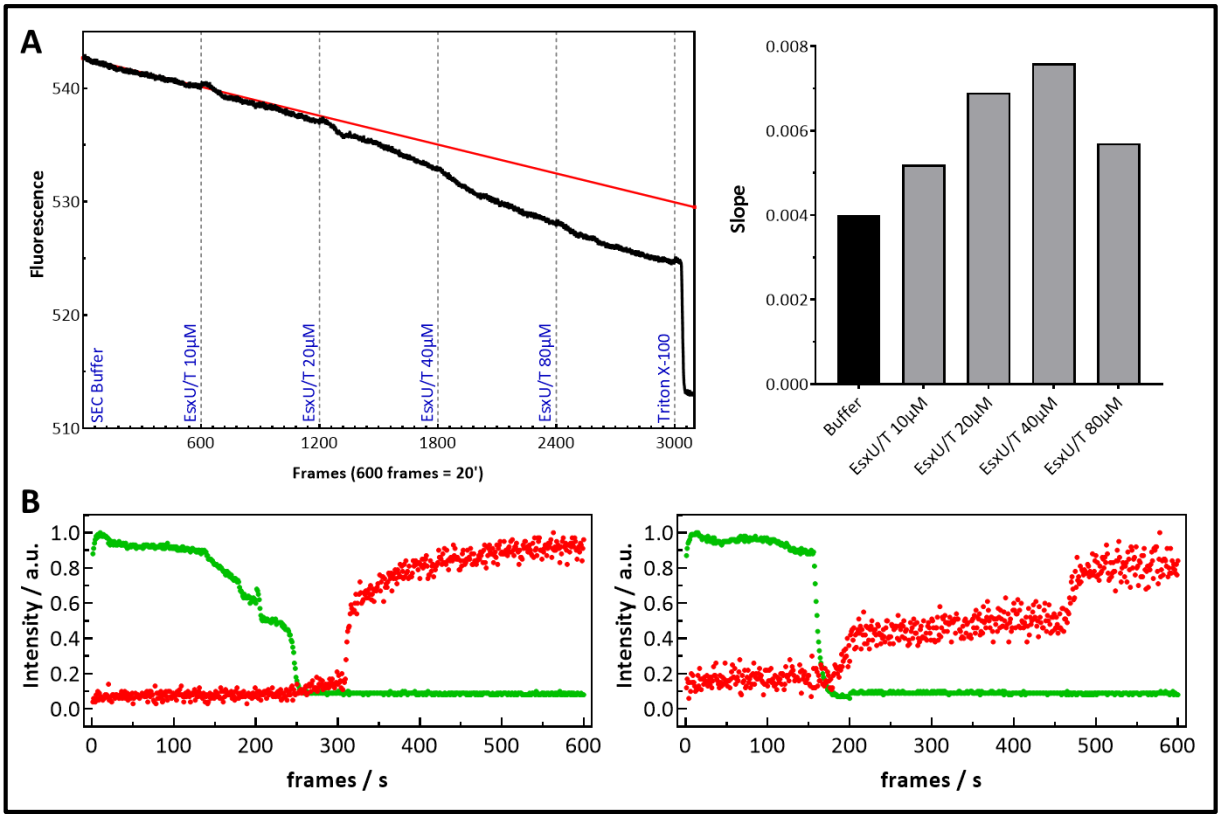

Figure 39. Dye influx and efflux through structures formed by EsxU/EsxT in DOPC membranes using the NanoSpot technique. DOPC bilayers were formed at 37°C and pH 7.2 on top of cavities filled with Atto488 carboxy fluorescence dye (green). **A:** Fluorescence (black curve) decreased as the EsxU/EsxT concentration increased up to 40 µM. Upon addition of Triton X-100 the fluorescence decreased abruptly. The red curve represents the tendency line of the loss of fluorescence if no protein would have been added. The sum of fluorescence signals from 300 cavities covered with DOPC membrane are plotted in this graph. **B:** Examples of single cavity analysis of experiments were two dyes were used. TexasRed-labelled dextran of 40,000 MW

was added outside the cavities before addition of EsxU/EsxT purified protein (final concentration=10 µM). The green dots represent the efflux of Atto488 carboxy efflux dye and the red dots represent the influx of TexasRed dye.

To obtain more information about the possible "pore" formed by the protein, a second fluorescent dye (TexasRed-labelled dextran of 40,000 MW) was added on top of the membrane before the addition of the heterodimer. Single-cavity analysis showed an increase in the fluorescence of the second dye in several cavities (Figure 39B), indicating the influx of dextran, and suggesting the formation of a higher order structure. Since dextran is polydisperse the diameter of the "pore" formed by EsxU/EsxT can only be given as a range.

Oriented Circular Dichroism (OCD)

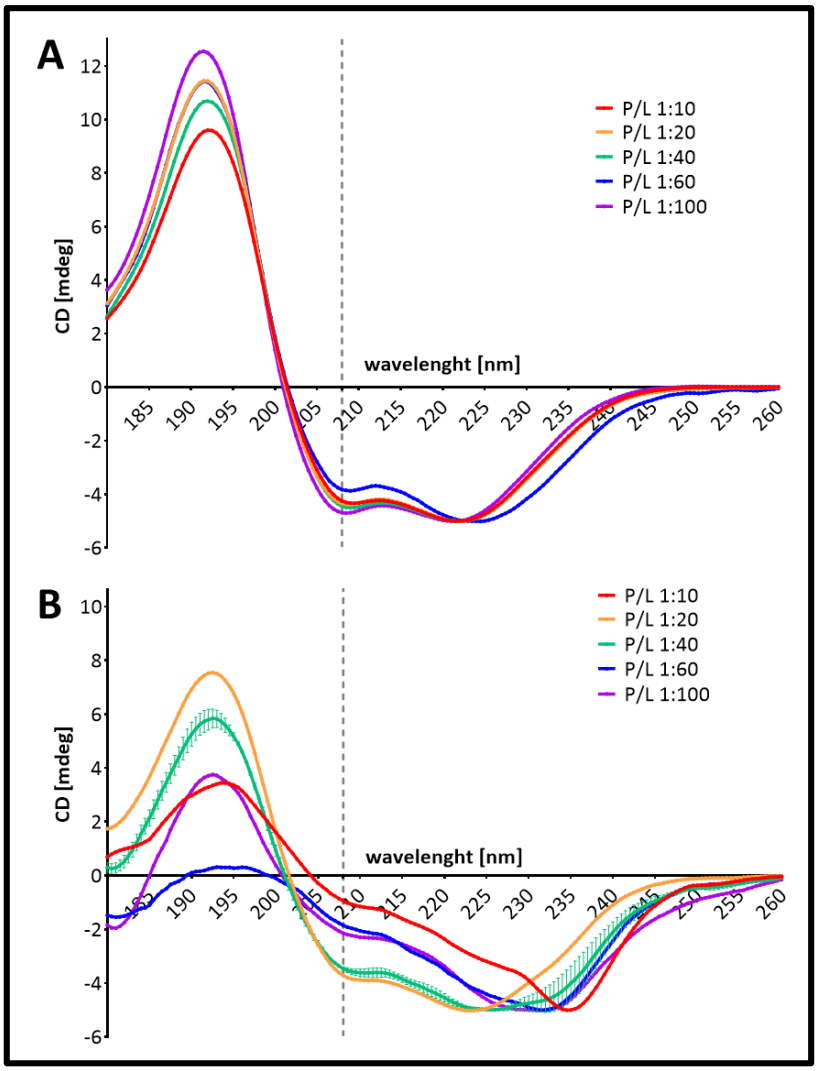

Figure 40. OCD profiles of Mab EsxU/EsxT in DOPC membranes. Experiments were performed using EsxU/EsxT, 10mM phosphate buffer, and DOPC in different protein/lipid (P/L) ratios. The dotted line at 208nm shows the distinguishing feature in the OCD spectra: if the absolute value of the amplitude decreases, approaching zero, it indicates that the protein is "tilted" in the membrane, approaching an "inserted" state [89]. **A:** pH 4.0 and **B:** pH 7.0. Spectra shown are representative of 1-3 different experiments.

To verify that the disruption of the DOPC membrane was due to insertion of the EsxU/EsxT complex and not caused by random aggregation of heterodimers on the bilayer surface, we used the UV-CD12 beamline at Karlsruhe Institute of Technology (KIT) to perform Oriented Circular Dichroism (OCD) experiments. This technique allows the elucidation of the orientation of proteins in membranes.

The line shape of OCD spectra showed that EsxU/EsxT adopted a classical α-helical conformation, as the curves presented a positive maximum at approximately 192 nm and two characteristic peaks of negative amplitude at 208 nm and 223 nm. In addition, inspection of the first negative peak of each OCD profile showed that the complex was indeed “tilted” in the membrane at both pH conditions (4.0 and 7.0), and that there was no protein/lipid (P/L)-dependent effect at pH 4.0 (Figure 40A). For reasons yet unknown, samples at pH 7.0 seemed to be not as stable as the ones at pH 4.0, generating curves of less amplitude and more variability within repeats (Figure 40B). DOPC forms membranes of 26.8 Ă of thickness, and can accommodate a peptide of 18 residues fully inserted. However, Mab EsxU and EsxT proteins contain approximately 40 aminoacids on each α-helix, making it very difficult for them to be fully inserted in a DOPC membrane and probably explaining this “tilted” orientation.

Planar supported tethered membranes approach

Knowing that the interaction between the EsxU/EsxT complex and the DOPC bilayers was due to protein insertion and not random aggregation on the surface, we used the **TethaPod** instrument to further characterize this interaction. In this approach, planar supported tethered membranes were built to study membrane conductance upon addition of a protein. Six independent experiments could be done at the same time, using buffers of different pH and adding protein to different final concentrations. In principle, when the membrane is formed and stability is reached, there is no conductance through the bilayer. If the protein of interest is added and interacts with the membrane, the conductance will increase as the protein inserts within the bilayer and allows a current to be established through the membrane.

Results showed that the conductance observed as a consequence of EsxU/EsxT interacting with DOPC membranes had a dose and pH-dependent behaviour, with the strongest effect visible at pH 3.0, followed by increased transmembrane conductance at pH 4.0. For pH values 5.0-7.0 the effects on the transmembrane conductance were minimal (Figure 41A). The same experiment was performed using purified EsxT homodimer (Figure 41C) and EsxU (Figure 41B). Data indicated that both purified EsxU and EsxT also interacted with the DOPC membranes, producing an even higher response in conductivity than the EsxU/EsxT heterodimer. When the protein concentration values were graphed on the x axis (second column of Figure 41), it could be observed that the increase of the conductance, however directly proportional to the final concentration, was not linear for all proteins tested.

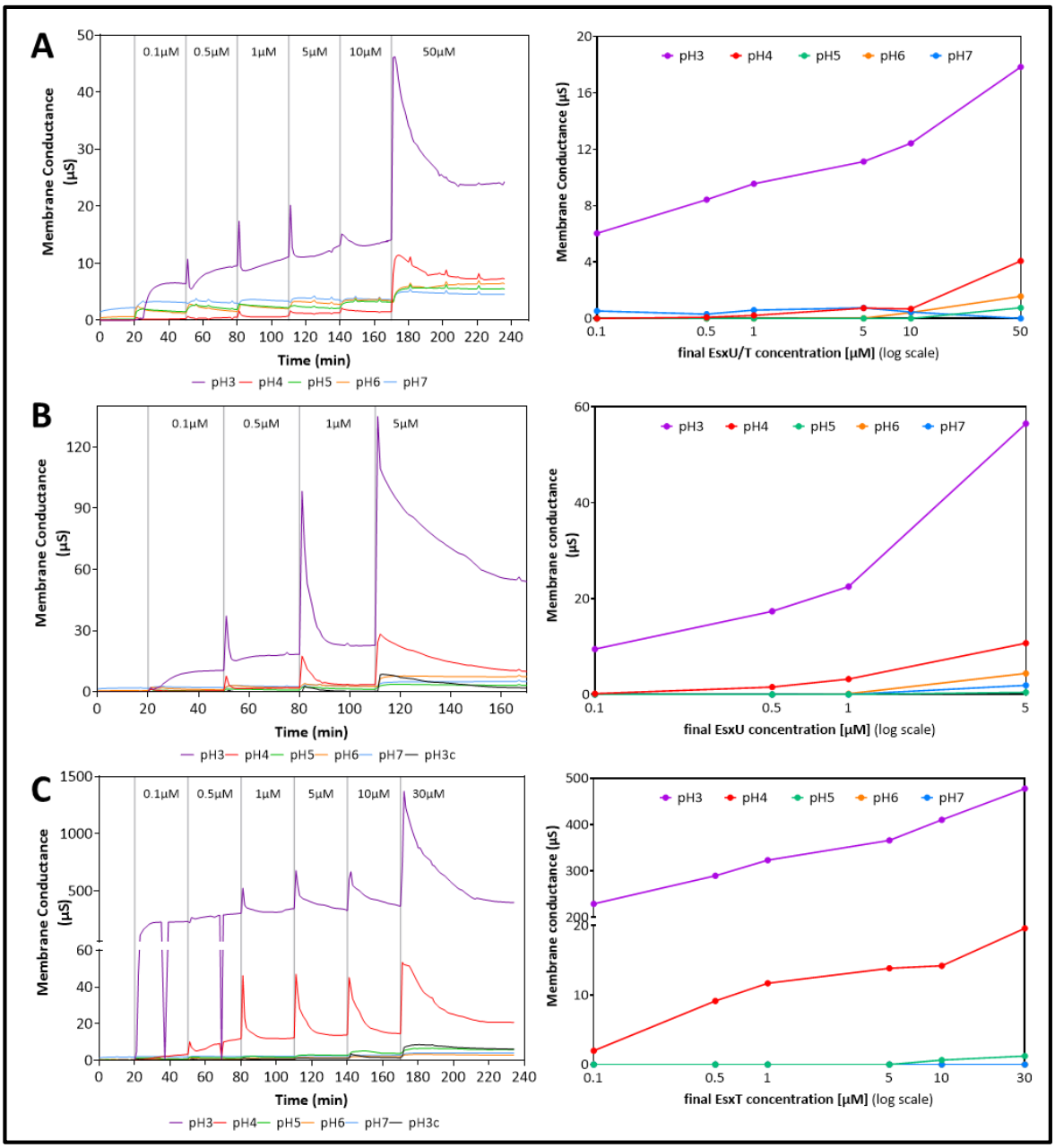

Figure 41. Conductance in DOPC membranes upon incubation with EsxU, EsxT and EsxU/EsxT. Planar supported DOPC bilayers were built on TethaPlates and the conductance of the membranes at 37°C was measured using the TethaPod instrument. **A:** EsxU/EsxT. **B:** EsxU. **C:** EsxT. Samples were measured at pH 3.0-7.0. Buffer at pH 3.0 was used as a control. Purified proteins were added every 30 min to reach different final concentrations: 0.1, 0.5, 1, 5, 10 and 50 µM for EsxU/EsxT; 0.1, 0.5, 1, and 5 µM for EsxU; 0.1, 0.5, 1, 5, 10 and 30 µM for EsxT. Experiments are representative of 3 different sets. pH 7.0 (blue), pH 6.0 (orange), pH 5.0 (green), pH 4.0 (red), pH 3.0 (purple), control (black).

Unsupported (free-standing) planar membranes

Finally, we performed experiments with unsupported planar DOPC bilayers. This approach allows us to change the pH of the buffer and the temperature, but also to apply a transmembrane voltage. For this purpose, we used a device in which we could perform four independent experiments at once, submitted the preparations to different transmembrane voltages, pH values and various concentrations of the EsxU/EsxT

heterodimer. As shown in Figure 42, heterogeneous transient lesions appeared at pH 7.2 and concentrations of 10 µM of EsxU/EsxT complex (green and brown boxes in diagram). When more complex was added, the lesions (pores) became stable.

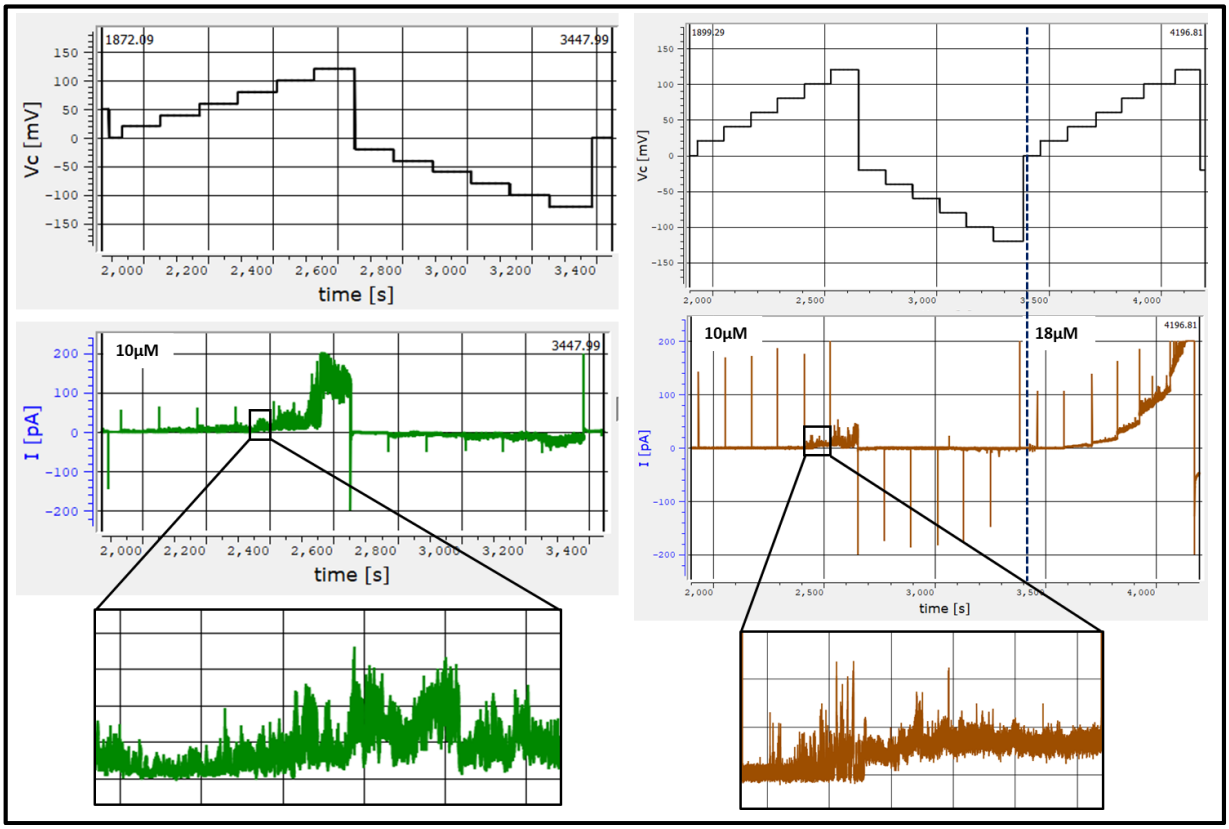

Figure 42. Current across DOPC membranes upon incubation with EsxU/EsxT at pH=7.2 and application of different voltages. Planar unsupported DOPC bilayers were built and the current across the membrane was measured upon addition of EsxU/EsxT at 36-37°C. Experiments were carried out in buffer at pH 7.2 and cavities of 100µm of diameter. Stimulus voltage with a duration of 2 min and amplitudes from -120mV to 120mV was applied and current response was recorded after addition of EsxU/EsxT to a final concentration of 10 µM or 18 µM. Note the heterogeneous transient lesions at 10 µM and the more stable lesions (pores) at 18 µM.

These pores were induced at +/-80mV but once formed, they were stable even at lower voltages, showing a symmetric behaviour in the I/V plot (Figure 43A, B). Furthermore, at pH 4.0, the pores were induced at lower voltages and were stable, showing an asymmetric curve in the I/V plot (Figure 43C, D). These experiments suggest that Mab EsxU/EsxT interaction with DOPC bilayers is both pH and voltage-dependent, and that the heterodimer is capable of forming stable pores.

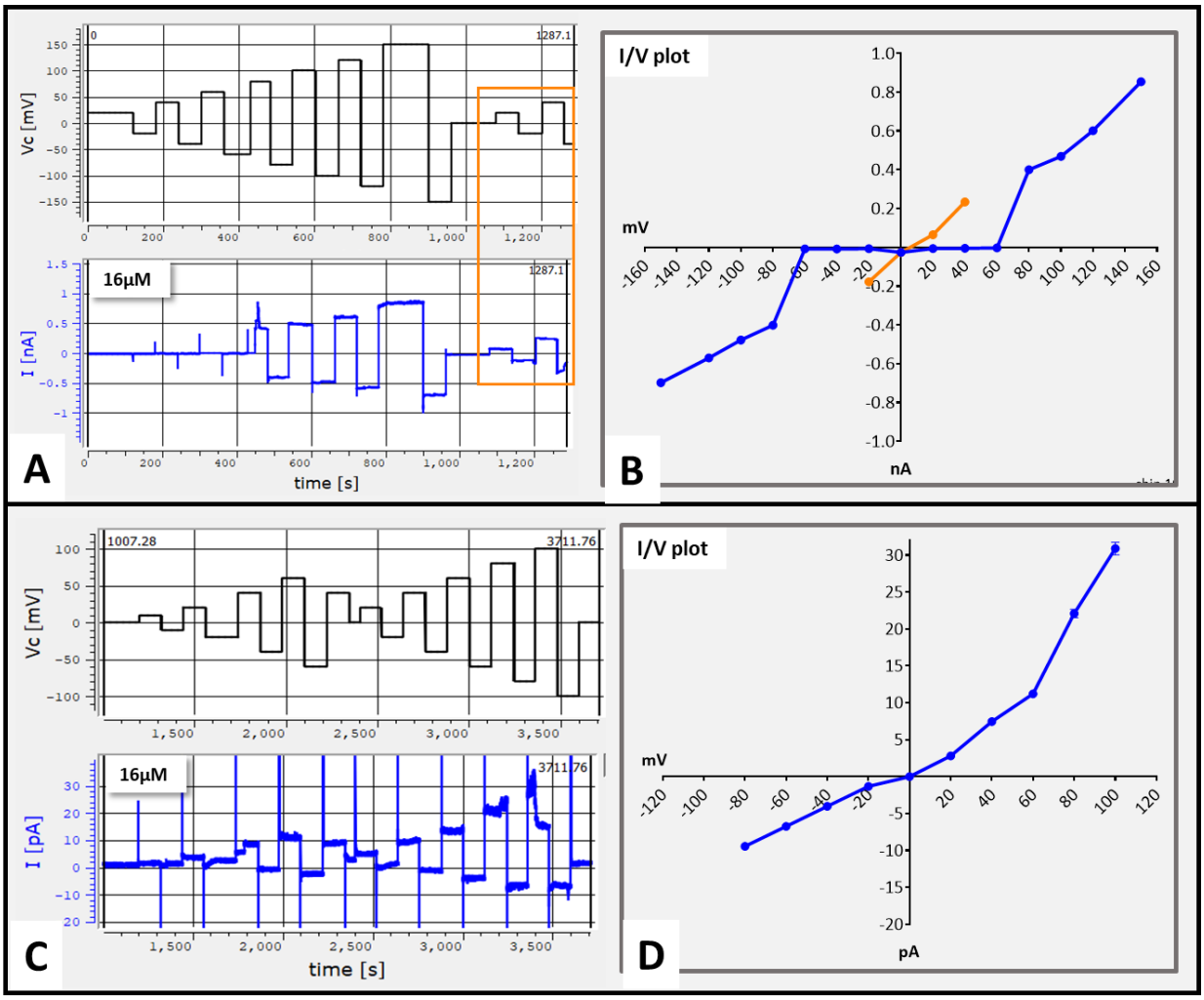

Figure 43. Current-voltage diagrams from unsupported DOPC membranes upon incubation with EsxU/EsxT. Planar unsupported DOPC bilayers were built and the current across the membrane was measured upon addition of EsxU/EsxT at 36-37°C. Experiments were carried out in buffer at pH 7.2 (A and B) and pH 4.0 (C and D) and cavities of 100 µm of diameter. **A:** Stimulus voltage with a duration of one minute and amplitudes from -150 mV to 150 mV was applied and current response was recorded after addition of 16 µM of EsxU/EsxT. Note that pores are induced at +/-80 mV. **B:** Current-voltage curve from the experiment shown in B. Note the symmetry of the curves. **C:** Stimulus voltage with a duration of 2 min and amplitudes from -100 mV to 100 mV was applied and current response was recorded after addition of 16 µM of EsxU/EsxT. Note the induction and stability of the pores formed. **D:** Current-voltage curve from the experiment shown in C. Note the asymmetry of the curve.

Considering all experiments together, results indicate that the EsxU/EsxT complex interacts with DOPC bilayers by inserting itself into the membrane, assuming a “tilted” position and probably adopting a higher order conformation. The conductance through the structure is pH, concentration and voltage-dependant, which gives insight on a possible regulating mechanism that depends on the pH. The heterodimer was shown to adopt a classical α-helical conformation and to have a pore-like behaviour.

3.3.2 EsxU/EsxT interacts with membranes formed with lipids extracted from Mab membranes

We next isolated Mab membranes and extracted the total lipids, which we then used in OCD experiments, becoming the first users who used bacteria-extracted lipids for these experiments at Karlsruhe Institute of Technology (KIT). The lipids formed very stable bilayers and, like with previous experiments with DOPC, the EsxU/EsxT complex was again found to be “tilted” in the membrane, in a P/L-dependent manner at pH 7.0, as shown in Figure 44.

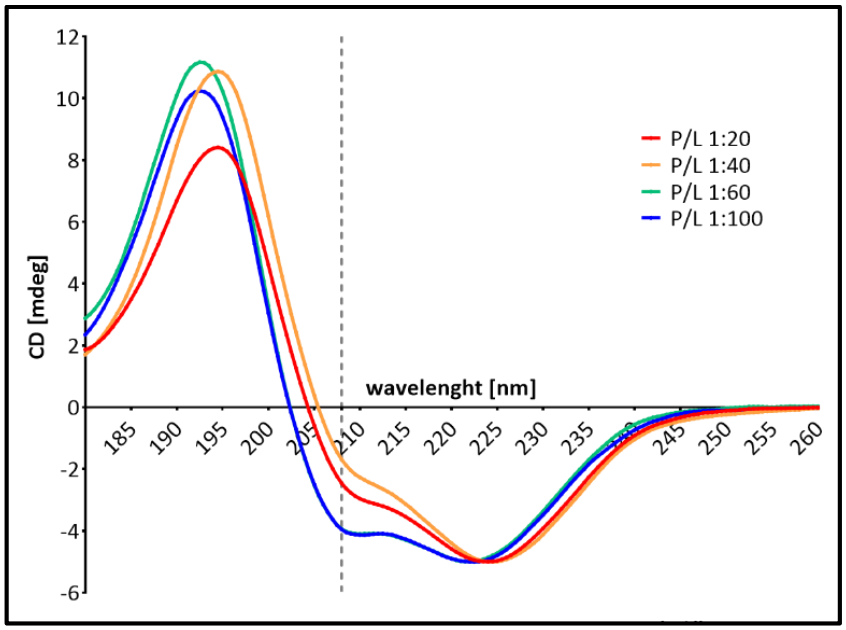

Figure 44. OCD profiles of Mab EsxU/EsxT in membranes formed with lipids isolated from Mab membranes. Experiments were performed using EsxU/EsxT, 10 mM phosphate buffer at pH 7.0, and lipids in different protein/lipid (P/L) ratios. Spectra shown are representative of 2 different experiments.

Considering the fact that the Mab lipid extract used contained a mixture of all membrane lipids that were combining to form a bilayer that probably didn’t exist in real life (as the lipids in the outer and inner membrane are different), we decided to separate the lipids from the outer (OM) and the inner membrane (IM) and perform experiments using supported (TethaPod) and unsupported (planar membranes) bilayers.

As shown in Figure 45, the conductance across the OM and IM was pH-dependent, having the lowest values at pH 5.0-7.0. Interestingly, this conductance didn’t depend on protein concentration, in contrast to the DOPC results shown earlier.

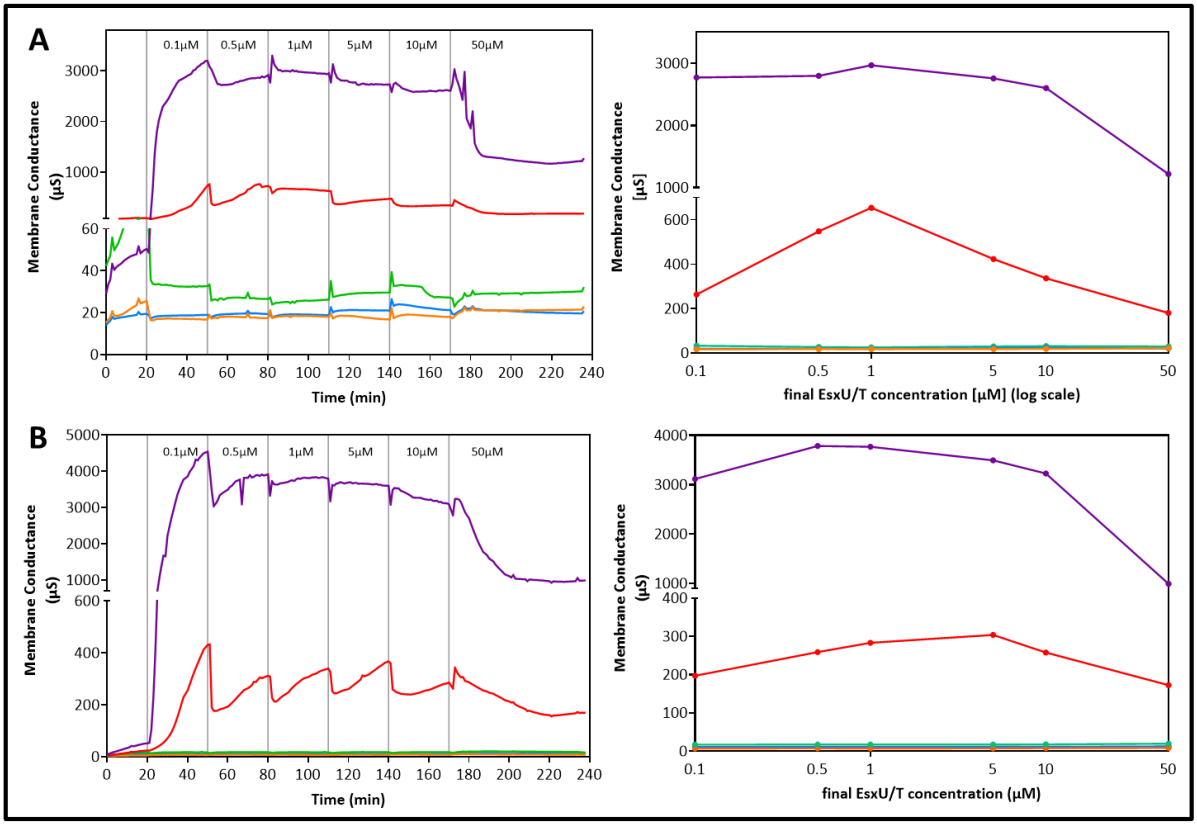

Figure 45. Conductance in membranes formed with lipids isolated from Mab inner (IM) and outer (OM) membranes upon incubation with EsxU/EsxT. Planar supported bilayers were built on TethaPlates and the conductance of the membranes at 37°C was measured using the TethaPod™ instrument. **A:** IM lipids **B:** OM lipids. Samples were measured at pH 3.0-7.0. Buffer at pH 3.0 was used as a control. Purified proteins were added every 30 min to reach different final concentrations: 0.1, 0.5, 1, 5, 10 and 50 µM for EsxU/EsxT. Experiments are representative of 3 different sets. pH 7.0 (blue), pH 6.0 (orange), pH 5.0 (green), pH 4.0 (red), pH 3.0 (purple), control (black).

Next, we carried out unsupported planar bilayer experiments. Using Mab IM lipids, we could achieve membrane formation at 37°C and pH 4.0 and pH 7.2. However, testing transmembrane voltages from 0 to +/- 120 mV no current could be measured upon addition of up to 30 µM EsxU/EsxT (data not shown). Using OM lipids, no membrane could be formed at 37°C and pH 7.2. At pH 4.0, low capacitance membranes could be formed and were tested applying transmembrane voltages from 0 to +/- 120 mV. Upon addition of EsxU/EsxT complex, transient lesions (some of them ending in membrane break) could be observed at different voltage values, without finding consistency in the experiments.

Taking together all results, using DOPC and Mab lipids, we observed that changes in the conductance and, hence, the interaction of the EsxU/T heterodimer with lipid bilayers was not only dependent on protein concentration, pH, and transmembrane voltage but also dependent on the lipid composition of the bilayer.

In summary, the conductance through the structure formed by EsxU/EsxT in lipid bilayers is pH, concentration, voltage and lipid-dependant, having more activity (higher conductance) at pH 4.0.

3.3.3 Mutations in the WXG and secretion motifs of EsxU/EsxT affect its interaction with DOPC membranes

To investigate how mutations in the WXG motif and the secretion signal sequence of Mab EsxU and EsxT would affect their interaction with DOPC membranes, 3 heterodimers carrying mutations were designed, overexpressed in *M. smegmatis* and purified. In the first mutant (EsxU/EsxT$_{A43W}$), a mutation in the AEG sequence of EsxT was introduced, converting it into a WEG sequence (WXG motif). As a result, both peptides of the new complex had WXG motifs. In the other 2 mutants (EsxU/EsxT$_{D87L}$ and EsxU/EsxT$_{D87N}$), the D residue in the secretion signal (HxxxD/ExxhxxxH) of EsxT was mutated either to residue L or N, leaving the heterodimeric complex with one WXG motif and no secretion signal. The 3 proteins were purified similarly to the WT and were resuspended in SEC buffer. Interestingly, all mutant proteins eluted as heterodimers (Figure 46A), indicating that the mentioned mutations did not affect heterodimerization. In addition, all proteins could be identified in a western blot using the anti-EsxU/EsxT antibody described in section 3.1.3 (Figure 46B).

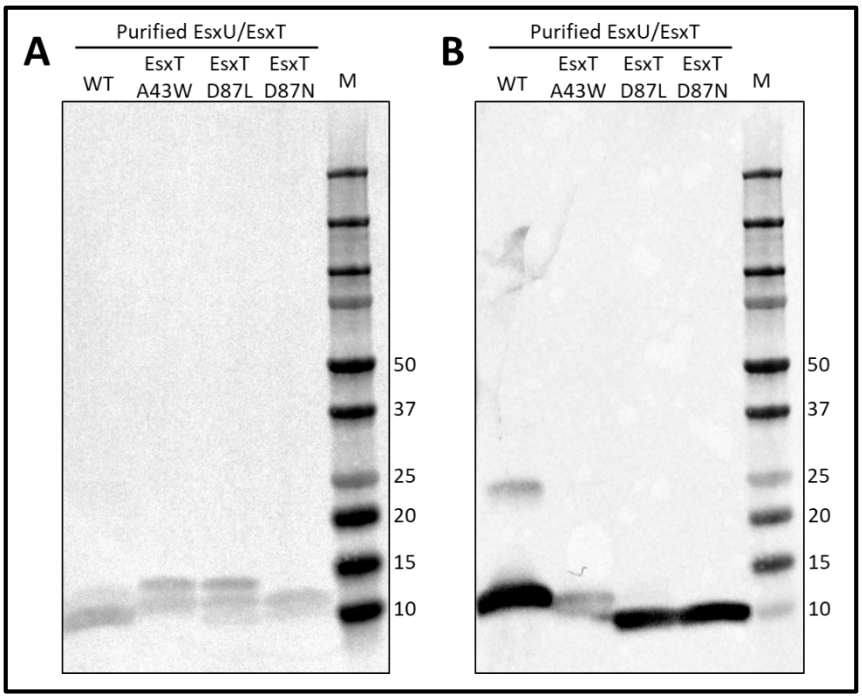

Figure 46. Purified EsxU/EsxT WT and mutant proteins. 5 µg of each purified protein were run in a 4-20% SDS-gel and transferred to a 0.2 µm nitrocellulose membrane. **A:** Ponceau-stained nitrocellulose membrane showing at least 2 bands for each sample. **B:** Western blot probed with anti-EsxU/EsxT antibody showing the presence of a band at approximately 10 kDa for all proteins, and a faint band at approximately 23 kDa for the WT protein.

Experiments using the TethaPod approach were conducted similarly to the ones previously described using the WT EsxU/EsxT heterodimer. As shown in Figure 47, the conductance had a dose and pH-dependent behaviour, with the strongest effect visible at pH 4.0. Among all 4 proteins tested, EsxU/EsxT$_{A43W}$ showed the highest conductance at both pH values, directly proportional to the concentration, and much higher than the one observed for the WT complex. EsxU/EsxT$_{D87L}$ and EsxU/EsxT$_{D87N}$ showed almost no interaction with the

membrane, suggesting that one WXG motif and one secretion signal are the minimum requirements for EsxU/EsxT interaction with DOPC membranes.

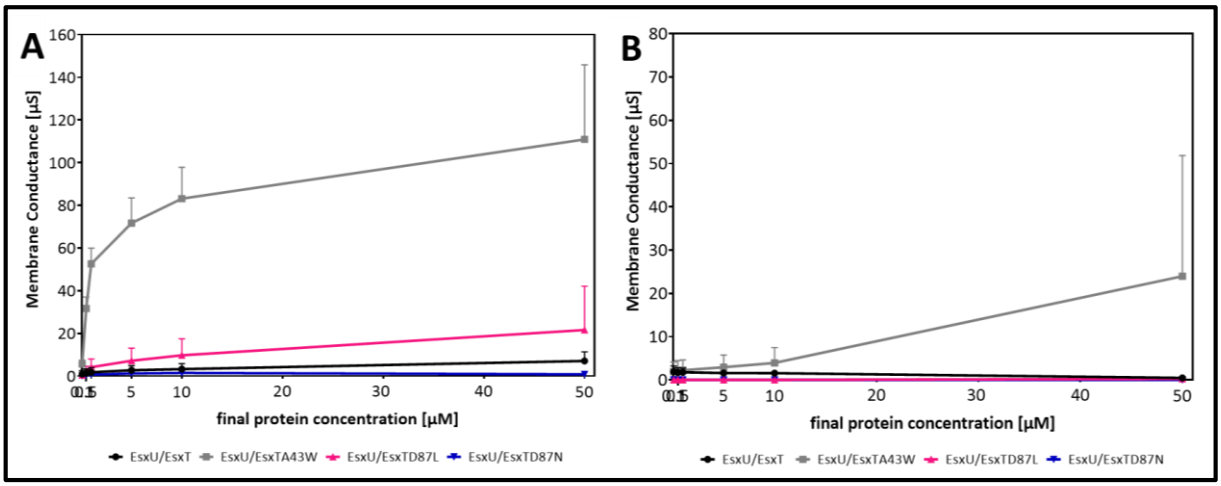

Figure 47. Conductance in DOPC membranes upon incubation with EsxU/EsxT WT complex and the mutant versions: EsxU/EsxT$_{A43W}$, EsxU/EsxT$_{D87L}$ and EsxU/EsxT$_{D87N}$. Planar supported DOPC bilayers were built on TethaPlates and the conductance of the membranes at 37°C was measured using the TethaPod^{TM} instrument at pH 4.0 **(A)** and pH 7.0 **(B)**. Purified complex was added every 30 min to reach different final concentrations: 0.1, 0.5, 1, 5, 10 and 50 µM. Buffers were used as negative controls. In the graphed values the conductance recorded for the negative controls has already been subtracted from the original values recorded for the heterodimers. Experiments are representative of 3 different sets.

Next, experiments with unsupported DOPC planar bilayers were performed. As shown in Figure 48, EsxU/EsxT$_{A43W}$ complex interacts with DOPC membranes at pH 7.2. Different to the behaviour of the WT complex, this interaction was not voltage-dependent. Most current readings were obtained at a transmembrane voltage of -80 mV. In addition, the current (I) vs time graphs indicated gated events (open-close) in several experiments. The difference in current between the “open” and “closed” states was approximately 5 pA, and intermediate states could sometimes be observed. At pH 4.0 and adding 16 µM of complex, 8 of the 15 membranes tested broke abruptly at different voltages, something not frequently observed in experiments with the WT protein.

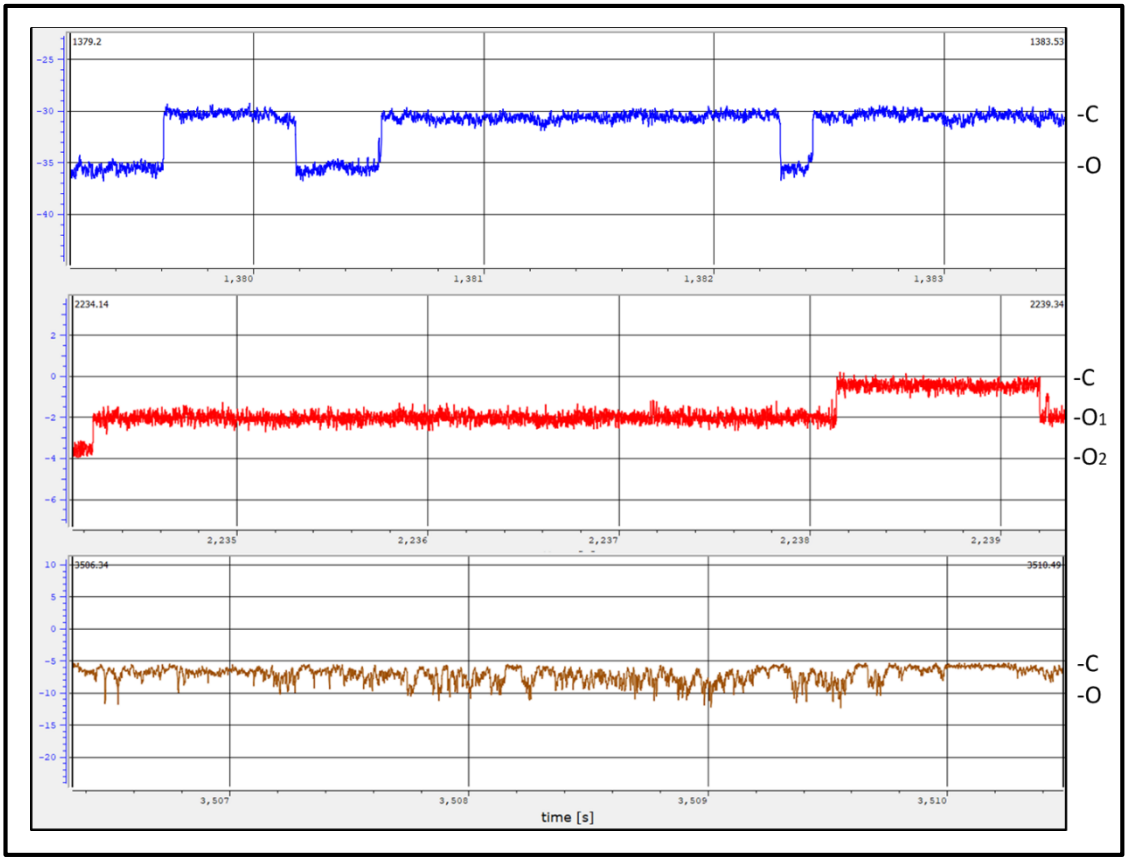

Figure 48. Current-time diagrams from unsupported DOPC membranes upon incubation with EsxU/EsxTA43W. Planar unsupported DOPC bilayers were built and the current across the membrane was measured upon addition of 16 µM of EsxU/EsxT$_{A43W}$ at 36-37°C. Experiments were carried out in buffer at pH 7.2 and cavities of 100 µm of diameter. A stimulus voltage of -80 mV was applied and current response (pA) was recorded. C = closed; O = open.

Similar experiments with mutants EsxU/EsxT$_{D87L}$ and EsxU/EsxT$_{D87N}$ at pH 4.0 and pH 7.2 showed no interaction with DOPC bilayers (data not shown).

In summary, these results suggest that the WXG motif modulates the interaction of the EsxU/EsxT heterodimer with lipid membranes. In the particular case of Mab EsxU/EsxT, a WXG motif on each monomer increases the interaction between the heterodimer and DOPC bilayers. Moreover, the presence of a secretion signal as described by Poulsen et al. [56] (HxxxD/ExxhxxxH) seems not to be required for heterodimerization. However, the results showed that at least one WXG motif and one secretion signal are required for EsxU/EsxT interaction with DOPC membranes.

4. DISCUSSION

In this study we have expanded the current knowledge on the Mab ESX-4 locus, in particular on two of its genes, *esxU* and *esxT.* We have characterized their expression, the organization and localization of the proteins they encode, and we have demonstrated a role for the EsxU/EsxT heterodimer in Mab pathogenicity and as mediators of pore formation in lipid bilayers. The most important findings of this work are: the elevated expression levels of *esxU* and *esxT* in Mab clinical isolates as compared to the type strain, the stable organization of the EsxU/EsxT complex as a 1:1 heterodimer that localizes in the mycomembrane, its ability to form pores in DOPC membranes and, in collaboration with colleagues from IRIM and UVSQ, its role in host-pathogen interaction and phagosomal escape.

Previously, the ESX-4 secretion system was considered non-functional due to the absence of the EccE structural component in most mycobacteria. Moreover, very few reports addressed the study of this mycobacterial system [51-54]. Mab ESX-4 attracted our interest when a recent investigation found this system to be functional and associated with virulence [53]. Considering the aforementioned study and the presence of only two T7SS in Mab (ESX-3 and ESX-4), we initially hypothesized that ESX-4 could be the key secretion system associated with Mab virulence and that EsxU and EsxT could fulfil a role comparable to EsxA and EsxB from Mtb, namely that EsxU and EsxT would be secreted and subsequently interact with host phagosomal membranes to facilitate the escape of mycobacteria from the intraphagosomal compartment.

Our first approach into the study of the Mab ESX-4 locus was to assess its gene expression pattern. RT-PCR results in the Mab reference strain indicated that *esxU* and *esxT* are expressed in similar quantities, supporting a 1:1 stoichiometry. Interestingly, our results also showed that *esxU* and *esxT* are expressed at significantly higher levels than the other genes encoded within the Mab ESX-4 operon. Further analysis of the secondary structure of the transcripts revealed that there are protective loops flanking the *esxU-esxT* mRNA (data not shown), probably stabilizing this part of the chain and keeping it from degradation, which could explain the higher expression levels observed for *esxU* and *esxT* in comparison to the other genes encoded in the operon. This protective effect has previously been reported in *Bacillus subtilis* for the *yukE* operon [90] and the *gapA* operon [91]. Based on the principle of parsimony, which states that a cell does not expend energy generating large quantities of transcripts it does not need and based on the fact that protective mechanisms would not evolve to avoid degradation of transcripts that are not required, these results suggest that EsxU and EsxT are important for the cell and are required during normal culture conditions. In addition, further experiments showed higher expression levels of *esxU* and *esxT* in Mab clinical strains in comparison to the reference strain, suggesting upregulation and, very likely, relevance during infection.

Using *M. smegmatis* as an expression platform we were able to overexpress Mab *esxU* and *esxT*. Our results showed that these genes, when expressed together, translate into proteins that form a soluble and stable 1:1 complex that can be purified as an un-tagged heterodimer, without the use of detergents. OCD experiments confirmed that the heterodimer has an α-helical conformation. Our results build upon previous studies that have characterized EsxU (Rv3445c) and EsxT (Rv3444c) of the Mtb ESX-4 system, showing that they form a 1:1 stable complex with predominantly α-helical conformation [85]. In the aforementioned study, both genes were cloned and expressed separately in *Escherichia coli*, found to form inclusion bodies, and were purified from the insoluble fraction of the cell lysate. This difference in solubility, also found in the present study when purifying EsxU and EsxT that were cloned and expressed individually, corroborates

that Esx protein pairs are more stable when together. Based on these findings, we conclude that Mab EsxU/EsxT exists mainly as a heterodimer that can be recognized and translocated by Mab ESX-4.

In 2014, it was proposed based on YukE (WXG substrate of the *Bacillus subtilis yuk* system) that the ESX secretion machinery needed only one signal to recognize and secrete a substrate. This signal was described as being composed of two features, a WXG motif located in the middle of one hairpin, and one C-terminal secretion signal (YxxxD/E) located on the other hairpin which upon dimerization would render both features on one side of the complex [92]. If this is true for all ESX substrates, the Mab EsxU/EsxT complex would be secreted as it fulfils these requirements. EsxU has a WXG motif and EsxT has a C-terminal signal (HxxxD/ExxhxxxH), which together would reside on one side of the heterodimer. Several structural studies have shown that ESX components EccB-E and MycP are arranged within the inner membrane, forming an oligomeric complex capable of translocating substrates [47, 48, 78, 93]. Our previous results indicate that Mab ESX-4 recognizes the EsxU/EsxT heterodimer and that it facilitates its translocation. However, *Bacillus subtilis* is a monoderm bacteria and upon translocation through the cytoplasmic membrane, substrates can reach the exterior of the cell. In the case of mycobacteria, which possesses an additional membrane (mycomembrane), this “exterior” would correspond to the space between both membranes (the periplasmic space) as the secretion machinery spans mainly the inner membrane. To reach the external environment, an associated porin-like structure is needed, but such an assembly has not yet been reported. From the periplasmic space, EsxU/EsxT appear to be mainly interacting with the mycomembrane as we have found large amounts of EsxU/EsxT in Mab membrane fractions, but not in the environment outside the mycobacterial cell. In addition, we could demonstrate a difference in density and cell aggregation between the WT and *ΔesxUΔesxT* DKO strains of the Mab S variants supporting the notion that the EsxU/EsxT heterodimer plays a role in supporting the structure of the bacterial cells. In addition, a disturbance in auto-aggregation suggests impaired quorum sensing. Izquierdo et al. have previously suggested that Mtb senses environmental changes via ESX-4 [54], after the ESX-1-mediated phagosomal escape. In addition, Clark et al. reported in their study that the deletion of the ESX-4 locus strikingly changed the colony morphology of *M. smegmatis*, suggesting that alterations in cell wall composition or structure may also be directly or indirectly associated to ESX-4 activation [51].

Further experiments in our study showed that the EsxU/EsxT heterodimer, by itself, had no lytic potential in human cells, and could not trigger any cytokine response in human phagocytes. This suggests that if the heterodimer would be in direct contact with the host cells, it could not lyse them, activate the inflammasome, or induce TNF-α secretion. Previous studies have shown activation of cytokine response upon incubation with Mab [53], however these experiments were done with whole bacteria, for which different immune activators can be suggested. In addition, no IFN-γ could be detected in an ELISpot test where PBMCs from a Mab infected patient were exposed to Mab EsxU/EsxT and EsxT. Similar results were found for Mtb EsxU and EsxT as they did not induce secretion of IFN-γ after PBMCs of a TB patient were stimulated with these proteins (separately) for 48 hours [85]. Incubation of human macrophages with the S and R variants of Mab in their wild-type and DKO forms resulted in no difference in the expression of different cytokines at different timepoints and MOI, again suggesting that EsxU/EsxT itself is not recognized by a receptor or a surface protein that could initiate an immune response. Furthermore, profiles of antibiotic resistance were similar among the wild-type and mutant strains, suggesting that EsxU/EsxT does not play a role in the protection of the bacteria through drug efflux.

While performing these experiments in Germany, our collaborators at IRIM and UVSQ were studying the differences in virulence between the WT and *ΔesxUΔesxT* DKO variants in the S Mab morphotype. Their findings clearly point to a role of EsxU/EsxT in host-pathogen interaction and in the fate of Mab inside the phagosome. In addition, our biophysical experiments demonstrate that the EsxU/EsxT heterodimer is capable of directly interact with lipid membranes in a way that is dependent on protein concentration, pH, transmembrane voltage and lipid composition. As we demonstrated that these proteins are highly abundant in the mycobacterial membrane, it appears possible that individual EsxU/EsxT heterodimers form a higher order structure, corresponding to an oligomeric arrangement of EsxU/EsxT.

Taking all results together, we can propose two models for the arrangement and possible function of EsxU/EsxT (Figure 49). The first model presents an oligomeric arrangement of EsxU/EsxT heterodimers associated to the mycomembrane, forming a channel. This channel allows to complete the secretion of substrates recognized by the ESX-4 inner membrane complex from the cytosol to the cell exterior. The substrates could be involved in quorum sensing, phagosomal escape, and other processes associated with virulence and host adaptation. The channel function (open/close, oligomerization, etc.) could respond to changes in pH and transmembrane voltage like the ones that occur when Mab is inside the phagosome. In other words, it could be regulated directly by changes in environmental conditions or indirectly by forming part of a regulon. According to this model, if EsxU/EsxT is absent, substrates involved in phagosomal escape cannot be secreted and therefore the mycobacteria remain inside the phagosome. Previous studies have reported that Mab is capable not only of surviving inside acidic phagosomes for up to 72 hours, but also of maintaining proliferative capacity afterwards [13] [94]. Therefore, under these conditions, Mab would evade the host immune system response even better and remain hidden within phagosomes, creating a reservoir of bacteria. Since phagosomal escape eventually triggers cell death, without phagosomal escape the phagocyte would internalize more bacteria but cells would survive, increasing the number of infected macrophages.

The second model proposes a number of EsxU/EsxT heterodimers associated to the mycomembrane, without any higher order organization (Figure 49). Upon phagocytosis, these heterodimers would come in close proximity with the inner leaflet of the phagolysosomal membrane. In response to a trigger such as a decrease in pH following phagosome-lysosome fusion, EsxU/EsxT interacts directly with the phagosomal membrane, resulting in a loss of membrane integrity and subsequent escape of the bacteria from the phagosome. Thus, in this model EsxU/EsxT would have a direct effect on phagosomal escape, which could also be modulated directly by the environment or indirectly by a signalling pathway.

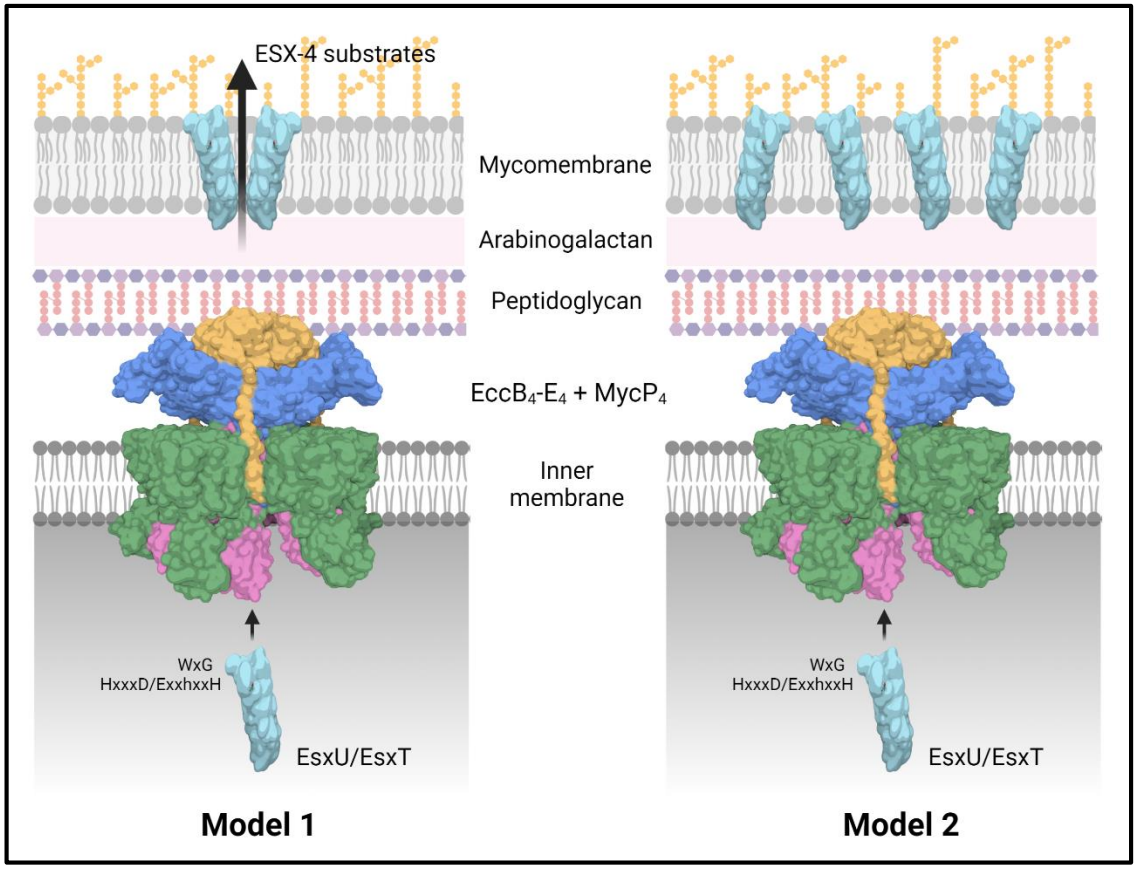

Figure 49: Proposed models for the organization and possible function of Mab EsxU/EsxT. The inner membrane organization of the components has been graphed in analogy to the structure published by Bunduc et al. [78]. The EsxU/EsxT heterodimer is represented based on its homologous in Mab, EsxE/EsxF. Figure created with BioRender.com.

Esx proteins have been classified as EsxA-like and EsxB-like WXG proteins based on their protein sequence, and most of what is believed comes from extending findings from studies addressing Mtb EsxA/EsxB. However, several studies suggesting other roles for the Esx proteins have been published. These studies have found distinct surface features [95], different expression profiles [96], and different nature of membrane interaction and cellular localization [97] when studying Esx pairs, which clearly points to distinct functional roles. For example, Mab EsxU and EsxT share only 26% and 37% sequence identity and 51% and 62% sequence homology with Mtb EsxU and EsxT, respectively. In addition, the WXG motif in these EsxT homologues is quite different. As presented here and in the study by Pandey et al. [85] these heterodimers have different localizations.

Based on the literature and our results, we propose that recognition, cellular localization, quaternary structure and function of Esx heterodimers is predetermined by the presence of WXG and secretion signals, the helix residue distribution, as well as the lipid composition of the target membrane. However, more research is required to further elucidate the exact roles of different Esx pairs among mycobacterial species and to understand how their function is regulated.

Finally, our findings point to a need for further investigations into the secretome of Mab WT and Mab *ΔesxUΔesxT* DKO strains, for example using mass spectrometry. Differences in the respective secretomes would confirm that EsxU/EsxT is involved in protein secretion, favouring

the first model proposed in this study. Second, further investigation of the structure of EsxU/EsxT is required, such as obtaining the heterodimer crystal structure, and performing single-particle analysis to elucidate the oligomeric conformation of the complex associated to the membrane. Third, a transcriptional analysis in Mab reference strain and in a *sigM* overexpressing strain is needed to verify if ESX-4 belongs to Mab SigM regulon. Identifying which genes are upregulated next to *esxU* and *esxT* could allow us to better understand the process of infection. Furthermore, in an effort to further investigate the effect of WXG motifs and secretion signals in the cellular localization of Mab EsxU/EsxT, experiments using Mab DKO complemented with the mutant proteins (EsxU/EsxT$_{A43W}$, EsxU/EsxT$_{D87L}$ and EsxU/EsxT$_{D87N}$) will be needed.

5. SUMMARY IN ENGLISH

Mycobacterium abscessus (Mab) is a nontuberculous mycobacterium capable of producing pulmonary and disseminated infections in humans. These infections are very difficult to treat due to innate and acquired antibiotic resistance that render a scenario of limited and suboptimal therapeutic options, the majority of which significantly reduce the patient's quality of life. The resistance mechanisms combined with the ability of Mab to evade the immune system via the formation of giant cords, to shield itself from antibiotic therapy though the induction of granulomas and biofilms, and to hide inside host phagocytes, represent a formidable set of virulence and defence mechanisms that turn Mab into one of the most challenging human pathogens. Understanding the foundations of its virulence and pathogenicity could unveil new ways for fighting Mab infections.

Secretion systems are associated with the transport of virulence factors and the persistence of mycobacteria within the immune cells. In particular, some Type VII secretion systems (T7SS or ESX) are involved in host-pathogen interactions. Mab possesses only ESX-3 and ESX-4. ESX-4 contains 5 genes encoding proteins that form a structure that spans the inner membrane, and 3 additional genes which products have not been previously characterized. However, a recent study proposed that ESX-4 was associated to Mab virulence. In this study, we have characterized two proteins from Mab ESX-4 locus, EsxU and EsxT, previously thought to be secreted factors.

Our results show that Mab EsxU and EsxT are helical proteins that form a 1:1 soluble heterodimer, as previously reported for other Esx protein pairs. Through cloning, expression and purification experiments we found that EsxU/EsxT is a substrate of Mab ESX-4 and that this system is functional. Subcellular localization suggests that the heterodimer associates with the mycomembrane, maintaining a weak bond with the inner membrane complex. Cytokine secretion and expression experiments indicate that this heterodimer does not activate an immune response on its own, nor induce lysis or apoptosis in human phagocytes, nor act as an efflux-pump protecting the bacteria from antibiotics. However, experiments conducted in collaboration with research groups at IRIM and UVSQ show that EsxU/EsxT has a role in host-pathogen interaction and in the fate of the mycobacteria inside the phagosome. RT-PCR experiments showed that both *esxU* and *esxT* are expressed in larger quantities than the ESX-4 structural components in the Mab ATCC 19977 type strain. Their expression levels are even greater in clinical Mab isolates, suggesting a critical role during infection. Nevertheless, *esxU* and *esxT* are not essential as evidenced by the successful generation of double knock-out strains by our collaborators. Biophysical experiments indicated that the EsxU/EsxT heterodimer interacts with membranes, probably forming a high-order porin-like structure, and that this interaction depends on the pH of the environment, the protein concentration, the transmembrane voltage, and the lipid composition of the membrane. By performing similar biophysical experiments with an EsxU/EsxT$_{A43W}$ mutant, we found that the WXG motif plays and important role in porin formation.

The present study presents, for the first time, an overview of the localization, roles and structure of the Mab EsxU/EsxT heterodimer, with insight on how mutations on the WXG motif affect the protein interaction with membranes. Further research is needed to clarify EsxU/EsxT function and relevance during infection. Likewise, a deeper investigation is required to fully understand the role of the WXG motifs and secretion signals in the localization and function of Esx proteins, and to study how these proteins evolved to fulfil different roles.

SUMMARY IN GERMAN

Mycobacterium abscessus (Mab) ist ein nichttuberkulöses Mykobakterium, das beim Menschen pulmonale und disseminierte Infektionen hervorrufen kann. Diese Infektionen sind aufgrund der angeborenen und erworbenen Antibiotikaresistenz sehr schwer zu behandeln. Somit stehen nur wenige und unzureichende therapeutische Optionen zur Verfügung, von denen die meisten die Lebensqualität der Patienten erheblich beeinträchtigen. Die Resistenzmechanismen in Verbindung mit der Fähigkeit von Mab, sich dem Immunsystem durch die Bildung von großen Schnurstrukturen zu entziehen, sich durch die Induktion von Granulomen und Biofilmen vor einer Antibiotikatherapie zu schützen und sich in den Phagozyten des Wirts zu verstecken, stellen ein beeindruckendes Spektrum von Virulenz- und Abwehrmechanismen dar, die Mab zu einem der herausforderndsten menschlichen Krankheitserreger machen. Das Verständnis der Grundlagen seiner Virulenz und Pathogenität könnte neue Wege zur Bekämpfung von Mab-Infektionen aufzeigen.

Sekretionssysteme sind mit dem Transport von Virulenzfaktoren und der Persistenz von Mykobakterien innerhalb der Immunzellen assoziiert. Insbesondere einige Typ-VII-Sekretionssysteme (T7SS oder ESX) sind an Wirt-Pathogen-Interaktionen beteiligt. Von diesen Systemen besitzt Mab nur ESX-3 und ESX-4. ESX-4 enthält 5 Gene, welche für Proteine kodieren, die eine die innere Membran überspannende Struktur bilden, sowie 3 weitere Gene, deren Produkte bisher nicht charakterisiert wurden. In einer aktuellen Studie wurde jedoch vorgeschlagen, dass ESX-4 mit der Virulenz von Mab in Beziehung steht. In dieser Studie haben wir die beiden Proteine EsxU und EsxT aus dem ESX-4-Lokus von Mab charakterisiert, von denen bisher angenommen wurde, dass sie sezerniert werden.

Unsere Ergebnisse zeigen, dass Mab EsxU und EsxT helikale Proteine sind, die ein lösliches Heterodimer im Verhältnis 1:1 bilden, wie bereits für andere Esx-Proteinpaare berichtet wurde. Durch Klonierungs-, Expressions- und Aufreinigungsexperimente haben wir herausgefunden, dass EsxU/EsxT ein Substrat von Mab ESX-4 ist und dass dieses System funktionell ist. Aufgrund der subzellulären Lokalisierung ist anzunehmen, dass das Heterodimer mit der Mykomembran assoziiert und eine schwache Bindung mit dem inneren Membrankomplex aufweist. Zytokinsekretions- und Expressionsexperimente deuten darauf hin, dass dieses Heterodimer weder selbst eine Immunantwort auslöst, noch Lyse oder Apoptose in menschlichen Phagozyten induziert, noch als Efflux-Pumpe agiert, die die Bakterien vor Antibiotika schützt. Experimente, die in Zusammenarbeit mit Forschungsgruppen am IRIM und am UVSQ durchgeführt wurden, zeigen jedoch, dass EsxU/EsxT eine Rolle bei der Wirts-Pathogen-Interaktion und beim Schicksal der Mykobakterien im Phagosom spielt. RT-PCR-Experimente zeigten, dass sowohl *esxU* als auch *esxT* in größeren Mengen als die ESX-4-Strukturkomponenten im Mab ATCC 19977-Typstamm exprimiert werden. Ihre Expressionswerte sind in klinischen Mab-Isolaten sogar noch höher, was auf eine entscheidende Rolle während der Infektion hindeutet. Dennoch sind esxU und esxT nicht essentiell, wie die erfolgreiche Erzeugung von Doppel-Knock-out-Stämmen durch unsere Kooperationspartner gezeigt hat. Biophysikalische Experimente wiesen darauf hin, dass das EsxU/EsxT-Heterodimer mit Membranen interagiert. Dabei bildet es vermutlich eine porinartige Struktur hoher Ordnung, und diese Interaktion hängt vom pH-Wert der Umgebung, der Proteinkonzentration, der Transmembranspannung und der Lipidzusammensetzung der Membran ab. Ähnliche biophysikalische Experimente mit einer EsxU/EsxT$_{A43W}$-Mutante ergaben, dass das WXG-Motiv eine wichtige Rolle bei der Porinbildung spielt.

Die vorliegende Studie gibt zum ersten Mal einen Überblick über die Lokalisierung, die Rolle und die Struktur des Mab-Heterodimers EsxU/EsxT und gibt Aufschluss darüber, wie Mutationen am WXG-Motiv die Interaktion des Proteins mit Membranen beeinflussen. Weitere Forschung ist erforderlich, um die Funktion und Relevanz von EsxU/EsxT während der Infektion zu klären. Ebenso ist eine tiefer gehende Untersuchung erforderlich, um die Rolle der WXG-Motive und der Sekretionssignale bei der Lokalisierung und Funktion der Esx-Proteine vollständig zu verstehen und um zu untersuchen, wie sich diese Proteine entwickelt haben, um unterschiedliche Aufgaben zu erfüllen.

6. LIST OF ABBREVIATIONS

CF	Cystic fibrosis
DOPC	Dioleoyl-phosphatidylcholine
Ecc	ESX conserved component
ESX	ESAT-6 secretion systems
EMBL	European Molecular Biology Laboratory
FZB	Forschungszentrum Borstel
GFP	Green fluorescent protein
GPL	Glycopeptidolipids
hIL-1β	Human interleukin one beta
hIL-8	Human interleukin eight
hIL-18	Human interleukin eighteen
hTNF-α	Human tumor necrosis factor alpha
hIFN-β	Human interferon beta
hIFN-γ	Human interferon gamma
hCCL3	Human chemokine (C-C motif) ligand 3
hCCL4	Human chemokine (C-C motif) ligand 4
IMAC	Immobilized metal affinity chromatography
IRIM	Institut de Recherche en Infectiologie de Montpellier
LDH	Lactate-Dehydrogenase
MA	Mycolic acids
Mab	*Mycobacterium abscessus*
MABC	*Mycobacterium abscessus complex*
MabsCIP	CIP 104536T type strain of *M. abscessus* subspecies *abscessus*
MAC	*Mycobacterium avium complex*
MATS	Microbial adherence to solvents
MIC	Minimal Inhibitory Concentration
NRZ	Reference Centre for Mycobacteria
NTM	Nontuberculous mycobacteria
OADC	Oleic Albumin Dextrose Catalase
OCD	Oriented Circular Dichroism
PBMC	Peripheral blood mononuclear cells
pDST	Phenotypic drug susceptibility testing
PMN	Polymorphonuclear neutrophils
R	Rough
RGM	Rapid-growing mycobacteria
RT-PCR	Real-time PCR
S	Smooth
SEC	Size exclusion chromatography
SEC-MALLS	Multi-angle light scattering coupled with size exclusion chromatography
SEM	Scanning electron microscopy
SGM	Slow-growing mycobacteria
T7SS	Type VII Secretion Systems
UVSQ	Université Versailles Saint-Quentin-en-Yvelines
WT	Wild-type

7. BIBLIOGRAPHY

1. Lee, M.R., et al., *Mycobacterium abscessus Complex Infections in Humans.* Emerg Infect Dis, 2015. **21**(9): p. 1638-46.
2. To, K., et al., *General Overview of Nontuberculous Mycobacteria Opportunistic Pathogens: Mycobacterium avium and Mycobacterium abscessus.* J Clin Med, 2020. **9**(8).
3. Jeon, D., *Infection Source and Epidemiology of Nontuberculous Mycobacterial Lung Disease.* Tuberc Respir Dis (Seoul), 2019. **82**(2): p. 94-101.
4. Bryant, J.M., et al., *Emergence and spread of a human-transmissible multidrug-resistant nontuberculous mycobacterium.* Science (New York, N.Y.), 2016. **354**(6313): p. 751-757.
5. Johansen, M.D., J.L. Herrmann, and L. Kremer, *Non-tuberculous mycobacteria and the rise of Mycobacterium abscessus.* Nat Rev Microbiol, 2020.
6. Victoria, L., et al., *Mycobacterium abscessus complex: A Review of Recent Developments in an Emerging Pathogen.* Front Cell Infect Microbiol, 2021. **11**: p. 659997.
7. Daley, C.L., et al., *Treatment of Nontuberculous Mycobacterial Pulmonary Disease: An Official ATS/ERS/ESCMID/IDSA Clinical Practice Guideline.* Clinical Infectious Diseases, 2020. **71**(4): p. e1-e36.
8. Jarand, J., et al., *Clinical and Microbiologic Outcomes in Patients Receiving Treatment for Mycobacterium abscessus Pulmonary Disease.* Clinical Infectious Diseases, 2011. **52**(5): p. 565-571.
9. Degiacomi, G., et al., *Mycobacterium abscessus, an Emerging and Worrisome Pathogen among Cystic Fibrosis Patients.* International journal of molecular sciences, 2019. **20**(23): p. 5868.
10. Maurer, F.P., et al., *Lack of antimicrobial bactericidal activity in Mycobacterium abscessus.* Antimicrob Agents Chemother, 2014. **58**(7): p. 3828-36.
11. Paulowski, L., et al., *C25-modified rifamycin derivatives with improved activity against Mycobacterium abscessus.* bioRxiv, 2021: p. 2021.07.12.452042.
12. Gutierrez, A.V., et al., *Glycopeptidolipids, a Double-Edged Sword of the Mycobacterium abscessus Complex.* Front Microbiol, 2018. **9**: p. 1145.
13. Roux, A.L., et al., *The distinct fate of smooth and rough Mycobacterium abscessus variants inside macrophages.* Open Biol, 2016. **6**(11).
14. Pawlik, A., et al., *Identification and characterization of the genetic changes responsible for the characteristic smooth-to-rough morphotype alterations of clinically persistent Mycobacterium abscessus.* Mol Microbiol, 2013. **90**(3): p. 612-29.
15. Tan, J.L., et al., *Genomic Comparisons Reveal Microevolutionary Differences in Mycobacterium abscessus Subspecies.* Frontiers in Microbiology, 2017. **8**(2042).
16. Bernut, A., et al., *Mycobacterium abscessus-Induced Granuloma Formation Is Strictly Dependent on TNF Signaling and Neutrophil Trafficking.* PLOS Pathogens, 2016. **12**(11): p. e1005986.
17. Bernut, A., et al., *Mycobacterium abscessus cording prevents phagocytosis and promotes abscess formation.* Proc Natl Acad Sci U S A, 2014. **111**(10): p. E943-52.
18. Dartois, V., *The path of anti-tuberculosis drugs: from blood to lesions to mycobacterial cells.* Nature Reviews Microbiology, 2014. **12**(3): p. 159-167.
19. Griffith, D.E., *Mycobacterium abscessus and Antibiotic Resistance: Same As It Ever Was.* Clinical Infectious Diseases, 2019. **69**(10): p. 1687-1689.
20. Chiaradia, L., et al., *Dissecting the mycobacterial cell envelope and defining the composition of the native mycomembrane.* Scientific Reports, 2017. **7**(1): p. 12807.
21. Jarlier, V. and H. Nikaido, *Mycobacterial cell wall: structure and role in natural resistance to antibiotics.* FEMS Microbiol Lett, 1994. **123**(1-2): p. 11-8.
22. DePas, W.H., M. Bergkessel, and D.K. Newman, *Aggregation of Nontuberculous Mycobacteria Is Regulated by Carbon-Nitrogen Balance.* mBio, 2019. **10**(4).
23. Bosserman, R.E. and P.A. Champion, *Esx Systems and the Mycobacterial Cell Envelope: What's the Connection?* Journal of Bacteriology, 2017. **199**(17): p. e00131-17.

24. III, J.O.F., *Reducing Human Exposure to Mycobacterium avium.* Annals of the American Thoracic Society, 2013. **10**(4): p. 378-382.
25. Brennan, P.J. and M.B. Goren, *Structural studies on the type-specific antigens and lipids of the mycobacterium avium. Mycobacterium intracellulare. Mycobacterium scrofulaceum serocomplex. Mycobacterium intracellulare serotype 9.* J Biol Chem, 1979. **254**(10): p. 4205-11.
26. Daffé, M., A. Quémard, and H. Marrakchi, *Mycolic Acids: From Chemistry to Biology*, in *Biogenesis of Fatty Acids, Lipids and Membranes*, O. Geiger, Editor. 2017, Springer International Publishing: Cham. p. 1-36.
27. Llorens-Fons, M., et al., *Trehalose Polyphleates, External Cell Wall Lipids in Mycobacterium abscessus, Are Associated with the Formation of Clumps with Cording Morphology, Which Have Been Associated with Virulence.* Front Microbiol, 2017. **8**: p. 1402.
28. Viljoen, A., et al., *Fast chemical force microscopy demonstrates that glycopeptidolipids define nanodomains of varying hydrophobicity on mycobacteria.* Nanoscale Horizons, 2020. **5**(6): p. 944-953.
29. Zulauf, K.E., J.T. Sullivan, and M. Braunstein, *The SecA2 pathway of Mycobacterium tuberculosis exports effectors that work in concert to arrest phagosome and autophagosome maturation.* PLOS Pathogens, 2018. **14**(4): p. e1007011.
30. van Winden, V.J.C., E.N.G. Houben, and M. Braunstein, *Protein Export into and across the Atypical Diderm Cell Envelope of Mycobacteria.* Microbiology Spectrum, 2019. **7**(4).
31. Dumas, E., et al., *Mycobacterial Pan-Genome Analysis Suggests Important Role of Plasmids in the Radiation of Type VII Secretion Systems.* Genome Biology and Evolution, 2016. **8**(2): p. 387-402.
32. Gröschel, M.I., et al., *ESX secretion systems: mycobacterial evolution to counter host immunity.* Nature Reviews Microbiology, 2016. **14**(11): p. 677-691.
33. Burts, M.L., et al., *EsxA and EsxB are secreted by an ESAT-6-like system that is required for the pathogenesis of Staphylococcus aureus infections.* Proceedings of the National Academy of Sciences of the United States of America, 2005. **102**(4): p. 1169-1174.
34. Huppert, L.A., et al., *The ESX System in Bacillus subtilis Mediates Protein Secretion.* PLOS ONE, 2014. **9**(5): p. e96267.
35. Newton-Foot, M., et al., *The plasmid-mediated evolution of the mycobacterial ESX (Type VII) secretion systems.* BMC Evol Biol, 2016. **16**: p. 62.
36. Letek, M., et al., *The Genome of a Pathogenic Rhodococcus: Cooptive Virulence Underpinned by Key Gene Acquisitions.* PLOS Genetics, 2010. **6**(9): p. e1001145.
37. Callahan, B., et al., *Conservation of Structure and Protein-Protein Interactions Mediated by the Secreted Mycobacterial Proteins EsxA, EsxB, and EspA.* Journal of Bacteriology, 2010. **192**(1): p. 326-335.
38. Akpe San Roman, S., et al., *A heterodimer of EsxA and EsxB is involved in sporulation and is secreted by a type VII secretion system in Streptomyces coelicolor.* Microbiology (Reading), 2010. **156**(Pt 6): p. 1719-1729.
39. Copeland, A., et al., *Complete genome sequence of Catenulispora acidiphila type strain (ID 139908T).* Standards in Genomic Sciences, 2009. **1**(2): p. 119-125.
40. Pukall, R., et al., *Complete genome sequence of Kribbella flavida type strain (IFO 14399T).* Standards in Genomic Sciences, 2010. **2**(2): p. 186-193.
41. Lagune, M., et al., *Conserved and specialized functions of Type VII secretion systems in non-tuberculous mycobacteria.* Microbiology, 2021. **167**(7).
42. Groschel, M.I., et al., *ESX secretion systems: mycobacterial evolution to counter host immunity.* Nat Rev Microbiol, 2016. **14**(11): p. 677-691.
43. Majlessi, L., et al., *Release of mycobacterial antigens.* Immunological Reviews, 2015. **264**(1): p. 25-45.
44. Ohol, Y.M., et al., *Mycobacterium tuberculosis MycP1 Protease Plays a Dual Role in Regulation of ESX-1 Secretion and Virulence.* Cell Host & Microbe, 2010. **7**(3): p. 210-220.

45. van Winden, V.J.C., et al., *Mycosins Are Required for the Stabilization of the ESX-1 and ESX-5 Type VII Secretion Membrane Complexes.* mBio, 2016. **7**(5): p. e01471-16.
46. van Winden, V.J.C., et al., *A Chimeric EccB-MycP Fusion Protein is Functional and a Stable Component of the ESX-5 Type VII Secretion System Membrane Complex.* J Mol Biol, 2020. **432**(4): p. 1265-1278.
47. Beckham, K.S., et al., *Structure of the mycobacterial ESX-5 type VII secretion system membrane complex by single-particle analysis.* Nat Microbiol, 2017. **2**: p. 17047.
48. Poweleit, N., et al., *The structure of the endogenous ESX-3 secretion system.* Elife, 2019. **8**.
49. Soler-Arnedo, P., et al., *Polarly Localized EccE₁ Is Required for ESX-1 Function and Stabilization of ESX-1 Membrane Proteins in Mycobacterium tuberculosis.* Journal of Bacteriology, 2020. **202**(5): p. e00662-19.
50. Chirakos, A.E., et al., *Modeling Tubercular ESX-1 Secretion Using Mycobacterium marinum.* Microbiology and Molecular Biology Reviews, 2020. **84**(4): p. e00082-19.
51. Clark, R.R., et al., *Direct cell-cell contact activates SigM to express the ESX-4 secretion system in Mycobacterium smegmatis.* Proc Natl Acad Sci U S A, 2018. **115**(28): p. E6595-E6603.
52. Gray, T.A., et al., *Intercellular communication and conjugation are mediated by ESX secretion systems in mycobacteria.* Science, 2016. **354**(6310): p. 347-350.
53. Laencina, L., et al., *Identification of genes required for Mycobacterium abscessus growth in vivo with a prominent role of the ESX-4 locus.* Proc Natl Acad Sci U S A, 2018. **115**(5): p. E1002-E1011.
54. Izquierdo Lafuente, B., et al., *Mycobacterium tuberculosis Toxin CpnT Is an ESX-5 Substrate and Requires Three Type VII Secretion Systems for Intracellular Secretion.* mBio, 2021. **12**(2): p. e02983-20.
55. Fedrizzi, T., et al., *Genomic characterization of Nontuberculous Mycobacteria.* Scientific Reports, 2017. **7**(1): p. 45258.
56. Poulsen, C., et al., *WXG100 protein superfamily consists of three subfamilies and exhibits an alpha-helical C-terminal conserved residue pattern.* PLoS One, 2014. **9**(2): p. e89313.
57. Stanley, S.A., et al., *Acute infection and macrophage subversion by Mycobacterium tuberculosis require a specialized secretion system.* Proceedings of the National Academy of Sciences, 2003. **100**(22): p. 13001-13006.
58. Tan, T., et al., *The ESAT-6/CFP-10 secretion system of Mycobacterium marinum modulates phagosome maturation.* Cellular Microbiology, 2006. **8**(9): p. 1417-1429.
59. Ma, Y., V. Keil, and J. Sun, *Characterization of Mycobacterium tuberculosis EsxA membrane insertion: roles of N- and C-terminal flexible arms and central helix-turn-helix motif.* J Biol Chem, 2015. **290**(11): p. 7314-22.
60. Peng, X. and J. Sun, *Mechanism of ESAT-6 membrane interaction and its roles in pathogenesis of Mycobacterium tuberculosis.* Toxicon, 2016. **116**: p. 29-34.
61. Wong, K.-W., *The Role of ESX-1 in Mycobacterium tuberculosis Pathogenesis.* Microbiology Spectrum, 2017. **5**(3).
62. Ariga, H. and N. Harada, *[Evolution of IGRA researches].* Kekkaku, 2008. **83**(9): p. 641-52.
63. Ripoll, F., et al., *Non mycobacterial virulence genes in the genome of the emerging pathogen Mycobacterium abscessus.* PLoS One, 2009. **4**(6): p. e5660.
64. Motohashi, K., *A simple and efficient seamless DNA cloning method using SLiCE from Escherichia coli laboratory strains and its application to SLiP site-directed mutagenesis.* BMC Biotechnology, 2015. **15**(1): p. 47.
65. Graewert, M.A., et al., *Adding Size Exclusion Chromatography (SEC) and Light Scattering (LS) Devices to Obtain High-Quality Small Angle X-Ray Scattering (SAXS) Data.* Crystals, 2020. **10**(11): p. 975.
66. Saini, G. *Bacterial hydrophobicity : assessment techniques, applications and extension to colloids*. 2010.

67. Serebriakova, E.V., et al., *[Evaluation of the hydrophobicity of bacterial cells by measuring their adherence to chloroform drops].* Mikrobiologiia, 2002. **71**(2): p. 237-9.
68. Au - Feltwell, T., et al., *Separating Bacteria by Capsule Amount Using a Discontinuous Density Gradient.* JoVE, 2019(143): p. e58679.
69. Au - Evans, B.C., et al., *Ex Vivo Red Blood Cell Hemolysis Assay for the Evaluation of pH-responsive Endosomolytic Agents for Cytosolic Delivery of Biomacromolecular Drugs.* JoVE, 2013(73): p. e50166.
70. van Zandbergen, G., et al., *Leishmania promastigotes release a granulocyte chemotactic factor and induce interleukin-8 release but inhibit gamma interferon-inducible protein 10 production by neutrophil granulocytes.* Infect Immun, 2002. **70**(8): p. 4177-84.
71. Reiling, N., et al., *Clade-Specific Virulence Patterns of Mycobacterium tuberculosis Complex Strains in Human Primary Macrophages and Aerogenically Infected Mice.* mBio, 2013. **4**(4): p. e00250-13.
72. Howard, S.T., et al., *Spontaneous reversion of Mycobacterium abscessus from a smooth to a rough morphotype is associated with reduced expression of glycopeptidolipid and reacquisition of an invasive phenotype.* Microbiology (Reading), 2006. **152**(Pt 6): p. 1581-1590.
73. Herold, C., et al., *Efficient Electroformation of Supergiant Unilamellar Vesicles Containing Cationic Lipids on ITO-Coated Electrodes.* Langmuir, 2012. **28**(13): p. 5518-5521.
74. Bi, H., et al., *Lipid Nanotube Formation Using Space-Regulated Electric Field above Interdigitated Electrodes.* ACS Nano, 2014. **8**(4): p. 3961-3969.
75. Kusters, I., A.M. van Oijen, and A.J.M. Driessen, *Membrane-on-a-Chip: Microstructured Silicon/Silicon-Dioxide Chips for High-Throughput Screening of Membrane Transport and Viral Membrane Fusion.* ACS Nano, 2014. **8**(4): p. 3380-3392.
76. Bürck, J., et al., *Conformation and Membrane Orientation of Amphiphilic Helical Peptides by Oriented Circular Dichroism.* Biophysical Journal, 2008. **95**(8): p. 3872-3881.
77. Gomez, M., et al., *sigA is an essential gene in Mycobacterium smegmatis.* Molecular Microbiology, 1998. **29**(2): p. 617-628.
78. Bunduc, C.M., et al., *Structure and dynamics of a mycobacterial type VII secretion system.* Nature, 2021. **593**(7859): p. 445-448.
79. Renshaw, P.S., et al., *Conclusive evidence that the major T-cell antigens of the Mycobacterium tuberculosis complex ESAT-6 and CFP-10 form a tight, 1:1 complex and characterization of the structural properties of ESAT-6, CFP-10, and the ESAT-6*CFP-10 complex. Implications for pathogenesis and virulence.* J Biol Chem, 2002. **277**(24): p. 21598-603.
80. Viljoen, A., et al., *A Simple and Rapid Gene Disruption Strategy in Mycobacterium abscessus: On the Design and Application of Glycopeptidolipid Mutants.* Front Cell Infect Microbiol, 2018. **8**: p. 69.
81. Busscher, H.J. and H.C. van der Mei, *How Do Bacteria Know They Are on a Surface and Regulate Their Response to an Adhering State?* PLOS Pathogens, 2012. **8**(1): p. e1002440.
82. Habimana, O., A.J.C. Semião, and E. Casey, *The role of cell-surface interactions in bacterial initial adhesion and consequent biofilm formation on nanofiltration/reverse osmosis membranes.* Journal of Membrane Science, 2014. **454**: p. 82-96.
83. Farniya, F., A. Jamalli, and T. Dadgar, *Physicochemical surface characteristics in different pathogenic bacteria.* Cogent Biology, 2019. **5**(1): p. 1638572.
84. Leisching, G., et al., *Virulence, biochemistry, morphology and host-interacting properties of detergent-free cultured mycobacteria: An update.* Tuberculosis (Edinb), 2016. **100**: p. 53-60.
85. Pandey, H., et al., *Biophysical and immunological characterization of the ESX-4 system ESAT-6 family proteins Rv3444c and Rv3445c from Mycobacterium tuberculosis H37Rv.* Tuberculosis (Edinb), 2018. **109**: p. 85-96.
86. Mohan, V.P., et al., *Effects of tumor necrosis factor alpha on host immune response in chronic persistent tuberculosis: possible role for limiting pathology.* Infect Immun, 2001. **69**(3): p. 1847-55.

87. Jafari, C., et al., *Rapid Diagnosis of Smear-negative Tuberculosis by Bronchoalveolar Lavage Enzyme-linked Immunospot.* American Journal of Respiratory and Critical Care Medicine, 2006. **174**(9): p. 1048-1054.
88. Patrick, K.L., S.L. Bell, and R.O. Watson, *For Better or Worse: Cytosolic DNA Sensing during Intracellular Bacterial Infection Induces Potent Innate Immune Responses.* Journal of Molecular Biology, 2016. **428**(17): p. 3372-3386.
89. Bürck, J., et al., *Oriented Circular Dichroism: A Method to Characterize Membrane-Active Peptides in Oriented Lipid Bilayers.* Accounts of Chemical Research, 2016. **49**(2): p. 184-192.
90. São-José, C., C. Baptista, and M.A. Santos, *Bacillus subtilis operon encoding a membrane receptor for bacteriophage SPP1.* J Bacteriol, 2004. **186**(24): p. 8337-46.
91. Ludwig, H., et al., *Transcription of glycolytic genes and operons in Bacillus subtilis: evidence for the presence of multiple levels of control of the gapA operon.* Mol Microbiol, 2001. **41**(2): p. 409-22.
92. Sysoeva, T.A., et al., *Dimer recognition and secretion by the ESX secretion system in Bacillus subtilis.* Proceedings of the National Academy of Sciences, 2014. **111**(21): p. 7653-7658.
93. Famelis, N., et al., *Architecture of the mycobacterial type VII secretion system.* Nature, 2019. **576**(7786): p. 321-325.
94. Ribeiro, G.M., et al., *Increased survival and proliferation of the epidemic strain Mycobacterium abscessus subsp. massiliense CRM0019 in alveolar epithelial cells.* BMC Microbiology, 2017. **17**(1): p. 195.
95. Ilghari, D., et al., *Solution Structure of the Mycobacterium tuberculosis EsxG·EsxH Complex: FUNCTIONAL IMPLICATIONS AND COMPARISONS WITH OTHER M. TUBERCULOSIS Esx FAMILY COMPLEXES*.* Journal of Biological Chemistry, 2011. **286**(34): p. 29993-30002.
96. Ryndak, M.B., et al., *Transcriptional profile of Mycobacterium tuberculosis replicating in type II alveolar epithelial cells.* PLoS One, 2015. **10**(4): p. e0123745.
97. Tak, U., T. Dokland, and M. Niederweis, *Pore-forming Esx proteins mediate toxin secretion by Mycobacterium tuberculosis.* Nature Communications, 2021. **12**(1): p. 394.

8. ACKNOWLEDGEMENTS

The present project was conceived by Project Leaders Prof. Florian Maurer, Prof. Matthias Wilmanns and Dr. Annabel Parret as part of the Infectophysics Consortium and funded by the Joachim Herz Foundation. They all have been the driving force for the development of this work, organizing, supervising and managing collaborations to obtain the best results possible. In line with this, the work presented here has been developed mainly at two institutes: EMBL-Hamburg and FZB. I would like to give special thanks to Prof. Ulrich Schaible and Prof. Thomas Gutsmann who welcomed me as part of their groups and organized my training so I could perform the different experiments conducted in their areas. Likewise, I would like to thank PD Dr. Norbert Reiling who suggested new experiments and always gave interesting insights to shape the investigation. I would also like to thank all teams, particularly the NRZ group who welcomed me and made sure I always had a spot somewhere at the offices during the pandemic-driven office rearrangements. In addition to the in-house collaboration, we hold collaborative efforts with the groups of Prof. Jean-Louis Herrmann at Université Versailles Saint-Quentin-en-Yvelines (UVSQ) and Prof. Laurent Kremer at Institut de Recherche en Infectiologie de Montpellier (IRIM), whose expertise in working with *Mycobacterium abscessus* and already established laboratory techniques made the progress of this research stronger. Their guidance and support has been crucial for the development of this work. Last but not least, I would like to extend special thanks to Dr. Astrid Sydow who organized everything I needed to come to Germany and helped me to surf through all required bureaucratic endeavours.

Furthermore, I would like to acknowledge the guidance and training I received from remarkable professionals, since the first day, which allowed me to discover research areas and techniques I haven't known before. With particular interest I would like to thank: Dr. Kate Beckham for training me in protein expression and purification, Dr. Diana Freires for helping me understand protein purification, Dr. Cecile Petit for being a dedicated collaborator at the EMBL when I moved to FZB, Dr. Tobias Dallenga for teaching me how to isolate human PMBCs, Dr. Christian Nehls for training me in the methods of planar membranes, light scattering and OCD, Dr. Laura Paulowski for training me in the methods of pore-spanning membranes (NanoSpot) and OCD and being a driving force to go to conferences and acquire essential devices, Dr. Matt Johansen at IRIM for generating the Mab mutant strains and Dr. Wassim Daher also at IRIM for conducting the cell fractionation and IF experiments. Likewise, I would like to extend special thanks to Prof. Thomas Gutsmann and Dr. Susanne Homolka for taking the SEM pictures at the Christian-Albrechts Universität zu Kiel, to Dr. Uwe Mamat for supporting me with mycobacterial fractionation, to Dr. Sven Müller-Loennies for isolating the lipids from Mab membranes, and to Dr. Jochen Bürck at Karlsruhe Institute of Technology (KIT) for his support and disposition during the OCD measurements.

I want to acknowledge the technical support of the wonderful technicians at EMBL-Hamburg and at FZB who helped me with the experiments. In particular, I would like to thank: Sonja Staack at EMBL-Hamburg for her expertise in protein purification, Anne Witt at NRZ for helping me with consumables ordering and logistics in general, Margrit Kernbach at NRZ for conducting the drug susceptibility testing and preparing Mab clinical isolates, Jacqueline Eich at Prof. Ulrich Schaible's laboratory for helping me with the live fluorescence microscopy, Carolin Golin at PD Dr. Norbert Reiling's laboratory for performing the infection and cytokine expression experiments in human macrophages, Sabrina Groth at Prof. Thomas Gutsmann's laboratory for performing the TethaPod experiments, and Veronika Susott and Ute Agge for helping with the isolation of Mab membrane lipids. Their invaluable contribution made this project possible.

9. CURRICULUM VITAE

Lebenslauf entfällt aus datenschutzrechtlichen Gründen.

Lebenslauf entfällt aus datenschutzrechtlichen Gründen.

Lebenslauf entfällt aus datenschutzrechtlichen Gründen.

Lebenslauf entfällt aus datenschutzrechtlichen Gründen.

Lebenslauf entfällt aus datenschutzrechtlichen Gründen.

10. Eidesstattliche Versicherung *[als letztes Blatt in die Dissertation einzubinden]*

Ich versichere ausdrücklich, dass ich die Arbeit selbständig und ohne fremde Hilfe verfasst, andere als die von mir angegebenen Quellen und Hilfsmittel nicht benutzt und die aus den benutzten Werken wörtlich oder inhaltlich entnommenen Stellen einzeln nach Ausgabe (Auflage und Jahr des Erscheinens), Band und Seite des benutzten Werkes kenntlich gemacht habe.
Ferner versichere ich, dass ich die Dissertation bisher nicht einem Fachvertreter an einer anderen Hochschule zur Überprüfung vorgelegt oder mich anderweitig um Zulassung zur Promotion beworben habe.
Ich erkläre mich einverstanden, dass meine Dissertation vom Dekanat der Medizinischen Fakultät mit einer gängigen Software zur Erkennung von Plagiaten überprüft werden kann.

Unterschrift: .....